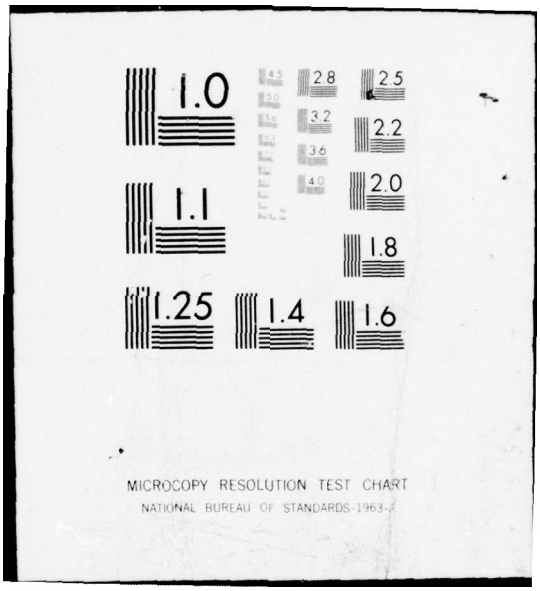
AD-A040 377 HARVARD UNIV CAMBRIDGE MASS GORDON MCKAY LAB F/G 9/5
THE BEVERAGE WAVE ANTENNA: CURRENTS, CHARGES AND ADMITTANCES. V--ETC(U)
FEB 77 R M SORBELLO F19628-76-C-0057
UNCLASSIFIED SCIENTIFIC-1 RADC-TR-77-82-VOL-1 NL

1 OF 2
AD
A040 377




1.0
1.1
1.25
1.4
1.6
1.8
2.0
2.2
2.5
2.8
3.2
3.6
4.0
4.5
5.0
5.6
MICROCOPY RESOLUTION TEST CHART
NATIONAL BUREAU OF STANDARDS-1963-A

AD A040377

RADC-TR-77-82, Vol. I (of two)
Scientific Report No. 1 (Vol. I)
February 1977

THE BEVERAGE WAVE ANTENNA: CURRENTS, CHARGES AND ADMITTANCES
Vol. I. Theoretical Analysis; Experimental Equipment and System Calibration

by

Robert M. Sorbello

Gordon McKay Laboratory, Harvard University
Division of Engineering and Applied Physics
Cambridge, MA 02138

Approved for public release;
distribution unlimited.

DDC
RECEIVED
JUN 9 1977
D

AD No.
DDC FILE COPY.

ROME AIR DEVELOPMENT CENTER
AIR FORCE SYSTEMS COMMAND
GRIFFISS AIR FORCE BASE, NEW YORK 13441

This report has been reviewed by the RADC Information Office (OI) and is releasable to the National Technical Information Service (NTIS). At NTIS it will be releasable to the general public, including foreign nations.

APPROVED:

JOHN F. McILVENNA
Project Engineer

APPROVED:

ALLAN C. SCHELL, Acting Chief
Electromagnetic Sciences Division

FOR THE COMMANDER:

Plans Office

UNCLASSIFIED

SECURITY CLASSIFICATION OF THIS PAGE (When Data Entered)

REPORT DOCUMENTATION PAGE

READ INSTRUCTIONS BEFORE COMPLETING FORM

1. REPORT NUMBER: RADC-TR-77-82, Vol. I (of two)	2. GOVT ACCESSION NO.
3. RECIPIENT'S CATALOG NUMBER	
4. TITLE (and Subtitle): THE BEVERAGE WAVE ANTENNA: CURRENTS, CHARGES AND ADMITTANCES. Vol. I. Theoretical Analysis; Experimental Equipment and System Calibration.	5. TYPE OF REPORT & PERIOD COVERED: Scientific Report No. 1 (Vol. I)
	6. PERFORMING ORG. REPORT NUMBER
7. AUTHOR(s): Robert M. Sorbello	8. CONTRACT OR GRANT NUMBER(s): F19628-76-C-0057 and Joint Services Electronics Program Contract N00014-75-C-0648
9. PERFORMING ORGANIZATION NAME AND ADDRESS: Gordon McKay Laboratory, Harvard University, Division of Engineering and Applied Physics, Cambridge, Mass. 02138	10. PROGRAM ELEMENT, PROJECT, TASK AREA & WORK UNIT NUMBERS: 61102F, 5635-06-01
11. CONTROLLING OFFICE NAME AND ADDRESS: Deputy for Electronic Technology (RADC/ETER), Hanscom AFB, MA 01731, Contract Monitor: John F. McIlvenna	12. REPORT DATE: February 1977
	13. NUMBER OF PAGES: 114
14. MONITORING AGENCY NAME & ADDRESS (if different from Controlling Office)	15. SECURITY CLASS. (of this report): UNCLASSIFIED
	15a. DECLASSIFICATION/DOWNGRADING SCHEDULE

16. DISTRIBUTION STATEMENT (of this Report)

Approved for public release; distribution unlimited.

17. DISTRIBUTION STATEMENT (of the abstract entered in Block 20, if different from Report)

18. SUPPLEMENTARY NOTES

19. KEY WORDS (Continue on reverse side if necessary and identify by block number)

horizontal-wire antennas over an imperfectly conducting half-space
Beverage wave antennas
effect of half-space; end effects
currents, charges and input admittances
theoretical analysis; experimental equipment and system calibration

20. ABSTRACT (Continue on reverse side if necessary and identify by block number)

This report presents the results of an experimental and theoretical investigation of the circuit properties of horizontal-wire antennas placed over an imperfectly conducting half-space. Particular emphasis is given to the Beverage wave antenna, a special type of horizontal-wire antenna placed in close proximity to the earth. Earlier work has generally assumed a free-space wave number on the wire, thus neglecting the effect of the half-space. The present study has carefully investigated experimentally the effect of the half-space on the properties

DD FORM 1 JAN 73 1473 EDITION OF 1 NOV 65 IS OBSOLETE

UNCLASSIFIED

SECURITY CLASSIFICATION OF THIS PAGE (When Data Entered)

157 000

20. ABSTRACT (Continued)

of the antenna (current, charge and input admittance) and has included this effect in all theories discussed.

The theoretical analysis, appearing in Part I of Vol. I, involves several aspects. The theory of King, Shen and Wu for horizontal wires over an imperfectly conducting half-space was verified experimentally. Discrepancies observed in certain cases were attributed to end effects, not accounted for in the theory. Two semi-empirical theories were subsequently developed which included contributions due to end effects. Both provided good agreement with the measured data. The theory of King was extended to include the Beverage wave antenna and comparison with measured results proved quite acceptable.

Distributions of current and charge as well as the input admittance were measured on dipole antennas and on Beverage wave antennas that ranged in length from $.5\lambda_0$ to $1.5\lambda_0$ and were placed at heights of from $.01\lambda_0$ to $.25\lambda_0$ above three different media - fresh water, salt water, and moist earth. A description of the experimental design and system calibration is contained in Part II of Vol. I. The measured data are presented and discussed in Vol. II (Part III of the report). The effects of the wire height and the parameters of the dissipative medium are noted. Special attention is given to the transmission-line nature of the measured currents and charges and to the measured wave number.

ACCESSION for
NTIS White Section
DDC Buff Section
UNANNOUNCED
JUSTIFICATION
BY
DISTRIBUTION/AVAILABILITY CODES
Dist. AVAIL. and/or SPECIAL

DDC
RECEIVED
JUN 9 1977
D

TABLE OF CONTENTS

VOLUME I — PAGE

Part I: Theoretical Analysis

1.1. Introduction. 1

1.2. The Theory of King et al. 4

1.3. Beverage Wave Antenna 9

1.4. Over-The-Horizon Radar. 12

1.5. Modified Beverage Antenna 14

1.6. Loaded Horizontal Wires Above a Half-Space. 19

1.7. Special Cases 30

1.8. Theoretical Refinements and End-Effect Considerations . . . 35

Part II: Experimental Equipment and System Calibration

2.1. Experimental Modeling 71

2.2. Half-Space Model and Choice of Operating Frequency. 73

2.3. Coaxial Measuring Line. 79

2.4. Impedance Measuring Probes. 83

2.5. Measurement of the Electrical Properties of Water 87

2.6. Measurement of the Electrical Properties of Earth 91

2.7. Measurement of Load Resistors 95

2.8. System Calibration. 95

REFERENCES 107

VOLUME II

Part III: Experimental Measurements

3.1. Introduction. 1

3.2. Measuring Procedure 3

3.3. Presentation of Measured Data for a Dipole Antenna Above a Dissipative Half-Space. 7

3.4. Presentation of Measured Data for the Modified Beverage Wave Antenna 82

3.5. End-Effect Correction 155

3.6. Broadband Characteristics of the Modified Beverage Antenna 157

3.7. Conclusions 159

APPENDIX A 163

APPENDIX B 168

REFERENCES 243

PART I

THEORETICAL ANALYSIS

1.1. Introduction

The importance of the presence of a plane earth in modifying the electromagnetic fields of elementary sources was recognized as early as 1909 by Sommerfeld [1]. The boundary-value problem associated with an infinitesimal electric dipole placed horizontally above a plane earth, as shown in Fig. 1.1, is by no means trivial. Since induced currents may extend far in from the surface of the interface, only the special case of a perfectly conducting earth can be treated by the straightforward image method. Solutions do exist in infinite-integral form, and asymptotic techniques have been utilized [2] to obtain analytic expressions valid over limited ranges of the various parameters. Several numerical approaches have also been attempted [3], [4]. They have been shown to give good agreement with previous asymptotic results and are able to be used beyond the ranges of validity of the asymptotic solutions. Unfortunately, these numerical evaluations are quite complex due to the singular nature of the Sommerfeld integrals and are also complicated by convergence problems over all ranges of the parameters.

The problem is even more difficult when finite-sized sources are considered. Specifically, for a center-driven antenna of finite length 2h, placed horizontally in medium 1 at a height d above a conducting or dielectric half-space, as shown in Fig. 1.2, the problem resolves itself into an evaluation of the changes produced in the current and charge distributions on the antenna by the presence of the half-space. Once these quantities have been obtained, the fields can be evaluated by simple integration [3]. One of the earliest and best known attempts [5] to solve this problem for an air-earth interface employed a transmission-line analogy, but imposed several serious assumptions which limited the range of validity to low frequencies, i.e., those frequencies for which the earth acts like a good conductor. More recent works [6], [7] have dealt with high-frequency effects, but these too impose restrictive assumptions. Until recently, most of the work [8]-[10] dealing with an antenna in air parallel to the earth or any other medium has assumed the distribution of current to be known and to be essentially that for an isolated antenna in air or over a perfect conductor. The effects of the proximity of the interface and of the constitutive properties

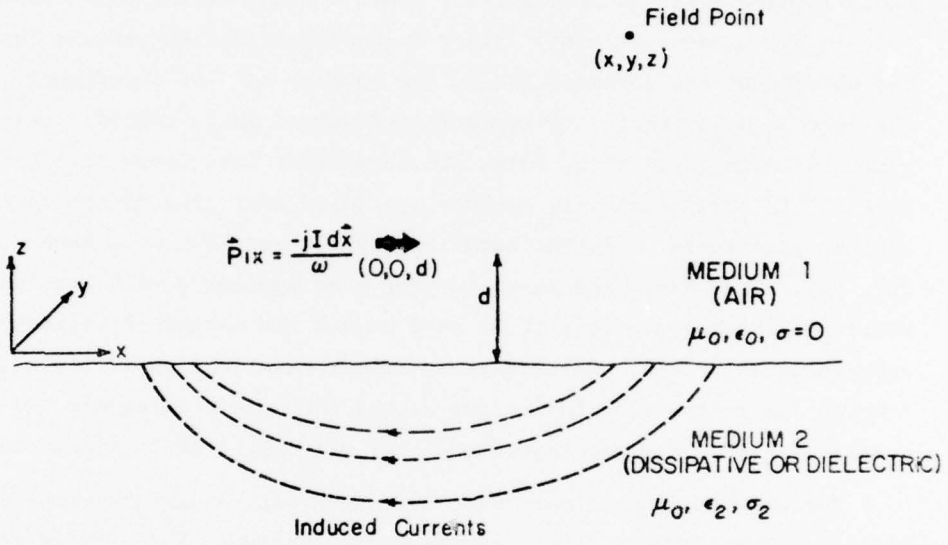


FIG. 1.1 INFINITESIMAL DIPOLE ABOVE AN IMPERFECT CONDUCTOR

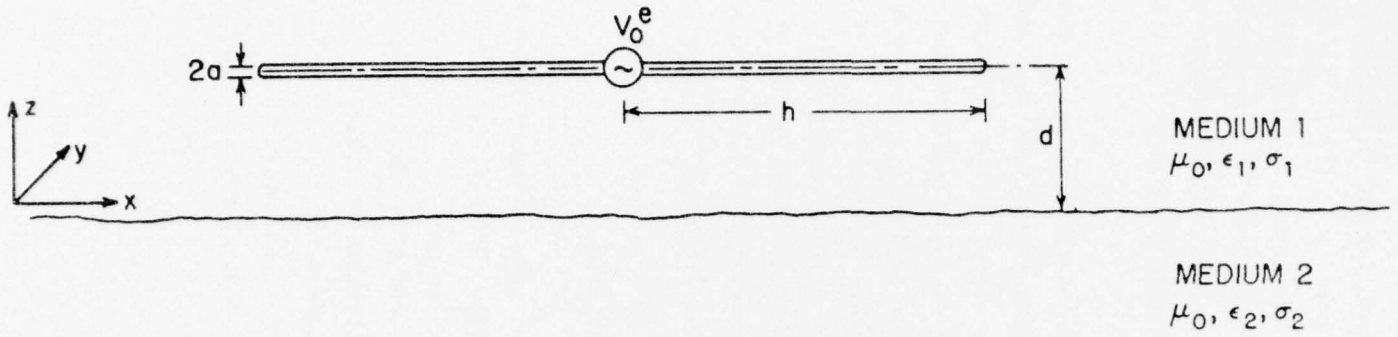


FIG. 1.2 HORIZONTAL WIRE ANTENNA OVER A CONDUCTING OR DIELECTRIC HALF-SPACE

of medium 2 on the antenna current distribution were neglected. Since it is possible to derive an integral equation for the current, several completely numerical approaches have been attempted [11], [12]. The difficulty with these methods lies in the fact that the kernel involves integrals and derivatives of Sommerfeld integrals, the solution of which can prove to be quite complex even for the straightforward moment-method technique [13]. At present, the exactness of any of these numerical methods is still to be determined.

To date, the best treatments of this problem can be found in two recent publications [14], [15]. Both are less restrictive than any of the previous works and both take into account the effect of the interface by solving for the complex wave number k_L on the wire. Wait deals exclusively with an infinitely long wire, while King is able to derive a zero-order expression for the current on a wire of finite length. Unfortunately, the paper by Wait leaves the solution for k_L in an unevaluated, modal-equation form unsuitable for further development. In the other treatment by King et al., an analytic expression is obtained for the wave number that lends itself to simple numerical evaluation. This treatment will prove to be quite useful for subsequent development in this report.

1.2. The Theory of King et al.

The theory for a horizontal wire over a conducting or dielectric half-space is closely related to two previous works [16], [17] which deal with the insulated and eccentrically insulated antennas. Through a limiting process which extends to infinity the outer medium of the eccentrically insulated antenna while keeping the distance between the conductor and the outer region constant, King was able to transform the formula for the wave number of the eccentrically insulated antenna into an expression which represents the wave number on a wire above an interface. King also showed that the zero-order current that exists on the wire is of transmission-line type.

The model for the problem is shown in Fig. 1.2. It depicts a center-driven dipole antenna of half-length h, placed horizontally in medium 1 at a height d above a plane half-space (medium 2) where the wave numbers of the two media are, respectively,

$$k_1 = \beta_1 - j\alpha_1 = \omega(\mu_1\xi_1)^{1/2} \tag{1.1a}$$

$$k_2 = \beta_2 - j\alpha_2 = \omega(\mu_2\xi_2)^{1/2} \tag{1.1b}$$

with

$$\xi_1 = \varepsilon_0(\varepsilon_{er1} - j\sigma_{e1}/\omega\varepsilon_0) \tag{1.2a}$$

$$\xi_2 = \varepsilon_0(\varepsilon_{er2} - j\sigma_{e2}/\omega\varepsilon_0) \tag{1.2b}$$

$$\varepsilon_{ei} = \varepsilon_0\varepsilon_{eri} \quad , \quad i = 1, 2 \tag{1.2c}$$

The ε_{eri} and σ_{ei}, $i = 1, 2$, are the real effective relative dielectric constants and real effective conductivities for the respective media. For most of the work considered, medium 1 is air and therefore $\varepsilon_{er1} = 1$ and $\sigma_{e1} = 0$. Furthermore, for nonmagnetic material it may be assumed that $\mu_1 = \mu_2 = \mu_0$.

The validity of King's theory is based upon the following assumptions:

$$|k_1 a| < 1 \quad , \quad a << h \tag{1.3a}$$

$$|k_2| >> |k_1| \tag{1.3b}$$

$$|k_1 d| << 1 \tag{1.3c}$$

Condition (1.3a) is merely the thin-wire approximation necessary to insure that no transverse current modes exist on the wire. Condition (1.3b) places a restriction on the media for which the theory is valid. For cases in which medium 1 is air, (1.3b) can be restated as:

$$(\varepsilon_{er2}^2 + \sigma_{e2}^2/\omega^2\varepsilon_0^2)^{1/4} >> 1 \tag{1.4}$$

For low-loss materials with $\sigma_{e2} << \omega\varepsilon_{e2}$, (1.4) reduces to $\varepsilon_{er2}^{1/2} >> 1$. Under this restriction, materials such as water ($\varepsilon_{er} \sim 81$) and moist earth ($\varepsilon_{er} \geq 20$) would be well within the range of validity of the theory. For low-loss and slightly less polarizable materials, conditions can exist at sufficiently low frequencies such that $\omega\varepsilon_0 << \sigma_{e2}$, thus insuring that (1.4) is satisfied. Condition (1.3c) places limitations on the height of the wire. For the cases in which medium 1 is air, this condition reduces to:

$$\beta_0 d << 1 \quad \text{or} \quad d/\lambda_0 << \pi/2 \tag{1.5}$$

In the original theoretical development, condition (1.3c) was believed to be essential; it was later postulated, however, that as long as h/d remains sufficiently large, no restriction on d is required. Experimental verification of this recent postulate along with an expanded discussion on condition (1.3c) will be dealt with later in Section 1.8.

Assuming that the above conditions can be satisfied in some way, King has shown that the total axial current on the antenna can be expressed as:

$$I(x) = \frac{jV_0^e}{2Z_c} \frac{\sin k_L(h - |x|)}{\cos k_L h} \quad , \quad |x| \leq h \tag{1.6}$$

where an $e^{j\omega t}$ time dependence has been assumed and

$$k_L = \beta_L - j\alpha_L = k_1 \left(1 + [2/\ell n(2d/a)]\{1/(2k_2 d)^2 - K_1(2k_2 d)/2k_2 d - j\pi I_1(2k_2 d) + 4k_2 d + j[2k_2 d/3 + (2k_2 d)^3/45 + (2k_2 d)^5/1575 + \ldots]\}\right)^{1/2} \tag{1.7}$$

$$Z_c = R_c + jX_c = (k_L \zeta_1 / 2\pi k_1) \cosh^{-1}(d/a) \tag{1.8}$$

with

$$\zeta_1 = (\mu_0/\xi_1)^{1/2} \tag{1.9}$$

In (1.7) K_1 and I_1 are modified Bessel functions of order 1 with complex argument [18]. Expression (1.6) is identical to that of the current distribution on two open-ended sections of transmission line with characteristic impedance Z_c and complex wave number k_L in series with two generators each with driving voltage $V_0^e/2$ at $z = 0$. Figure 1.3 depicts an equivalent mathematical model for the physical situation shown in Fig. 1.2. The effect of the presence of medium 2 can be seen in the expression for k_L which is dependent on the height of the wire and the constitutive properties of the medium over which it is placed.

To complete the transmission-line analogy, expressions for the effective line constants per unit length may be obtained by using the following

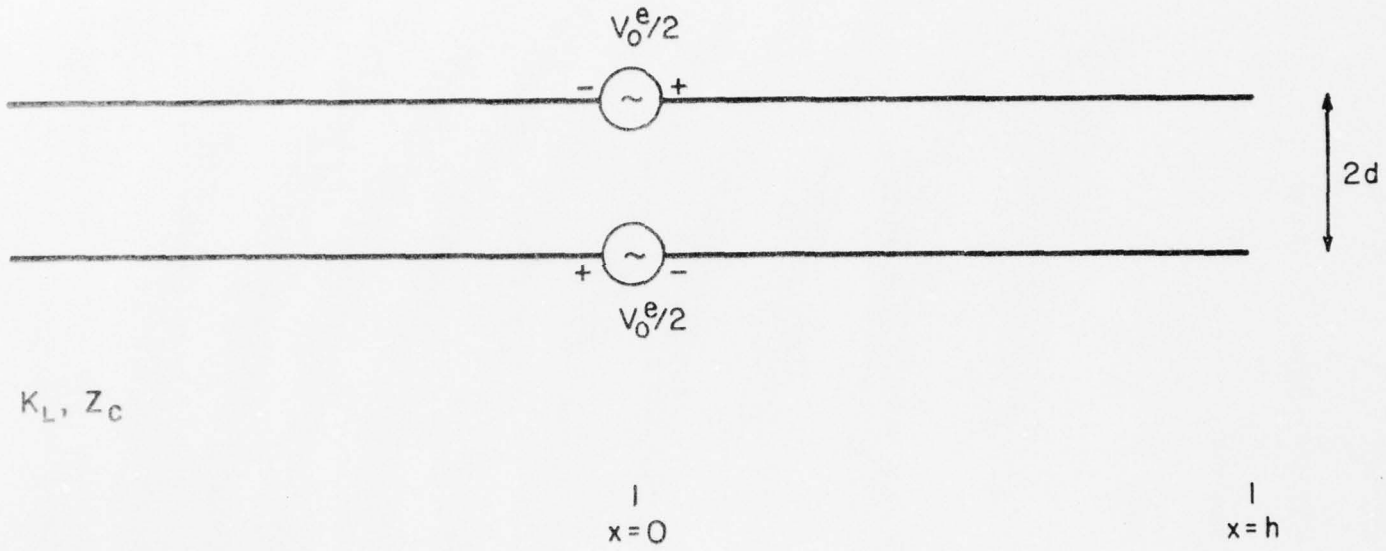


FIG. 1.3 MATHEMATICAL MODEL FOR HORIZONTAL WIRE OVER A DISSIPATIVE HALF-SPACE.

definitions: $k_L^2 = z_L y_L$ and $Z_c^2 = z_L/y_L$. Therefore,

$$y_L = g_L + jb_L = jk_L/Z_c = j2\pi\omega\varepsilon_{el}/\ell n(2d/a) \tag{1.10}$$

Setting $b_L \equiv \omega c_L$, it follows that

$$g_L = 2\pi\sigma_{el}/\ell n(2d/a) \tag{1.11a}$$

$$c_L = 2\pi\varepsilon_{el}/\ell n(2d/a) \tag{1.11b}$$

Likewise,

$$z_L = r_L + jx_L = jk_L Z_c = (jk_L^2\zeta_1/2\pi k_1)\ell n(2d/a) \tag{1.12}$$

With (1.7) and the fact that $k_1\zeta_1 = \omega\mu_0$,

$$z_L = z^e + z_2^i = j\omega\ell^e + z_2^i \tag{1.13}$$

with

$$\ell^e = (\mu_0/2\pi)\ell n(2d/a) \tag{1.14}$$

$$z_2^i = (j\omega\mu_0/\pi)\{1/(2k_2d)^2 - K_1(2k_2d)/2k_2d - j\pi I_1(2k_2d)/4k_2d + j[2k_2d/3 + (2k_2d)^3/45 + (2k_2d)^5/1575 + \ldots]\} \tag{1.15}$$

The driving-point admittance of the antenna can be shown to be:

$$Y_{in}(x) = I(0)/V_0^e = (j/2Z_c)\tan k_L x \tag{1.16}$$

where (1.16) is obtained from (1.6) by setting $z = 0$ to impose the driving-point condition.

The charge distribution per unit length can be obtained through the equation of continuity, viz.,

$$dI(x)/dx + j\omega q(x) = 0 \tag{1.17}$$

It is

$$q(x) = \frac{V_0^e k_L}{2Z_c \omega} \frac{\cos k_L(h - x)}{\cos k_L h} \quad , \quad x > 0 \tag{1.18}$$

Symmetry arguments are used to show that $q(x) = -q(-x)$ and, as a result, $q(x)$ is easily determined for $x < 0$. At $x = 0$ the charge is discontinuous due to the presence of the generator.

Thus, subject to conditions (1.3a,b,c), King has shown that a horizontal-wire antenna over a half-space can be modeled mathematically as a lossy, open-circuited transmission line with the values of k_L and Z_c determined by the height of the wire and by the properties of the medium over which it is placed. Note that the transmission-line analogy exists only in the mathematical sense in describing the form of the current distribution. Conventional transmission lines radiate little or no electromagnetic energy, yet this transmission-line-like antenna can be shown to produce significant far-field radiation (provided $p_{e2} = \sigma_{e2}/\omega\varepsilon_{e2}$ does not become infinitely large). This also follows from the fact that the only loss mechanism on the wire, accounted for by α_L, is radiation.

1.3. Beverage Wave Antenna

An important type of wire antenna which is placed horizontally above the earth is the Beverage wave antenna [19]. It was originally proposed in 1923 by H. H. Beverage as a receiving antenna for long-range, low-frequency (30 Kc) communication between the United States and Europe. As shown in Fig. 1.4, it consists of a straight wire, one or more wavelengths long, placed at electrically small heights ($.001\lambda_0$ - $.1\lambda_0$) above and parallel to the ground and resistively terminated at both ends to obtain a matched condition which will induce a traveling wave of current along the wire. In the traveling-wave mode, the Beverage antenna can be shown to possess good unidirectional radiation characteristics which prove to be quite useful in the LF to HF bands in which arrays become impractical.

A simple explanation of the Beverage antenna's unidirectional property can be seen in Fig. 1.5. Due to the fact that the medium over which the antenna is placed is not a perfect conductor, the incoming wave front is not perpendicular to the medium but has a forward tilt of 1° to 10° depending on

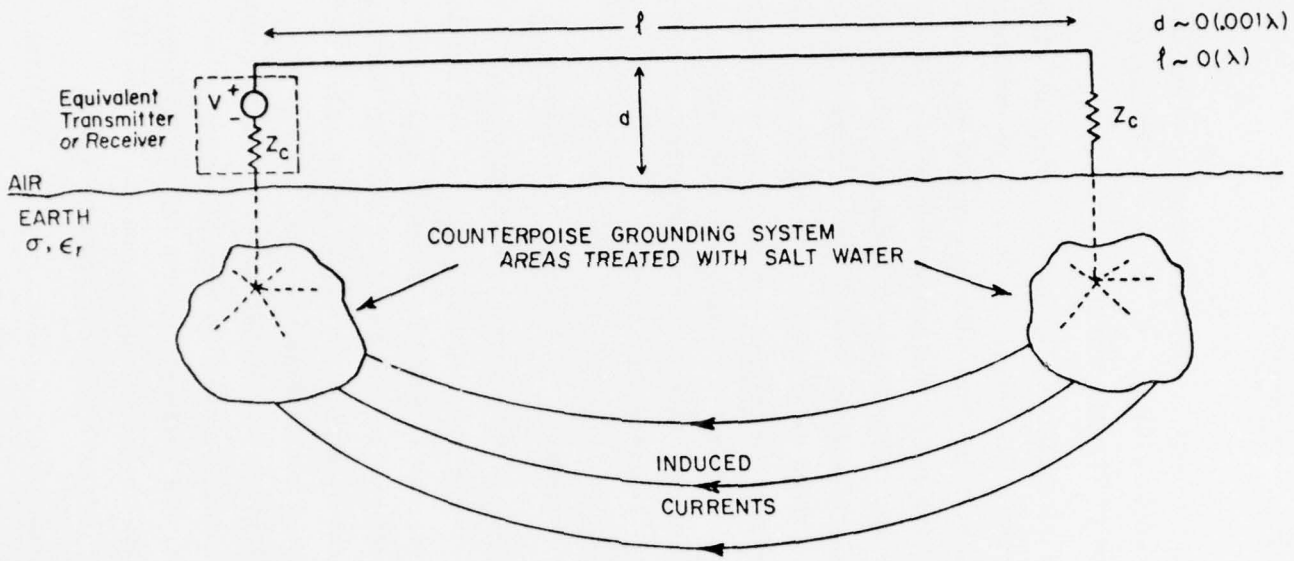


FIG. 1.4 CONVENTIONAL BEVERAGE WAVE ANTENNA WITH COUNTERPOISE GROUNDING SYSTEM.

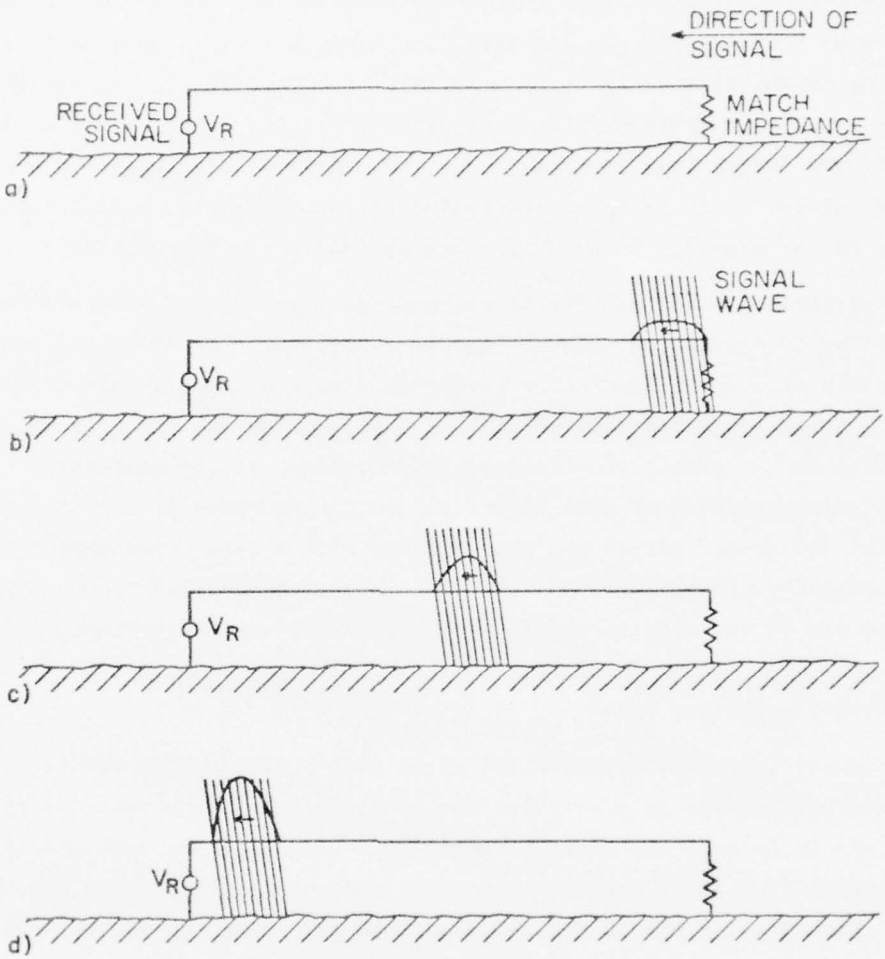


FIG. 1.5 BUILDING UP OF WAVE ON BEVERAGE ANTENNA AS INCIDENT WAVE PROGRESSES

the frequency and the characteristics of the medium. This tilt induces a wave on the wire which builds gradually in intensity as it travels along the wire, coupling energy from the wave front. By proper matching at the receiving end of the wire, this signal may be captured. Likewise, if the wave front were traveling in the opposite direction, a large signal would also build up on the wire along the direction of the wave front, but all this energy would ultimately be dissipated in the matched load. Thus, with no significant reflections from the load, the signal at the receiving end would be negligible. From reciprocity considerations, a similar unidirectional behavior can be expected when the antenna is used as a transmitting element.

For proper operation of this antenna the earth must be sufficiently conducting to provide an adequate ground connection. If this condition does not exist, it becomes impossible to obtain a good match. In his original work, Beverage incurred difficulties of this type due to the poor soil conductivity in the area. To alleviate this problem, it was necessary to bury a counterpoise system at each ground connection as shown in Fig. 1.4. By treating the ground around the counterpoise with a highly concentrated salt-water solution, Beverage found that this further alleviated the matching problem and he was able to obtain the desired antenna properties.

1.4. Over-The-Horizon Radar

Current interest in horizontal wires over a dissipative medium and in the Beverage antenna in particular has been generated by a consideration of their use in an over-the-horizon radar [20]. Due to their high operating frequencies (> 1 GHz), conventional radar systems are limited to line-of-sight operation. Proposed OTH radar systems are being considered with operating frequencies in the HF band (3 - 30 MHz). Specifically, the HF band can be shown to have important properties which can be exploited for wider radar coverage. As shown in Fig. 1.6(a), HF radiation has the ability to propagate beyond the line-of-sight either by ground waves diffracting around the curvature of the earth or by sky waves being reflected from the ionosphere. The main interest appears to be in sky-wave propagation since coverage from radar of this type can range from a minimum of 1000 to 4000 km or more. This method can extend the coverage of conventional ground-based radar by an order of magnitude. Higher susceptibility to noise and random scattering effects off the ionosphere are the chief drawbacks of this method.

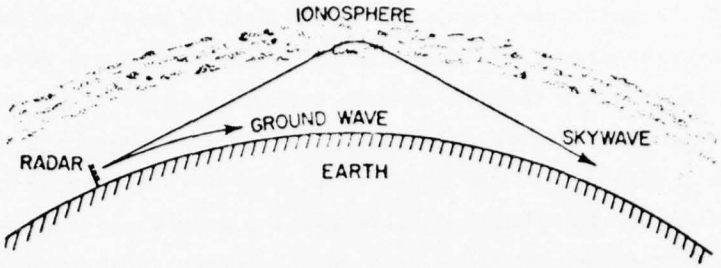


FIG. 1.6(a). GEOMETRY OF SKY-WAVE AND GROUND-WAVE PROPAGATION

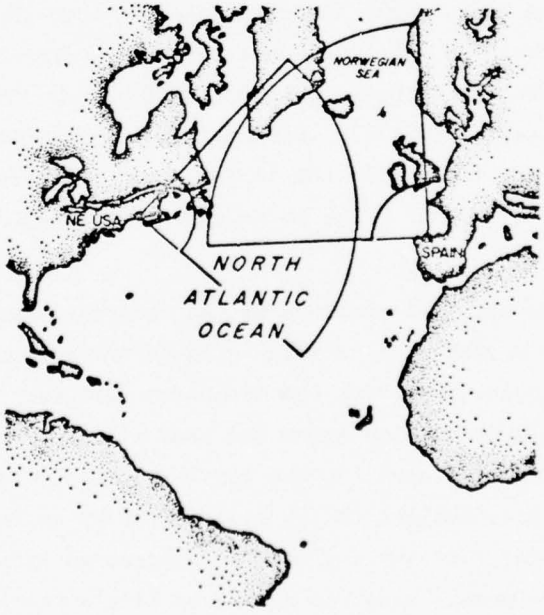


FIG. 1.6(b). POSSIBLE OVER-THE-HORIZON RADAR COVERAGE AREA

Ground-wave propagation at HF with its ability to diffract around the curvature of the earth can provide improved detection of aircraft flying at low angles of elevation. With a range of coverage that can extend from 200 to 400 km, its capabilities are clearly less than those of sky-wave radar. But ground-wave radar can be quite useful in providing partial coverage over the sky wave's skip zone. The chief advantage of this type of coverage is the elimination of atmospheric effects and the associated influences on diurnal and nocturnal propagation. The main drawback is obviously in the range of coverage which is somewhat limited due to the rapid attenuation of the ground wave. A typical area of coverage for an OTH radar system is shown in Fig. 1.6(b).

The Beverage antenna as well as arrays of Beverage antennas are presently being considered as the chief radiating elements in a proposed OTH radar system. The ability of the Beverage antenna to launch both unidirectional sky- and surface-wave patterns plus its simplicity of design make it a logical choice.

1.5. Modified Beverage Antenna

As was pointed out previously, both the efficiency and the gain of the Beverage antenna can be severely hampered unless proper ground conditions exist. In recent tests on the Beverage antenna for OTH-radar use, it has been shown that different methods of grounding can cause the antenna properties to differ substantially [21]. Compounding this problem is the fact that over poorly conducting soils the impedance of the ground return path (Fig. 1.7) can be sufficiently high so as to make a match difficult to obtain.

To overcome the apparent problems of the Beverage antenna it becomes necessary to devise a method of driving which avoids making any physical contact with the ground. Consider the situation depicted in Fig. 1.8(a) where the imperfectly conducting earth has been replaced by a perfect conductor. In analyzing this case for the dipole antenna, the effect of the perfect conductor is equivalent to its replacement by an image antenna. For $2\beta_0 d << 1$, Fig. 1.8(a) represents a double, open-ended transmission line with equivalent wave number equal to β_0. From King's theory it is apparent that the only difference introduced by the presence of an imperfect earth

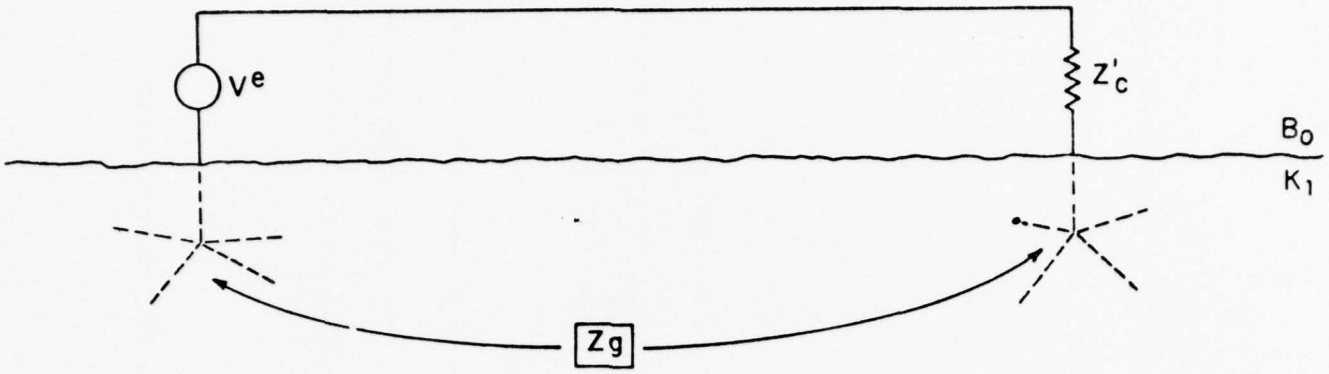


FIG. 1.7 DISTRIBUTED GROUND IMPEDANCE ASSOCIATED WITH CONVENTIONAL BEVERAGE ANTENNA

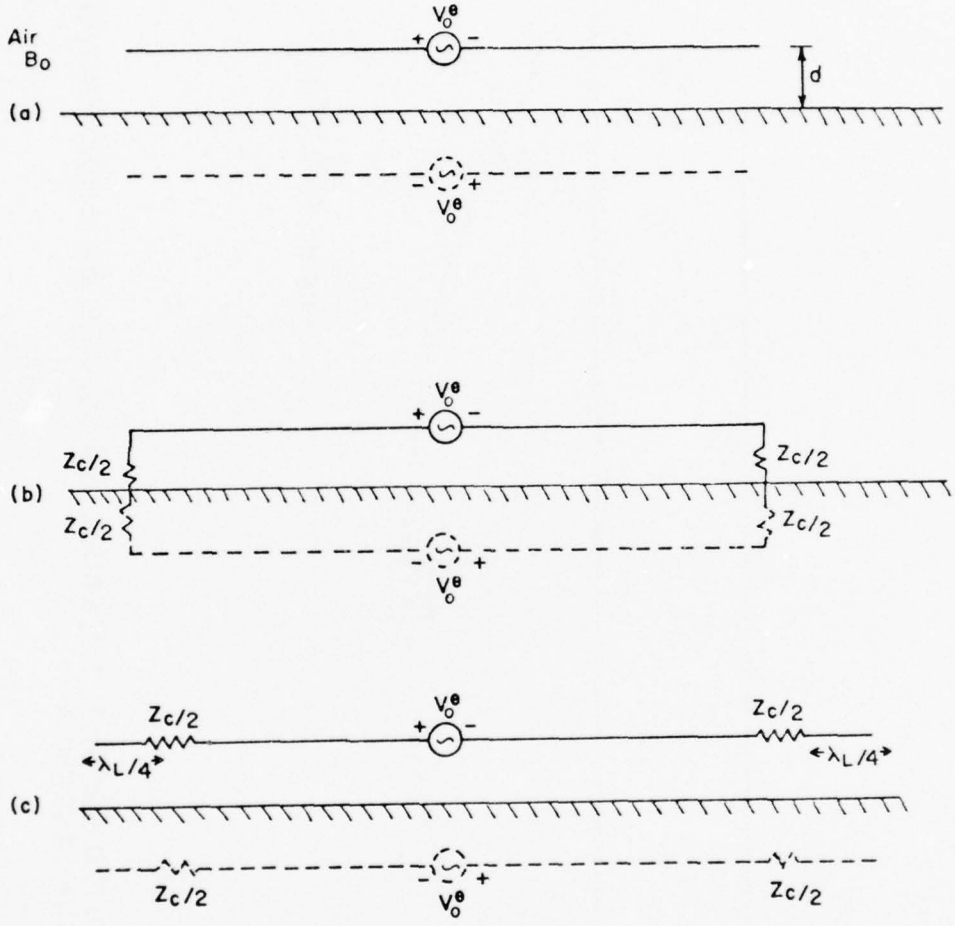


FIG. 1.8. WIRES OVER A PERFECT CONDUCTOR

is to modify the wave number by the complex factor given in (1.7). To obtain a matched condition on the transmission line in Fig. 1.8(a), it is necessary to place proper loads between the wire and the ground plane. As shown in Fig. 1.8(b), the presence of the perfect conductor necessitates loading the wire with only half the characteristic impedance since the equivalent of the other half is contained in the image. To avoid making any contact with the ground plane while still maintaining a match, the wire can be loaded at both ends with $Z_c/2$ and a section of wire equal in length to $\lambda_L/4$ (Fig. 1.8c). Figures 1.8(b) and 1.8(c) now have equivalent matched conditions up to the resistor, $Z_c/2$. In Fig. 1.8(c) an additional standing wave exists on the quarter-wave section. Matching in Fig. 1.8(c) is possible due to the fact that the quarter-wavelength section transforms back to the resistor as a high reactance or short circuit and represents a pseudo-ground connection at that point. As in Fig. 1.8(a), replacing the perfect conductor in Fig. 1.8(c) with an imperfect earth merely involves analyzing a loaded transmission line with modified wave number (1.7) and characteristic impedance (1.8). Thus, Fig. 1.8(c) represents a technique by which matching can be obtained without making any physical contact with the earth [15], [22].

The previous discussion assumes that the wire is close enough to the interface so that a transmission-line type current can be assumed. Presumably, as the height of the wire is increased, a gradual transition to an antenna-type current occurs. The point at which this transition occurs will be the subject of subsequent experimental investigation. The question that remains is: When the height is such that the transmission-line approximation is not entirely correct, can the matching technique of Fig. 1.8(c) still be employed? The answer to this is contained in the comprehensive work done by Altshuler [23]. This work emphasizes that, to at least a zero-order approximation, the antenna in free space is very similar to an open-ended transmission line since both require that the axial current vanish at the ends and both have standing-wave type current distributions. For the antenna, the latter similarity is true only in a very restrictive sense. By using this type of approximate similarity, it was shown that traveling-wave current distributions can also be obtained on an isolated antenna in free space by proper resistive loading backed with a quarter-wave resonant element.

The reason for this transmission-line-like similarity can be observed

when comparing the expression for the current on a double, open-ended, center-driven transmission line with wave number $k_L = \beta_0$ to that for the zero-order current on a center-driven dipole in free space. For the transmission line it can be shown that the current is given by (1.6) with $k_L = \beta_0$. Likewise, the zero-order current on the center-driven dipole is given by:

$$I_0(x) = \frac{j2\pi V_0^e \sin \beta_0(h - |x|)}{\zeta_0 \psi \cos \beta_0 h} \quad , \quad |x| \leq h \tag{1.19}$$

It is evident that the two expressions are identical when the following correspondence is made:

$$Z_c \iff \frac{\zeta_0 \psi}{4\pi} = 30\psi \tag{1.20}$$

where

$\zeta_0 = \zeta_1$ free-space wave impedance

$$\psi \approx \Omega - 2 \tag{1.21a}$$

$$\Omega \approx 2 \ln(2h/a) \tag{1.21b}$$

The quantity ψ is a commonly used expansion parameter in antenna theory [24] and is a somewhat arbitrarily defined quantity which relates the ratio of the vector potential at any cross section on the outside surface of the antenna to the total axial current in the conductor at that cross section. It can be shown that this ratio is reasonably constant over all parts of the antenna except near the ends where the current is small. Inspection of (1.21b) shows that ψ is not independent of the antenna length and, therefore, an exact TEM correspondence cannot be expected. What can be ascertained, however, is an order-of-magnitude value for the "pseudo-characteristic impedance" required to obtain a traveling-wave distribution on the antenna. Through experimental means Altshuler was able to obtain a more accurate value for this impedance.

Thus, in the limiting cases of both the transmission-line mode ($k_2 \to \infty$) and the free-space antenna ($k_2 \to 0$) a matched condition can be obtained by proper impedance loading, backed by a quarter-wave section of line. With

this understanding, a modified Beverage antenna, as shown in Fig. 1.8(c), for use over all ranges of k_2 was proposed to replace the conventional Beverage antenna. With the elimination of the original grounding-system problem and the ability to match over all ranges of k_2, this type of arrangement will be shown to facilitate antenna operations and, at the same time, to possess all the desired properties of the conventional Beverage antenna.

1.6. Loaded Horizontal Wires Above a Half-Space

The analysis of the modified Beverage antenna can be implemented by simply extending King's theory in Section 1.2 for the horizontal wire to cover the case of loaded wires as well. Since King's theory derives a lossy transmission-line form as the zero-order behavior of the unloaded wire, standard transmission-line techniques can be readily extended to the loaded wire. The important quantities necessary for the analysis are the line wave number k_L, (1.7), and the equivalent characteristic impedance Z_c, (1.8), both of which depend only on the height d of the wire and the properties of the medium over which it is placed.

For reasons that are discussed in the separate treatment of the field patterns [25], the loaded-dipole configuration with asymmetrical driving point, shown in Fig. 1.9, will be considered initially for the general case with any combination of lengths (ℓ_1, ℓ_2, ℓ_3, ℓ_4) and values of loads (Z_1, Z_2). Subsequent to this analysis, the special case of the modified Beverage antenna with $Z_1 = Z_2 = Z_c$ and $\ell_2 = \ell_4 = \lambda_L/4$ can be evaluated easily. The approach to the solution begins with the utilization of the compensation theorem whereby the antenna loads can be replaced with fictitious voltage generators, as seen in Fig. 1.10(a). With this simplification the solution for the antenna current involves the use of the analogy developed from King's theory which shows that the mathematical equivalent of Fig. 1.10a can be modeled as a transmission line driven by three generators, as depicted in Fig. 1.10(b). When dealing with linear systems, as in this case, the superposition principle applies and therefore the solution to Fig. 1.10(b) can be obtained by superimposing the individual solutions of Figs. 1.11(a)-(c). In each case only one set of generators is present while the other two pairs have been replaced by short circuits.

The current distribution on an arbitrarily loaded transmission line

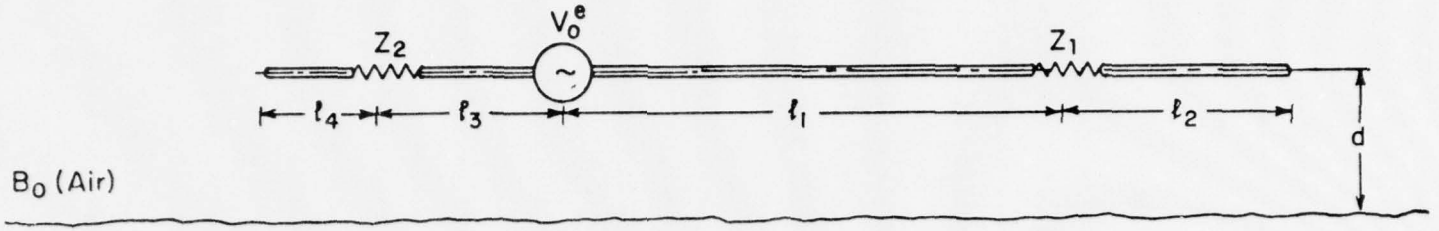


FIG. 1.9 ASYMMETRICALLY DRIVEN LOADED ANTENNA ABOVE DISSIPATIVE HALF-SPACE

$V_1 = I_T(\ell_1) Z_1$
$V_2 = I_T(-\ell_3) Z_2$
$S = \ell_1 + \ell_2$
$q = \ell_3 + \ell_4$

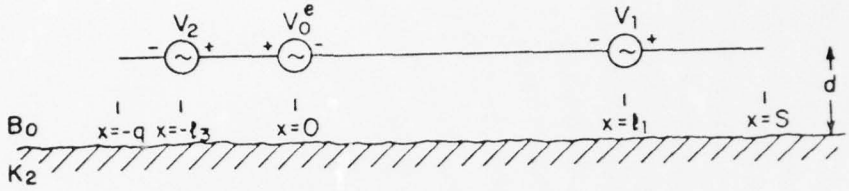


FIG. 1.10a REPLACEMENT OF IMPEDANCES WITH EQUIVALENT VOLTAGE SOURCES

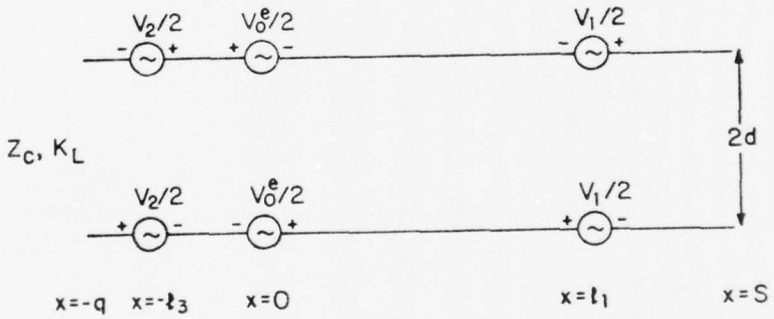
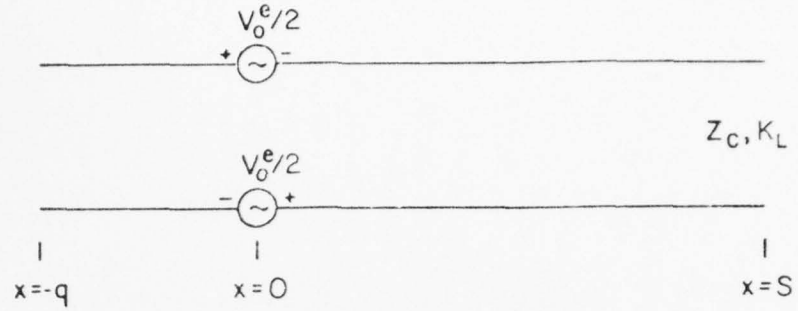
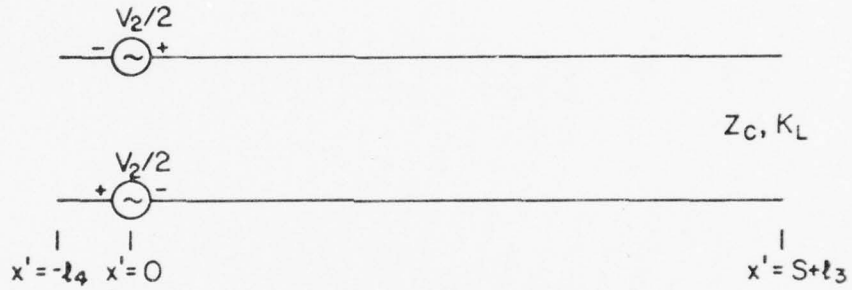


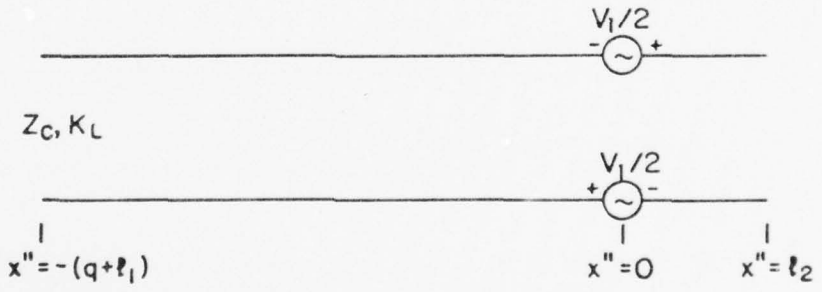
FIG. 1.10b TRANSMISSION LINE, MATHEMATICAL EQUIVALENT FOR LOADED ANTENNA ABOVE HALF-SPACE



a)



b)



c)

FIG. 1.11 INDIVIDUAL CASES a, b and c SUPERIMPOSED FOR TOTAL SOLUTION OF LOADED ANTENNA.

when driven by a pair of arbitrarily placed point generators, as illustrated in Fig. 1.12, can be expressed as [26]

$$I(x) = \frac{V_0^e}{Z_c} \frac{\sinh \theta_{0q'} \sinh(\gamma_L w + \theta_s)}{\sinh(\gamma_L s + \theta_s + \theta_{0q'})} \quad , \qquad 0 \leq x \leq s \tag{1.22}$$

where

$$\gamma_L = jk_L \quad ; \quad w = s - x \tag{1.23}$$

In (1.22) $\theta_{0q'}$ is the complex terminal function of impedance $Z_{0q'}$ looking to the left from the generator and θ_s is the complex terminal function of the load Z_s. The following expressions apply:

$$Z_{0q'} = Z_c \coth(\gamma_L q + \theta_q) \tag{1.24}$$

and

$$\theta_{0q'} = \coth^{-1}(Z_{0q'}/Z_c) = \gamma_L q + \theta_q \tag{1.25}$$

where θ_q is the complex terminal function at the load Z_q and is expressed as:

$$\theta_q = \coth^{-1}(Z_q/Z_c) \tag{1.26a}$$

Similarly,

$$\theta_s = \coth^{-1}(Z_s/Z_c) \tag{1.26b}$$

With the above substitutions (1.22) may be rewritten as:

$$I(x) = \frac{V_0^e}{Z_c} \frac{\sinh(\gamma_L q + \theta_q)\sinh(\gamma_L w + \theta_s)}{\sinh(\gamma_L s + \gamma_L q + \theta_s + \theta_q)} \quad , \qquad 0 \leq x \leq s \tag{1.27}$$

In an analogous manner the current on the section of transmission line $-q \leq x \leq 0$ may be expressed as:

$$I'(x) = \frac{V_0^e}{Z_c} \frac{\sinh(\gamma_L s + \theta_s)\sinh(\gamma_L y + \theta_q)}{\sinh(\gamma_L s + \gamma_L q + \theta_s + \theta_q)} \quad , \qquad -q \leq x \leq 0 \tag{1.28}$$

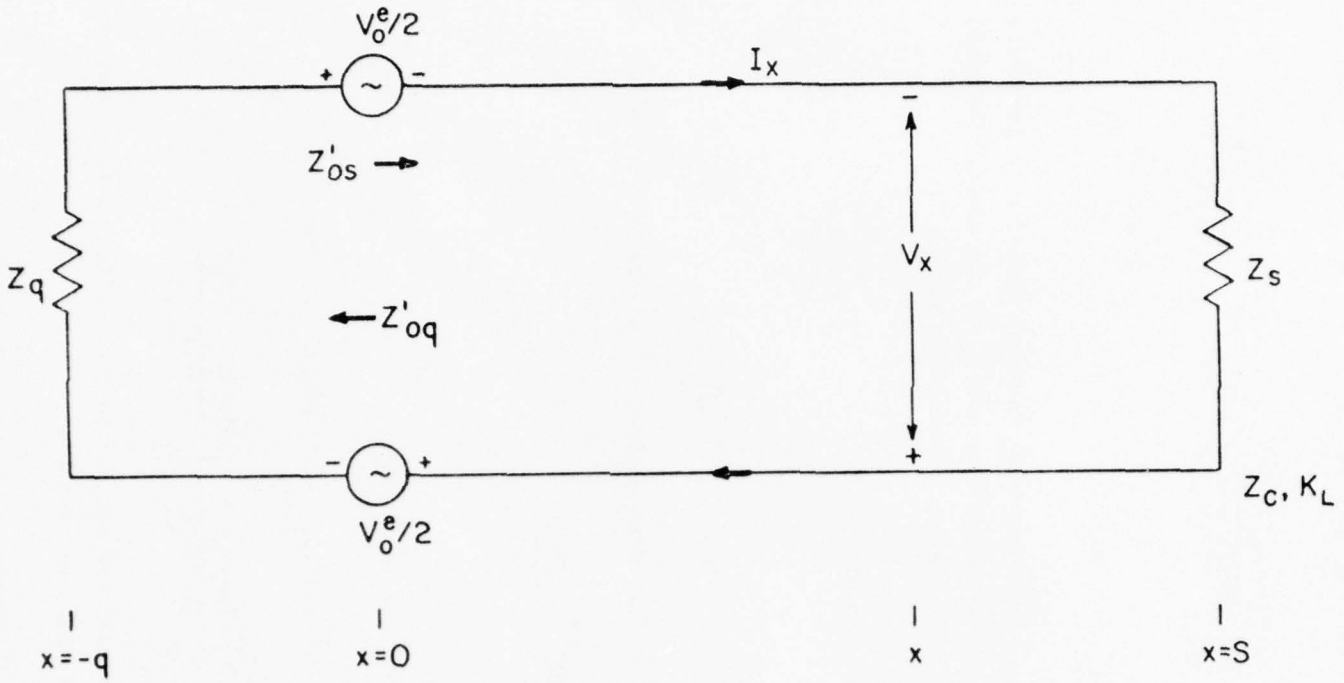


FIG. 1.12 TRANSMISSION LINE DRIVEN BY POINT GENERATORS AT ARBITRARY DISTANCE FROM LOADED ENDS.

where

$$y = q + x$$

For the cases in which the terminal impedances can be modeled as ideal open circuits, it is apparent that $Z_s = Z_q = \infty$ and $\theta_{\text{open-ckt}} = 0$.

By utilizing the above formulas the three cases in Fig. 1.11 can be analyzed conveniently. For Fig. 1.11(a) the current expressions are:

$$I_1(x) = \frac{V_0^e}{Z_c} \frac{\sinh(\gamma_L q)\sinh[\gamma_L(s - x)]}{\sinh(\gamma_L q + \gamma_L s)} \quad , \qquad 0 \leq x \leq s \tag{1.29}$$

and

$$I_1'(x) = \frac{V_0^e}{Z_c} \frac{\sinh(\gamma_L s)\sinh[\gamma_L(q + x)]}{\sinh(\gamma_L q + \gamma_L s)} \quad , \qquad -q \leq x \leq 0 \tag{1.30}$$

where

$$s = \ell_1 + \ell_2 \quad , \quad q = \ell_3 + \ell_4$$

For Fig. 1.11(b) it is necessary first to write the current expressions with respect to the origin of the fictitious generators at $x' = 0$ and then to shift to the origin of the externally applied source at $x = 0$. The procedure is as follows:

$$I_2(x') = \frac{V_2}{Z_c} \frac{\sinh(\gamma_L \ell_4)\sinh\{\gamma_L[(s + \ell_3) - x']\}}{\sinh[\gamma_L \ell_4 + \gamma_L(s + \ell_3)]} \quad , \quad 0 \leq x' \leq s + \ell_3 \tag{1.31}$$

$$I_2'(x') = \frac{V_2}{Z_c} \frac{\sinh[\gamma_L(s + \ell_3)]\sinh[\gamma_L(\ell_4 + x')]}{\sinh[\gamma_L \ell_4 + \gamma_L(s + \ell_3)]} \quad , \quad -\ell_4 \leq x' \leq 0 \tag{1.32}$$

Shifting to the point $x = 0$ involves the substitution of $x' = x + \ell_3$ in (1.31) and (1.32). Performing this substitution gives:

$$I_2(x) = \frac{V_2}{Z_c} \frac{\sinh(\gamma_L \ell_4)\sinh[\gamma_L(s - x)]}{\sinh[\gamma_L \ell_4 + \gamma_L(s + \ell_3)]} \quad , \qquad -\ell_3 \leq x \leq s \tag{1.33}$$

and

$$I_2'(x) = \frac{V_2}{Z_c} \frac{\sinh[\gamma_L(s + \ell_3)]\sinh[\gamma_L(q + x)]}{\sinh[\gamma_L \ell_4 + \gamma_L(s + \ell_3)]} \quad , \quad -q \leq x \leq -\ell_3 \qquad (1.34)$$

Following a similar procedure for the case in Fig. 1.11(c) with the subsequent shift in origin gives:

$$I_3(x) = \frac{V_1}{Z_c} \frac{\sinh[\gamma_L(q + \ell_1)]\sinh[\gamma_L(s - x)]}{\sinh[\gamma_L(s + q)]} \quad , \quad \ell_1 \leq x \leq s \qquad (1.35)$$

and

$$I_3'(x) = \frac{V_1}{Z_c} \frac{\sinh(\gamma_L \ell_2)\sinh[\gamma_L(q + x)]}{\sinh[\gamma_L(s + q)]} \quad , \quad -q \leq x \leq \ell_1 \qquad (1.36)$$

If the principle of superposition is used, the total current that exists on the transmission line can be shown to be:

$$I_T = I_1 - I_2 - I_3 \quad \text{and} \quad I_T' = I_1' - I_2' - I_3' \qquad (1.37)$$

With (1.37) and (1.23) the total current is

$$I_T(x) = (V_0^e \sin k_L q - V_2 \sin k_L \ell_4)\left[\frac{j \sin k_L(s - x)}{Z_c \sin k_L(s + q)}\right]$$

$$- j \frac{V_1}{Z_c} \frac{\sin k_L \ell_2 \sin k_L(q + x)}{\sin k_L(s + q)} \quad , \quad 0 \leq x \leq \ell_1 \qquad (1.38a)$$

$$I_T(x) = (V_0^e \sin k_L q - V_2 \sin k_L \ell_4)\left[\frac{j \sin k_L(s - x)}{Z_c \sin k_L(s + q)}\right]$$

$$- j \frac{V_1}{Z_c} \frac{\sin k_L(q + \ell_1)\sin k_L(s - x)}{\sin k_L(s + q)} \quad , \quad \ell_1 \leq x \leq s \qquad (1.38b)$$

$$I_T'(x) = (V_0^e \sin k_L s - V_1 \sin k_L \ell_2)\left[\frac{j \sin k_L(q + x)}{Z_c \sin k_L(s + q)}\right]$$

$$- j \frac{V_2}{Z_c} \frac{\sin k_L \ell_4 \sin k_L(s - x)}{\sin k_L(s + q)} \quad , \quad -\ell_3 \leq x \leq 0 \qquad (1.38c)$$

$$I_T'(x) = (V_0^e \sin k_L s - V_1 \sin k_L \ell_2)\left[\frac{j \sin k_L(q + x)}{Z_c \sin k_L(s + q)}\right]$$

$$- j\frac{V_2}{Z_c}\frac{\sin k_L(s + \ell_3)\sin k_L(q + x)}{\sin k_L(s + q)} \quad , \quad -q \leq x \leq -\ell_3 \qquad (1.38d)$$

It is now necessary to solve for the fictitious voltage generators, V_1 and V_2, in terms of the externally applied voltage V_0^e. This is accomplished by solving for $I_T(\ell_1)$ and $I_T'(-\ell_3)$ while noting that $V_1 = I_T(\ell_1)Z_1$ and $V_2 = I_T'(-\ell_3)Z_2$. From (1.38a-d) it follows that:

$$I_T(\ell_1) = [V_0^e \sin k_L q - V_2 \sin k_L \ell_4 - V_1 \sin k_L(q + \ell_1)]$$

$$\times\left[\frac{j \sin k_L \ell_2}{Z_c \sin k_L(s + q)}\right] \qquad (1.39)$$

$$I_T'(-\ell_3) = [V_0^e \sin k_L s - V_1 \sin k_L \ell_2 - V_2 \sin k_L(s + \ell_3)]$$

$$\times\left[\frac{j \sin k_L \ell_2}{Z_c \sin k_L(s + q)}\right] \qquad (1.40)$$

By substituting expressions for $I_T(\ell_1)$ and $I_T'(-\ell_3)$ in terms of V_1 and V_2, respectively, into (1.39) and (1.40) it can be shown that these reduce to:

$$V_1[Z_c \sin k_L(s + q) + jZ_1 \sin k_L \ell_2 \sin k_L(\ell_1 + q)]$$

$$= jZ_1 \sin k_L \ell_2 (V_0^e \sin k_L q - V_2 \sin k_L \ell_4) \qquad (1.41)$$

$$V_2[Z_c \sin k_L(s + q) + jZ_2 \sin k_L \ell_4 \sin k_L(s + \ell_3)]$$

$$= jZ_2 \sin k_L \ell_4 (V_0^e \sin k_L s - V_1 \sin k_L \ell_2) \qquad (1.42)$$

These equations can be placed in the following form:

$$AV_1 + A''V_2 = A' \qquad (1.43a)$$

$$B''V_1 + BV_2 = B' \qquad (1.43b)$$

where

$$A = Z_c \sin k_L(s + q) + jZ_1 \sin k_L\ell_2 \sin k_L(q + \ell_1) \tag{1.44a}$$

$$A'' = jZ_1 \sin k_L\ell_2 \sin k_L\ell_4 \tag{1.44b}$$

$$A' = jZ_1V_0^e \sin k_L\ell_2 \sin k_Lq \tag{1.44c}$$

$$B = Z_c \sin k_L(s + q) + jZ_2 \sin k_L\ell_4 \sin k_L(s + \ell_3) \tag{1.44d}$$

$$B'' = jZ_2 \sin k_L\ell_4 \sin k_L\ell_2 \tag{1.44e}$$

$$B' = jZ_2V_0^e \sin k_L\ell_4 \sin k_Ls \tag{1.44f}$$

By using Cramer's rule, expressions for V_1 and V_2 can be obtained as follows:

$$V_1 = \frac{\begin{vmatrix} A' & A'' \\ B' & B \end{vmatrix}}{\begin{vmatrix} A & A'' \\ B'' & B \end{vmatrix}} = \frac{A'B - B'A''}{AB - B''A''} \tag{1.45}$$

$$V_2 = \frac{\begin{vmatrix} A & A' \\ B'' & B' \end{vmatrix}}{\begin{vmatrix} A & A'' \\ B'' & B \end{vmatrix}} = \frac{AB' - B''A}{AB - A''B''} \tag{1.46}$$

After performing the indicated operations, the final expressions for V_1 and V_2 are:

$$V_1 = \{jZ_1V_0^e \sin k_L\ell_2[Z_c \sin k_Lq \sin k_L(s + q) + jZ_2 \sin k_Lq \sin k_L\ell_4 \times \sin k_L(s + \ell_3) - jZ_2 \sin k_Ls \sin^2 k_L\ell_4]\}/D \tag{1.47}$$

$$V_2 = \{jZ_2V_0^e \sin k_L\ell_4[Z_c \sin k_Ls \sin k_L(s+q) + jZ_1 \sin k_Ls \sin k_L\ell_2 \times \sin k_L(q+\ell_1) - jZ_1 \sin k_Lq \sin^2 k_L\ell_2]\}/D \quad (1.48)$$

where

$$D = Z_c^2 \sin^2 k_L(s+q) + jZ_2Z_c \sin k_L(s+q) \sin k_L\ell_4 \sin k_L(s+\ell_3) + jZ_1Z_c \sin k_L(s+q) \sin k_L\ell_2 \sin k_L(q+\ell_1) - Z_1Z_2 \sin k_L\ell_2 \times \sin k_L\ell_4 \sin k_L(s+\ell_3)\sin k_L(q+\ell_1) + Z_1Z_2 \sin^2 k_L\ell_2 \sin^2 k_L\ell_4 \quad (1.49)$$

Therefore, the current distribution on the asymmetrically driven, doubly loaded wire antenna above a dissipative half-space (Fig. 1.9) is given by (1.38a-d) with the appropriate substitutions (1.7), (1.8), (1.47), (1.48) and (1.49). Since the mathematical model in Fig. 1.10(b) involves a two-wire line, in order to obtain the exact current and input impedance expressions for Fig. 1.9 where only a single conductor is present, the following identity applies:

$$|I|_{ant} = 2|I|_{transmission\ line} \quad (1.50)$$

This is equivalent to having point generators of V_0^e rather than $V_0^e/2$ in the above analysis. This additional factor of 2 must be accounted for in (1.38a-d) to obtain the correct current expression for Fig. 1.9. The complete current can be written as:

$$I(x) = \begin{cases} A \sin k_L(s-x) + B \sin k_L(q+x), & 0 \le x \le \ell_1 \quad (1.51a) \\ A \sin k_L(s-x) + C \sin k_L(s-x), & \ell_1 \le x \le s \quad (1.51b) \\ D \sin k_L(q+x) + E \sin k_L(s-x), & -\ell_3 \le x \le 0 \quad (1.51c) \\ D \sin k_L(q+x) + F \sin k_L(q+x), & -q \le x \le -\ell_3 \quad (1.51d) \end{cases}$$

where

$$A = \frac{2j(V_0^e \sin k_L q - V_2 \sin k_L \ell_4)}{Z_c \sin k_L(s+q)} \tag{1.52a}$$

$$B = \frac{-2jV_1 \sin k_L \ell_2}{Z_c \sin k_L(s+q)} \tag{1.52b}$$

$$C = \frac{-2jV_1 \sin k_L(q+\ell_1)}{Z_c \sin k_L(s+q)} \tag{1.52c}$$

$$D = \frac{2j(V_0^e \sin k_L s - V_1 \sin k_L \ell_2)}{Z_c \sin k_L(s+q)} \tag{1.52d}$$

$$E = \frac{-2jV_2 \sin k_L \ell_4}{Z_c \sin k_L(s+q)} \tag{1.52e}$$

$$F = \frac{-2jV_2 \sin k_L(s+\ell_3)}{Z_c \sin k_L(s+q)} \tag{1.52f}$$

and V_1 and V_2 are given by (1.47) and (1.48) with (1.49).

1.7. Special Cases

Several special cases of the preceding problem, which will prove to be of considerable interest, are considered in this section.

Case I: Symmetric Drive Point and Loading

When the antenna in Fig. 1.9 is center-driven and $\ell_1 = \ell_3$, $\ell_2 = \ell_4$, and $Z_1 = Z_2$, the current expressions become considerably more simple than those in (1.51). First of all, $I(x) = I(-x)$ for any point x along the wire due to symmetry. Symmetry considerations also lead to the conclusion that $V_1 = V_2$ so that (1.41) and (1.42) can be equated to give the following identity:

$$V_1 = V_2 = \frac{jZ_1 V_0^e \sin k_L \ell_2}{2(Z_c \cos k_L s + jZ_1 \cos k_L \ell_1 \sin k_L \ell_2)} \tag{1.53}$$

With this value for V_1 substituted into (1.38a-d), the current that exists on the symmetrically loaded dipole antenna can be shown to be:

$$I_T(x) = \frac{jV_0^e \sin k_L(s - |x|)}{Z_c \cos k_L s}$$

$$+ \frac{Z_1 V_0^e \sin^2 k_L \ell_2 \cos k_L x}{Z_c \cos k_L s(Z_c \cos k_L s + jZ_1 \sin k_L \ell_2 \cos k_L \ell_1)} \quad ,$$

$$0 \leq |x| \leq \ell_1 \qquad (1.54a)$$

$$I_T(x) = \frac{jV_0^e \sin k_L(s - |x|)}{Z_c \cos k_L s}$$

$$+ \frac{V_0^e Z_1 \sin k_L \ell_2 [\sin k_L \ell_2 + \sin k_L(s + \ell_1)] \sin k_L(s - |x|)}{2Z_c \sin k_L s \cos k_L s(Z_c \cos k_L s + jZ_1 \sin k_L \ell_2 \cos k_L \ell_1)} \quad ,$$

$$\ell_1 \leq |x| \leq s \qquad (1.54b)$$

The input admittance of this antenna is given as:

$$Y_{in} = \frac{I_T(0)}{V_0^e} = -\frac{j \tan k_L s}{Z_c}$$

$$+ \frac{Z_1 \sin^2 k_L \ell_2}{Z_c \cos k_L s(Z_c \cos k_L s + jZ_1 \sin k_L \ell_2 \cos k_L \ell_1)} \qquad (1.55)$$

If the continuity equation given in (1.17) is utilized, the charge distribution is:

$$Q_T(x) = \frac{V_0^e k_L \cos k_L(s - x)}{Z_c \omega \cos k_L s}$$

$$- \frac{jk_L Z_1 V_0^e \sin^2 k_L \ell_2 \sin k_L x}{\omega Z_c \cos k_L s(Z_c \cos k_L s + jZ_1 \sin k_L \ell_2 \cos k_L \ell_1)} \quad ,$$

$$0 \leq x \leq \ell_1 \qquad (1.56a)$$

and

$$Q_T(x) = \frac{V_0^e k_L \cos k_L(s - x)}{Z_c \omega \cos k_L s}$$

$$- \frac{jV_0^e Z_1 k_L \sin k_L \ell_2 [\sin k_L \ell_2 + \sin k_L(s + \ell_1)] \cos k_L(s - x)}{\omega Z_c \sin k_L s \cos k_L s (Z_c \cos k_L s + jZ_1 \sin k_L \ell_2 \cos k_L \ell_1)} \quad ,$$

$$\ell_1 \leq x \leq s \qquad (1.56b)$$

where the odd-symmetry relation for charge, $Q_T(x) = -Q_T(-x)$, can be used for the other half of the dipole. In all three sets of equations, (1.54), (1.55) and (1.56), the right-hand term represents an added factor to the unloaded antenna term due to the presence of Z_1 in the wire.

Case II: Symmetrically Driven Modified Beverage Antenna

The center-driven modified Beverage antenna can be analyzed from Case I when the following restrictions are imposed:

$$Z_1 = Z_c \quad ; \quad \ell_2 = \lambda_L/4$$

Using the fact that

$$\sin k_L \ell_2 = \sin(\beta_L - j\alpha_L)\ell_2 = \sin \beta_L \ell_2 \cosh \beta_L \ell_2 - j \cos \beta_L \ell_2 \sinh \beta_L \ell_2$$

$$\cos k_L \ell_2 = \cos(\beta_L - j\alpha_L)\ell_2 = \cos \beta_L \ell_2 \cosh \beta_L \ell_2 + j \sin \beta_L \ell_2 \sinh \beta_L \ell_2$$

and the above restriction on ℓ_2, one obtains

$$\sin k_L \ell_2 = \cosh \alpha_L \ell_2 \qquad (1.57)$$

$$\cos k_L \ell_2 = j \sinh \alpha_L \ell_2 \qquad (1.58)$$

Substituting (1.57) and (1.58) into the first part of (1.54) results in:

$$I_T(x) = \frac{V_0^e}{Z_c \cos k_L s} \left[j \sin k_L(s - |x|) + \frac{\cosh^2 \alpha_L \ell_2 \cos k_L x}{(\cos k_L s + j \cosh \alpha_L \ell_2 \cos k_L \ell_1)} \right]$$

$$0 \leq |x| \leq \ell_1 \qquad (1.59)$$

By using the following identities along with (1.59),

$$\sin k_L(s - x) = \sin k_L s \cos k_L x - \cos k_L s \sin k_L x$$

$$\cos k_L \ell_1 = \cos k_L(s - \ell_2) = j \sinh \alpha_L \ell_2 \cos k_L s + \cosh \alpha_L \ell_2 \sin k_L s$$

the current distribution for the modified Beverage antenna can be expressed as:

$$I_{BEV}(x) = \frac{V_0^e}{Z_c \cos k_L s} \{-j \cos k_L s \sin k_L |x| + \cos k_L x \left[j \sin k_L x + \frac{\cosh^2 \alpha_L \ell_2}{\cos k_L s(1 - \sinh \alpha_L \ell_2 \cosh \alpha_L \ell_2) + j \cosh^2 \alpha_L \ell_2 \sin k_L s} \right] \} ,$$

$$0 \leq |x| \leq \ell_1 \qquad (1.60)$$

A similar procedure for the current expression on the quarter-wave section leads to:

$$I_{BEV}(x) = \frac{V_0^e \sin k_L(s - |x|)}{Z_c \cos k_L s} \times \left[j + \frac{2 \cosh^2 \alpha_L \ell_2 \sin^2 k_L s + (j/2) \sin^2 k_L s \sinh^2 \alpha_L \ell_2}{\sin^2 k_L s + j2 \cosh^2 \alpha_L \ell_2 \sin^2 k_L s - (1/2) \sinh^2 \alpha_L \ell_2 \sin^2 k_L s} \right]$$

$$\ell_1 \leq |x| \leq s \qquad (1.61)$$

The input admittance for the antenna is:

$$Y_{BEV} = \frac{I_{BEV}(0)}{V_0^e} = \frac{1}{Z_c \cos k_L s} \left\{ j \sin k_L s + \frac{\cosh^2 \alpha_L \ell_2}{\cos k_L s[1 - (1/2) \sinh^2 \alpha_L \ell_2] + j \cosh^2 \alpha_L \ell_2 \sin k_L s} \right\} \qquad (1.62)$$

As before, the distribution of charge can be easily obtained from the continuity equation and (1.60) and (1.61).

As a check on (1.60), the limiting case in which $\alpha_L = 0$ and $\beta_L = \beta_0$ may be investigated. If these restrictions are imposed on (1.60), the modified Beverage antenna current reduces to:

$$I_{BEV}(x) = \frac{V_0^e}{Z_c} e^{j\beta_0|x|} \quad ; \quad \alpha_L = 0 \quad , \quad \beta_L = \beta_0 \quad , \quad 0 \leq |x| \leq \ell_1 \tag{1.63}$$

This is the current that would exist on a lossless transmission line of infinite length or one that is perfectly matched. As a limiting case, this would be the anticipated result if (1.60) truly represented the current on a matched transmission line with arbitrary complex wave number k_L. Interestingly enough, due to the matching technique for the modified Beverage arrangement, the current distribution is not of the form $\exp(jk_L|x|)$. This is the form usually assumed to exist on the conventional Beverage antenna.

Case III: Asymmetrically Driven Modified Beverage Antenna

For reasons that become apparent when dealing with the field patterns [25], the asymmetrically driven Beverage antenna is of great practical importance. Specifically for the case in which $\ell_1 >> \ell_3$ or in the limit $\ell_3 = 0$, it will be shown to possess a unidirectional surface-wave radiation pattern identical to the conventional Beverage antenna, thereby proving to be of fundamental importance in over-the-horizon (OTH) radar usage. Because of the asymmetry of the problem, a simple reduction for the current as in Cases I and II does not occur. Despite this, (1.51) can be simplified for the asymmetric case with $\ell_3 = 0$, $\ell_2 = \ell_4 = \lambda_L/4$, and $Z_1 = Z_2 = Z_c$. With these restrictions the current on the wire can be written as:

$$I(x) = \begin{cases} A \sin k_L(s - x) + B \sin k_L(x + \ell_2) \quad , & 0 \leq x \leq \ell_1 \quad (1.64a) \\ A \sin k_L(s - x) + C \sin k_L(s - x) \quad , & \ell_1 \leq x \leq s \quad (1.64b) \\ D \sin k_L(x + \ell_2) + F \sin k_L(x + \ell_2) \quad , & -\ell_2 \leq x \leq 0 \quad (1.64c) \end{cases}$$

where

$$A = \frac{2j \sin k_L \ell_2}{Z_c \sin k_L(s + \ell_2)} (V_0^e - V_2) \tag{1.65a}$$

$$B = \frac{-2jV_1 \sin k_L \ell_2}{Z_c \sin k_L(s + \ell_2)} \tag{1.65b}$$

$$C = \frac{-2jV_1 \sin k_L s}{Z_c \sin k_L(s + \ell_2)} \tag{1.65c}$$

$$D = \frac{2j(V_0^e \sin k_L s - V_1 \sin k_L \ell_2)}{Z_c \sin k_L(s + \ell_2)} \tag{1.65d}$$

$$F = \frac{-2jV_2 \sin k_L s}{Z_c \sin k_L(s + \ell_2)} \tag{1.65e}$$

and

$$V_1 = jZ_c^2 V_0^e \sin^2 k_L \ell_2 \sin k_L(s + \ell_2)/D \tag{1.66a}$$

$$V_2 = jZ_c^2 V_0^e \sin k_L \ell_2 [\sin k_L s \sin k_L(s + \ell_2) + j \sin^2 k_L s \sin k_L \ell_2 - j \sin^3 k_L \ell_2]/D \tag{1.66b}$$

with

$$D = Z_c^2[\sin^2 k_L(s + \ell_2) - \sin^2 k_L \ell_2 \sin^2 k_L s + \sin^4 k_L \ell_2 + 2j \sin k_L(s + \ell_2) \sin k_L s \sin k_L \ell_2] \tag{1.66c}$$

The input impedance and charge distribution can be obtained from the straightforward methods previously used.

1.8. Theoretical Refinements and End-Effect Considerations

The theoretical developments presented to this point assume implicitly that the ends of the antenna can be treated as perfect open circuits. Discrepancies between the measured results contained in Volume II of this report and the theoretical predictions indicate that an end-effect correction may have to be incorporated into King's theory and the related theory for the modified Beverage antenna in order to obtain better agreement. It was assumed initially that the discrepancies which occurred between the measured

wave numbers and those predicted by (1.7) were primarily due to a violation of condition (1.3c). This condition was believed to be essential since it was felt that only at electrically close spacings would the dominant behavior of the current be similar to a transmission-line form. It was assumed that as d/λ_0 became large the influence of the interface would diminish and the form of the current would become more like an antenna in free space. This is, of course, true to a large extent, but what was not understood clearly was how and at what range of d/λ_0 the effect of the interface would become negligible. In light of this situation, it was decided initially to use the measured wave numbers in the zeroth-order expressions for the current, charge and impedance in those cases for which (1.7) appears not to hold. This semi-empirical approach produced good results for the current and charge distributions but was less than satisfactory for the input admittance.

Subsequently, a closer examination of the problem by Professor T. T. Wu revealed that condition (1.3c) was never needed in the theoretical developments in Section 1.2. Due to the fact that, when d/λ_0 approaches infinity, the transmission-line form of the current must eventually be transferred into a form more representative of an antenna in free space, a condition on the spacing d must exist. Professor Wu postulated that this condition would not only involve d but also the antenna half-length h. The condition postulated by Wu states that as long as h/d remains large the transmission-line form for the current will be valid and (1.7) will give the correct wave number. When d becomes large, it is necessary for h to become increasingly larger in order for this condition to hold. Obviously, for the isolated antenna case when $d \to \infty$ the condition on h/d can never be met. The question of exactly how large h/d must be for this condition to hold together with an experimental verification of this postulate will be treated in the following subsection.

Once this postulate had been verified, it was then necessary to determine what had caused the discrepancies observed in Part III (Volume II) between the measured and theoretical wave numbers. As pointed out previously, ideal open circuits never actually exist. The question of significant end effects and the influence they may have on the measured wave numbers then arises. Studies on the reflection coefficient (a manifestation of the end effect) at the end of a finite antenna in free space have been made by a

number of authors [27], [28]. It has been shown that for electrically long antennas the current can be viewed as an incident wave, i.e., the current on an infinitely long antenna, and a reflected wave which is the incident wave modified by a reflection coefficient. For the isolated antenna the solution for the reflection coefficient is a complicated procedure involving the Weiner-Hopf technique. It was anticipated that the problem would be much more complex for a wire in the presence of a dissipative half-space. In view of this, no attempt was made to solve analytically for the reflection coefficient at the end of a wire above a dissipative half-space. Instead, the end effects were determined experimentally from the measured data presented in Volume II. Using the measured end corrections with the theoretical wave number given by (1.7), a new semi-empirical solution was developed and compared to the measured data. This solution was found to give good agreement for the current and charge distributions as well as the input admittance. This is discussed in more detail later in the section.

Experimental Verification of the Condition on d/λ_0

An experimental procedure was devised to verify Wu's postulate concerning the condition on d/λ_0 necessary for the validity of King's theory in Section 1.2. Since the end effect was believed to be the cause of the observed discrepancies between the measured and theoretical results, it was necessary to be able to eliminate all influence of end effects while measuring the wave numbers on the antennas. With open-ended antennas this could be accomplished only if the wire were infinitely long. However, measurements on extremely long antennas were not possible with the existing experimental apparatus since the total length of the water tank was only approximately 3 meters.

Attention was then directed to the fact that in precise transmission-line measurements made with a slotted line, short-circuit terminations are ordinarily preferred to open circuits. This is usually because the short circuit possesses less of an end effect and thus establishes a more precise plane of reference. The imaging effect of the short circuit, whereby the measuring line appears to be doubled in length, provides a termination with almost ideal characteristics. Since the transmission-line behavior of wire antennas in the presence of a dissipative half-space had been verified previously, it was decided to measure the wave numbers for these antennas when terminated by a short circuit. It was hoped that this would eliminate the

end effects encountered in the conventional open-circuited configuration.

The measurements were performed using basically the same equipment as described in Part II and used to obtain the data presented in Part III. This involved, essentially, the use of the water tank and coaxial measuring line. The short-circuit termination was made out of a large 4' by 4' sheet of aluminum. A small plug was attached to the aluminum sheet and then inserted into the end of the 1/8" antenna tubing to ensure good electrical contact with the aluminum sheet. To further ensure good electrical contact between the end of the antenna and the aluminum sheet, the area around the contact point was painted with a silver conducting paint. The aluminum sheet was presumed to be large enough so that most of the field at the end of the antenna, both above and below the water, would be reflected back. If this were not the case, end effects from a less than ideal short circuit would invalidate the measurements. It is obvious that if the aluminum sheet is large enough, it can model a perfect image plane. The cumulative result of the two image planes, the one against which the antenna is driven and the terminating plane, is to create a successive series of images whose net effect is to give the appearance of an infinitely long antenna. This proved to be most beneficial since the wave numbers could then be measured with a minimum influence from end effects. Hence, if Wu's postulate is correct, the wave numbers determined by this method should agree with results obtained from (1.7).

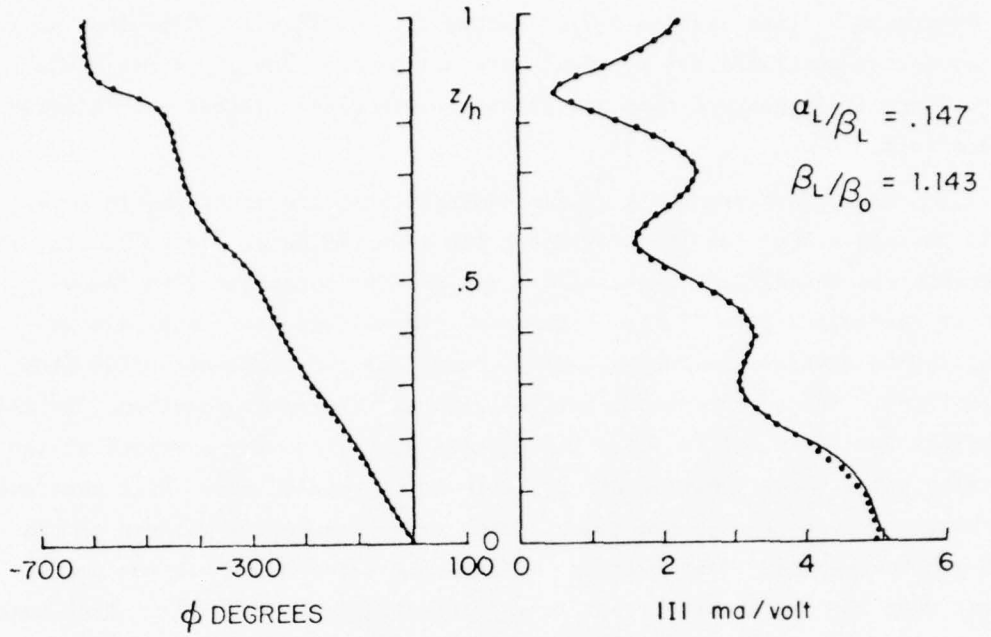
The measurements were made on terminated antennas placed over a fresh-water solution identical to that used in Part III. The electrical properties of this solution were determined to be $\varepsilon_r = 82$ and $\sigma = 0.092$ mhos/m at 18° C. The current and charge distributions were measured on a section of antenna, $1.5\lambda_0$ in length, at heights of $d/\lambda_0 = .01, .02, .05, .1, .13$ and .25 above the fresh-water interface. In all cases the section was terminated with a short circuit. From these distributions the corresponding wave numbers were determined with simple transmission-line relationships. This involves using the distance between successive nulls to determine β_L and the following relationship

$$ISWR = \frac{|I|_{max}}{|I|_{min}} \approx S_I = \frac{\cosh(\alpha_L w_1 + \rho_s)}{\sinh(\alpha_L w_2 + \rho_s)} \tag{1.67}$$

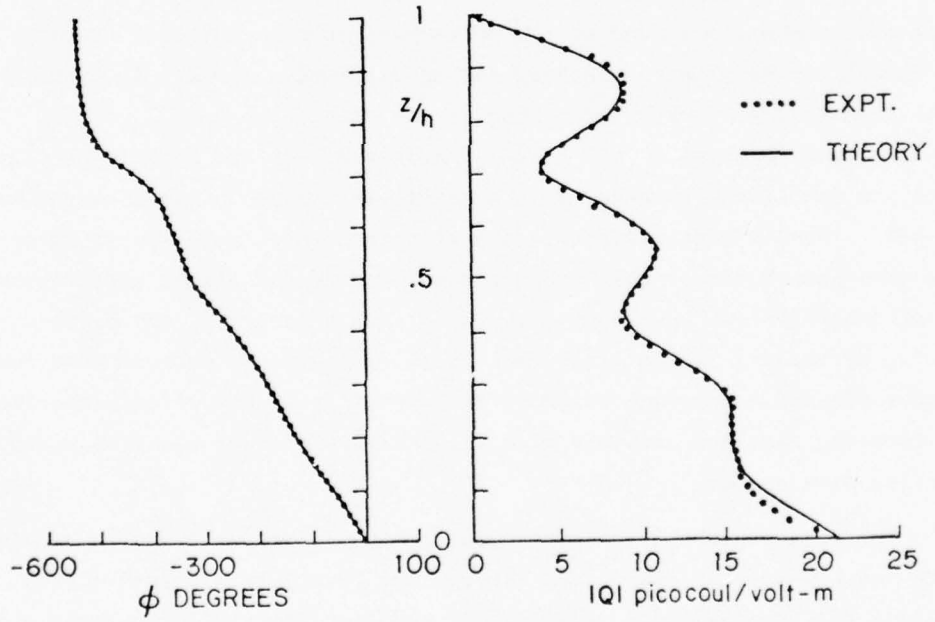
to determine α_L [see Section 3.3 in Volume II, eq. (3.4)]. Note that in the manipulation of (1.67) the terminal attenuation function ρ_s is set equal to zero since it is assumed that the short-circuit plane creates a negligible end effect.

The measured current and charge distributions are presented in Figs. 1.13 through 1.18. The dots represent the measured data, the solid line represents the theoretical expression based on King's results with the wave number determined from (1.7). Elementary transmission-line analysis was utilized to develop the theoretical formulas for the short-circuited line from (1.6). The agreement for both current and charge is excellent for all spacings including $d/\lambda_0 = .25$. The largest variations are observed at the driving point where junction effects were not accounted for. Note that even without any end-effect corrections added, the agreement is good up to the end of the antenna. This further confirms the assumption that the image plane used for the short circuit is sufficiently large to reflect back nearly all of the incident field at the end of the antenna. Figure 1.19 compares the theoretical wave numbers given by (1.7) with the measured values determined from the above data. Also displayed are the corresponding effective wave numbers measured on the open-ended antenna for each spacing. The agreement between the theoretical and measured wave numbers is excellent with less than a 5% error occurring at any spacing up to $d/\lambda_0 = .25$. It is evident from the curves that as d/λ_0 increases, the end effect associated with the open-ended antenna has a dramatic influence on the measured wave numbers. When standard transmission-line techniques are used to determine the wave number for an open-ended antenna and no end-effect corrections are made, the effective wave number tends to give a larger β_L and α_L than predicted by theory. It is clear that if (1.7) gives the correct wave number, a more plausible approach would be to determine the end effect experimentally from the data and use this with (1.7) rather than to use a measured effective wave number.

The data presented appear to confirm the assertion of Wu. Certainly with the end effects eliminated through the short-circuit termination, it is obvious that the measured wave numbers and distributions of current and charge agree quite well with theoretical predictions up to spacings as high as $d/\lambda_0 = .25$. With the arrangement of the two image planes, the antenna appears to be infinite in extent so that the condition that h/d be large is

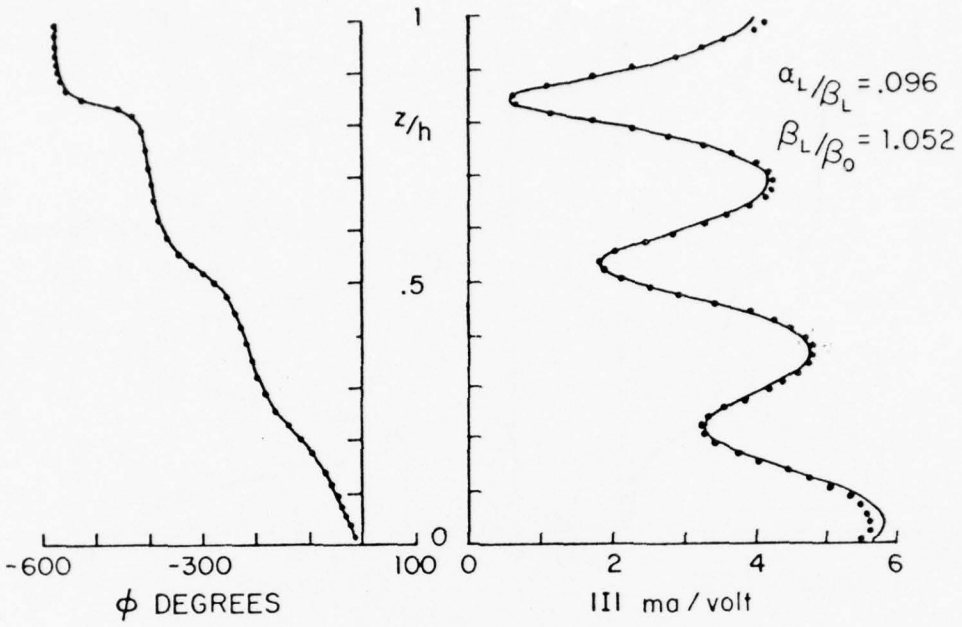


a.) CURRENT DISTRIBUTION

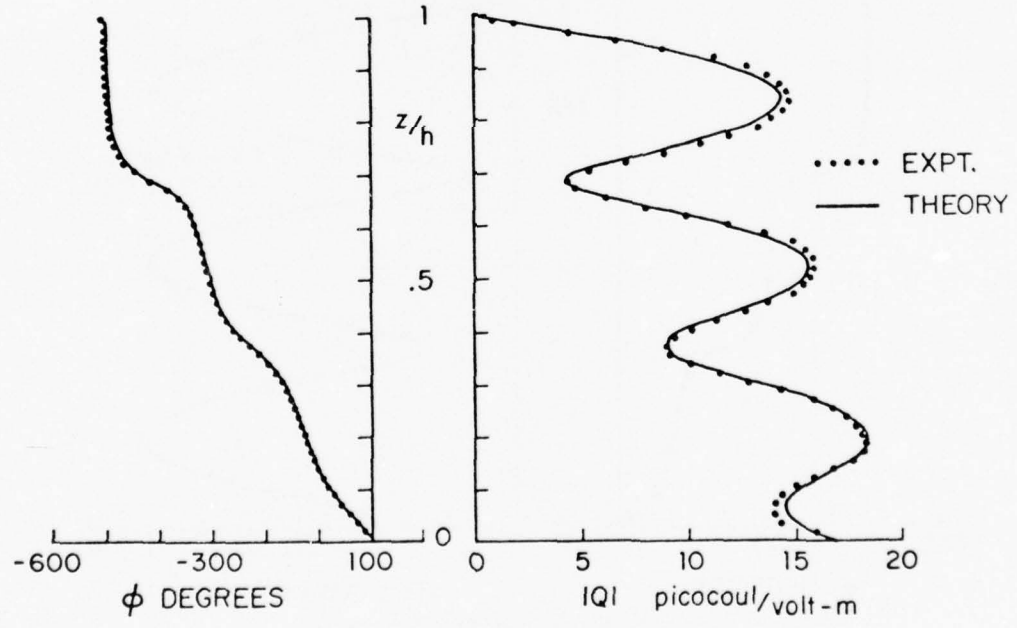


b.) CHARGE DISTRIBUTION

FIG. 1.13. CURRENT AND CHARGE DISTRIBUTION ON SHORT-CIRCUITED MONOPOLE OVER FRESH WATER; $h/\lambda_0 = 1.5$ AND $d/\lambda_0 = .01$.

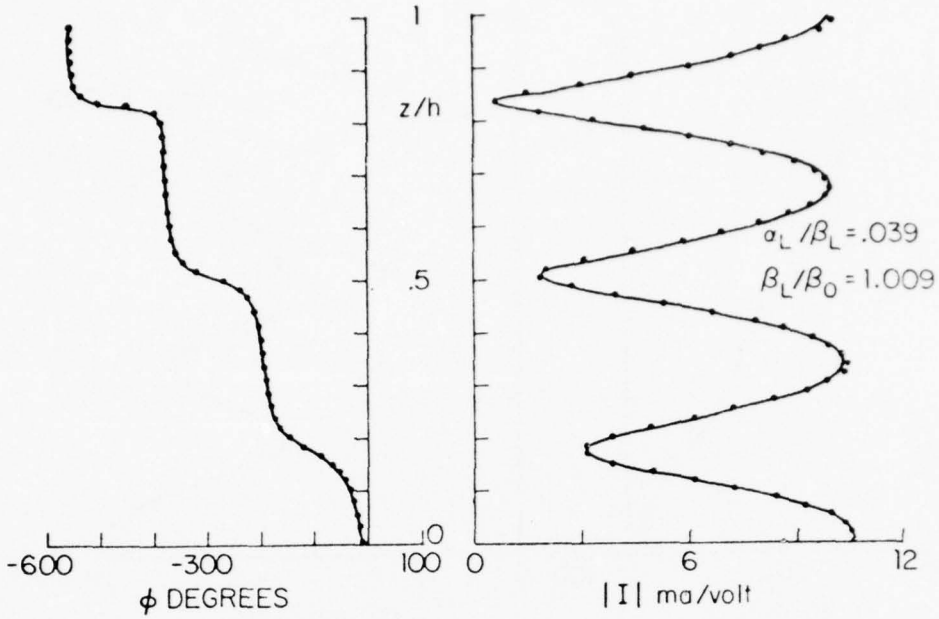


a.) CURRENT DISTRIBUTION

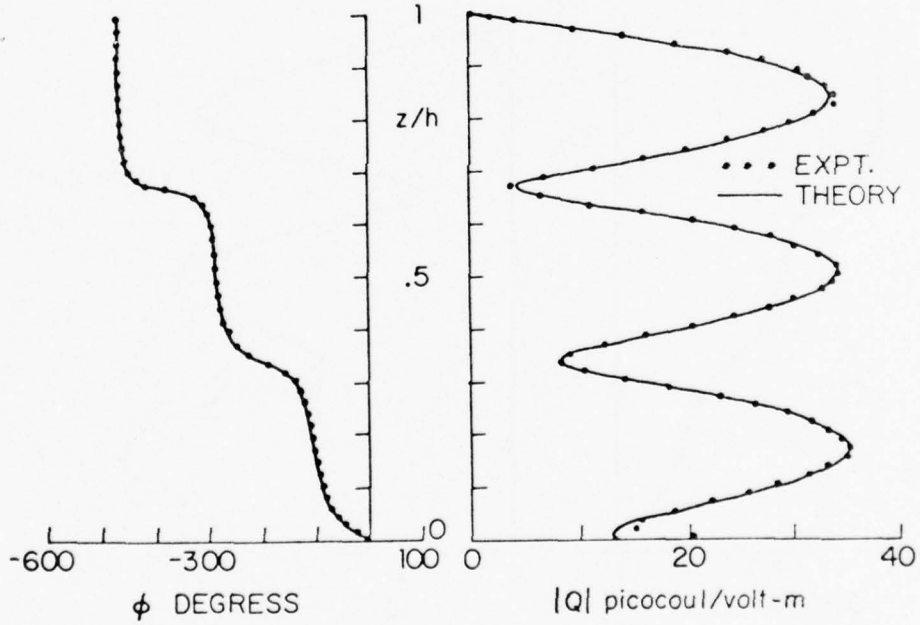


b.) CHARGE DISTRIBUTION

FIG. 1.14. CURRENT AND CHARGE DISTRIBUTION ON SHORT-CIRCUITED MONOPOLE OVER FRESH WATER; $h/\lambda_0 = 1.5$ AND $d/\lambda_0 = .02$.

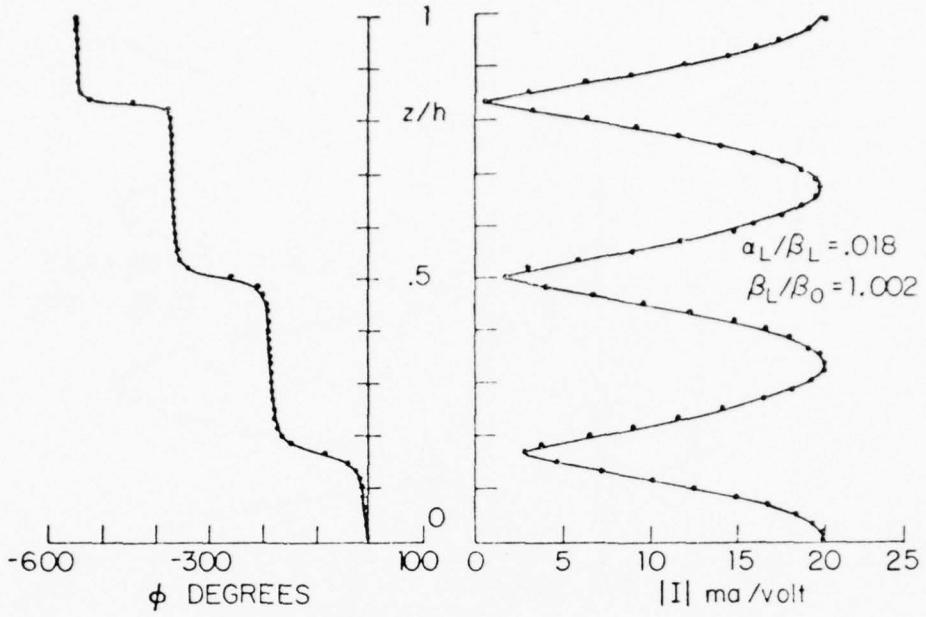


a) CURRENT DISTRIBUTION

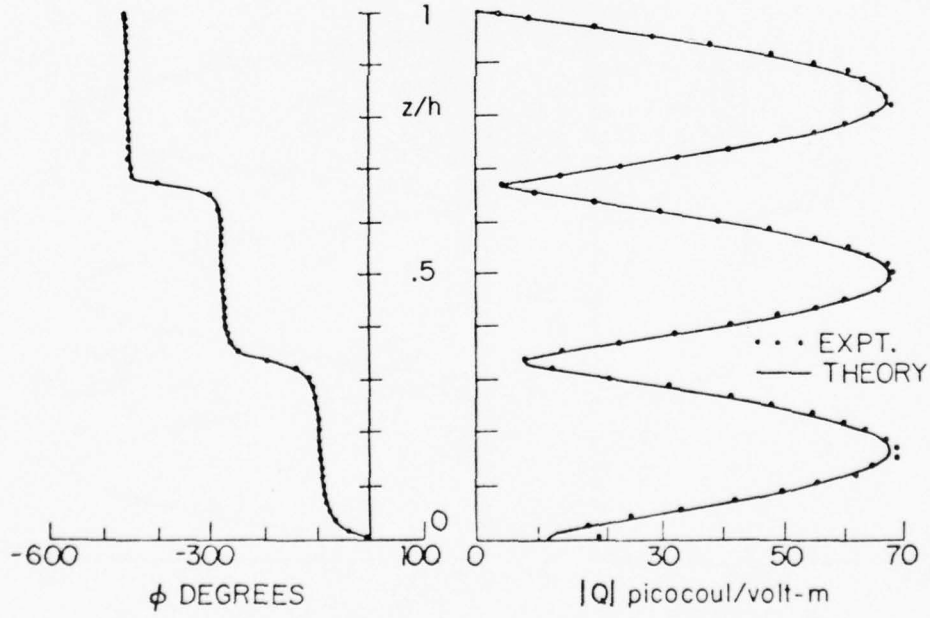


b) CHARGE DISTRIBUTION

FIG. 1.15. CURRENT AND CHARGE DISTRIBUTION ON SHORT-CIRCUITED MONOPOLE OVER FRESH WATER; $h/\lambda_0 = 1.5$ AND $d/\lambda_0 = .05$.

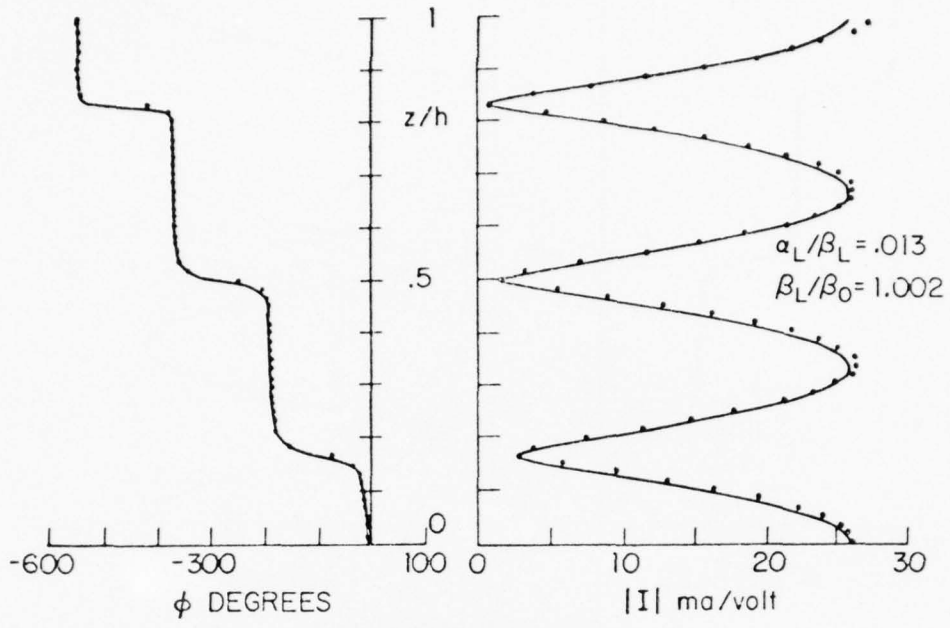


a) CURRENT DISTRIBUTION

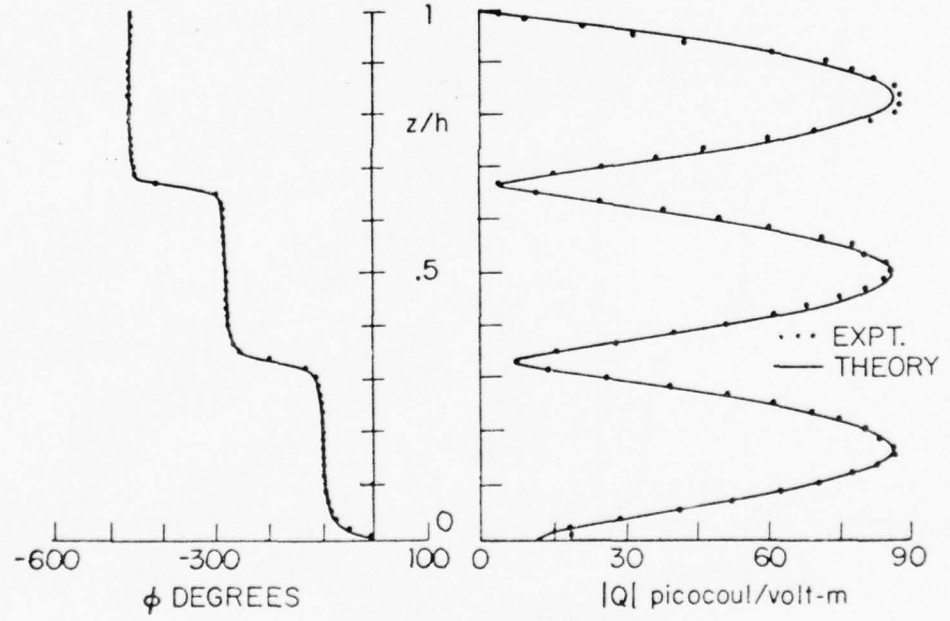


b) CHARGE DISTRIBUTION

FIG. 1.16. CURRENT AND CHARGE DISTRIBUTION ON SHORT-CIRCUITED MONOPOLE OVER FRESH WATER; h/λ_0=1.5 AND d/λ_0 = .1.

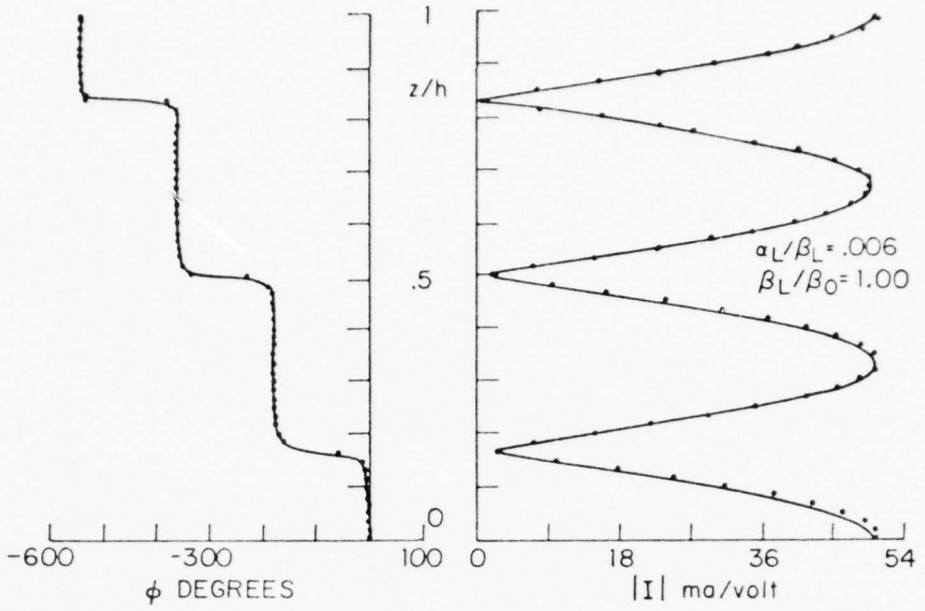


a) CURRENT DISTRIBUTION

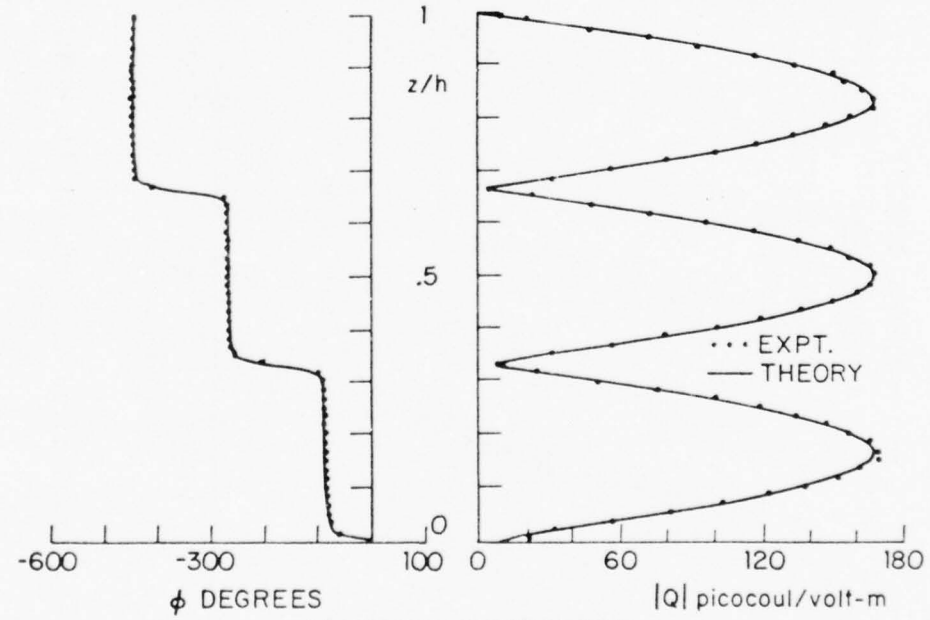


b) CHARGE DISTRIBUTION

FIG. 1.17. CURRENT AND CHARGE DISTRIBUTION ON SHORT-CIRCUITED MONOPOLE OVER FRESH WATER; $h/\lambda_0 = 1.5$ AND $d/\lambda_0 = .13$



a) CURRENT DISTRIBUTION



b) CHARGE DISTRIBUTION

FIG. 1.18. CURRENT AND CHARGE DISTRIBUTION ON SHORT-CIRCUITED MONOPOLE OVER FRESH WATER; $h/\lambda_0 = 1.5$ AND $d/\lambda_0 = .25$.

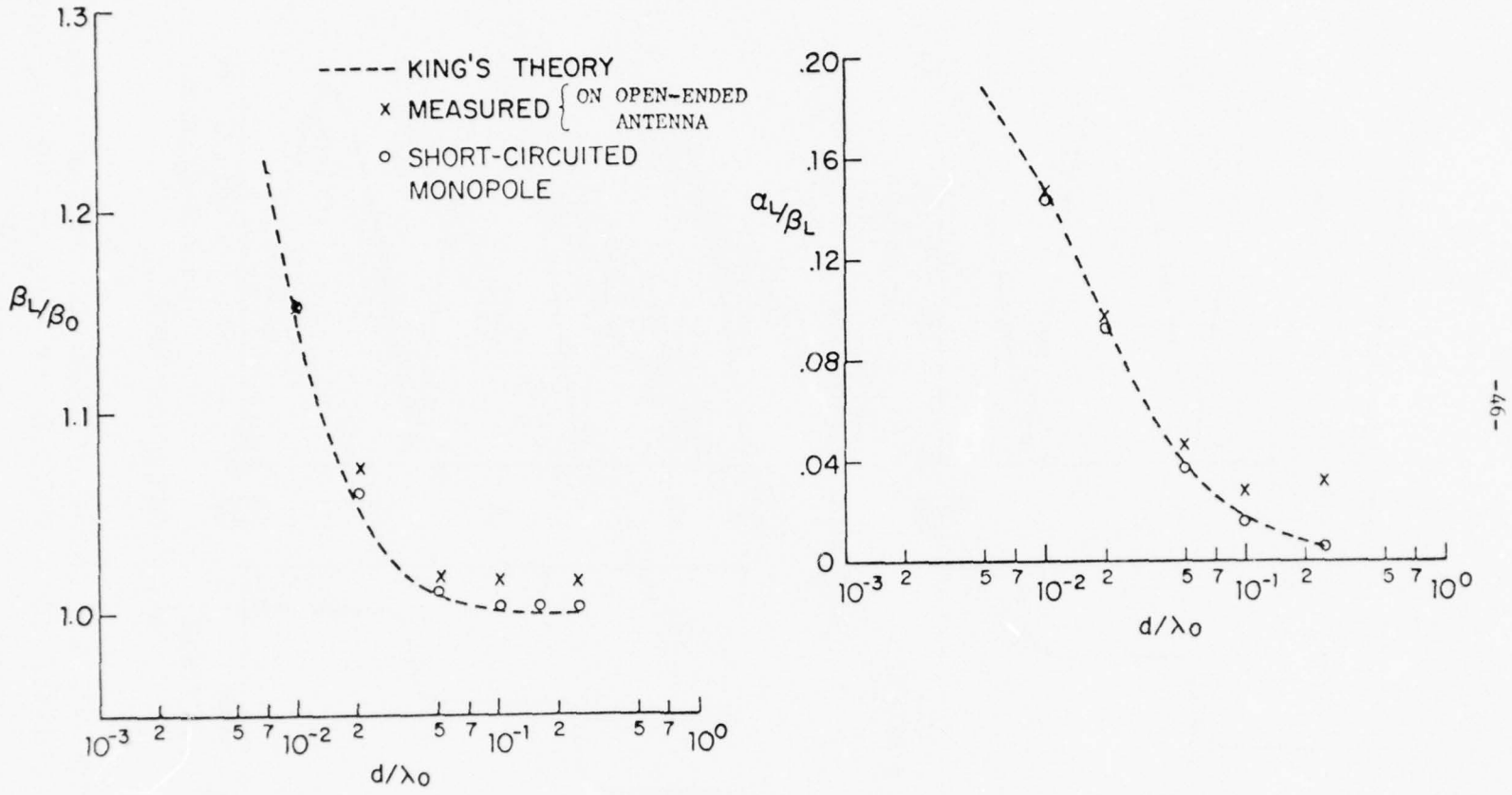


FIG. 1.19. WAVENUMBER ON HORIZONTAL WIRE OVER FRESH WATER;
$\varepsilon_r = 82$ AND $Pe = .067$

always enforced. Thus, it has been confirmed that for h sufficiently large (1.7) will hold for any spacing d except in the limit $d \to \infty$. The case of antennas of finite length remains to be investigated. The limitations on d/λ_0 for this situation are discussed later in the following subsection.

End-Effect Corrections for Finite Antennas Over a Dissipative Half-Space

It is demonstrated in Part III (Volume II) that, for d/λ_0 sufficiently small (approximately $< .02$), equations (1.6) and (1.7) correctly describe the current distribution on a dipole antenna above a dissipative half-space when $|k_2| >> |k_1|$. At larger values of d/λ_0 end effects cause variations to occur between the theoretical predictions and the measured data. It turns out that there is a connection between these end effects and the actual radiation mechanism of the antenna. In the original development by King [29] the wave number for the antenna was derived with the assumption that the radiation into air is negligible compared with the radiation into the dissipative medium. This is a direct consequence of condition (1.3b). For very small values of d/λ_0, the influence of the medium on the antenna is quite large and this is a good assumption. When d/λ_0 becomes sufficiently large, however, the influence of the half-space begins to diminish and the antenna may begin to radiate a significant amount of energy into the air. This radiation has not been accounted for in the original King theory and will result in an additional loss being observed in the measured data. This added loss can be seen in the measured α_L which is larger than that predicted by the theory. The larger attenuation was, of course, an effective α_L which includes the loss due to the end effect.

The radiation from a wire antenna placed sufficiently high above a dissipative half-space involves two different mechanisms. For the transmission-line-type mode in which all the radiation is into the half-space, the radiation loss is described by a distributed quantity, α_L. In this case the radiation is parcelled out to individual segments of the antenna circuit. In contrast, the energy that is radiated into the air is more characteristic of a free-space antenna and, thus, can be shown to be a property of the entire radiating circuit. Unlike the transmission-line mode in which the radiation is a distributed quantity, the conventional antenna-type radiation is described by a lumped parameter which is determined by the entire radiating structure. In the work done by Shen [28] it is shown that for long antennas in free space the loss associated with the radiation can be taken into

account by a complex terminating impedance. The antenna current can then be described as a combination of an infinitely long antenna current I_∞ and a reflected current that consists of I_∞ modified by a complex reflection coefficient. This reflection coefficient is related to the terminating impedance which accounts for the radiation loss.

It was decided that it would be possible to use a similar approach to treat the finite center-driven dipole antenna above a dissipative half-space as a two-wire transmission line with complex wave number determined by (1.7) and terminated at both ends in a complex impedance. It has been shown that with $|k_2| >> |k_1|$ and $d/\lambda_0 \leq .02$ the end effects are insignificant and, correspondingly, the radiation loss into the air is small. For this situation the terminating impedance is very large and approaches the value for an ideal open circuit. At greater values of d/λ_0 the end effects and radiation losses can be accounted for by the terminating impedance. Ideally, one would like to develop an analytic expression for the terminating impedance which would depend on the height of the wire and the properties of the medium over which it is placed. However, due to the anticipated complexity of this formulation, an experimental approach was initiated instead.

With the addition of the terminating impedance it is necessary to modify (1.6), (1.16) and (1.18) slightly in order to account for this factor. As shown previously, the current distribution for a doubly-terminated two-wire transmission line as depicted in Fig. 1.12 can be given by (1.27) and (1.28). For a center-driven section of transmission line with equal terminating impedances at each end, it is a straightforward procedure to show that:

$$I(x) = \frac{V_0^e}{Z_c} \frac{\sinh(\gamma_L w + \theta_s)}{2\cosh(\gamma_L h + \theta_s)} \quad , \qquad |x| \leq h \tag{1.68}$$

where

$$w = h - |x| \tag{1.69a}$$

$$\gamma_L = jk_L \tag{1.69b}$$

$$\theta_s = \coth^{-1}(Z_s/Z_c) = \rho_s + j\phi_s \tag{1.69c}$$

The quantity θ_s is the complex terminal function which accounts for both the

capacitive end effect and the radiation loss. The complex terminal function is composed of the terminal attenuation function ρ_s and the terminal phase function Φ_s. The quantity ρ_s contributes to the increased value of α_L as observed in Part III and Φ_s accounts for the shift which occurs between the measured and theoretical curves. In a straightforward manner (1.68) can be expressed in a form similar to (1.6) as follows:

$$I(x) = \frac{jV_0^e}{2Z_c} \frac{\sin k_L[(h - |x|) + \theta_s^*]}{\cos k_L(h + \theta_s^*)} \quad , \quad |x| \leq h \tag{1.70}$$

where

$$\theta_s^* = \Phi_s/k_L - j\rho_s/k_L = \Phi_s^* - j\rho_s^* \tag{1.71}$$

A comparison of (1.70) and (1.6) shows that they are identical except for the additional θ_s^* factor in the trigonometric arguments. Similarly, it can be shown that the input admittance and charge distribution differ only by the extra θ_s^* factor from King's original expressions. The modified expressions are as follows:

$$Y_{in}(x) = \frac{I(0)}{V_0^e} = \frac{j}{2Z_c} \tan k_L(x + \theta_s^*) \tag{1.72}$$

$$Q(x) = \frac{V_0^e k_L}{2Z_c \omega} \frac{\cos k_L[(h - x) + \theta_s^*]}{\cos k_L(h + \theta_s^*)} \quad , \quad x > 0 \tag{1.73}$$

By a similar procedure the expressions developed for the Beverage wave antenna can be modified for end effects. This merely involves incorporating the additional θ_s^* term into the equations.

The complex terminal function θ_s was determined experimentally with the aid of a computer program developed by Shen and Lee [30]. The program utilizes a least-squares-error criterion to best-fit the measured current data to the following form:

$$I(x) = Ae^{-jk_L x} + Be^{jk_L x} \tag{1.74}$$

Using the measured data, the program optimizes the real and imaginary parts

of A and B as well as α_L and β_L. A Newton-Raphson iteration technique was used to obtain better approximations for α_L and β_L. It should be pointed out that (1.70) and (1.74) can be shown to be equivalent representations for the current distribution on a center-driven, doubly end-loaded transmission line. For this equivalence the following relationships hold:

$$A = V_0^e Z_c/(Z_0 + Z_c)(1 + 2\Gamma_s e^{-2jk_L h}) \tag{1.75a}$$

$$B = V_0^e Z_c \Gamma_s e^{-2jk_L h}/(Z_0 + Z_c)(1 - 2\Gamma_s e^{-2jk_L h}) \tag{1.75b}$$

where Z_0 is given by (1.24) with q = s and Γ_s is the complex reflection coefficient defined as:

$$\Gamma_s = (Z_s - Z_c)/(Z_s + Z_c) = e^{-2\theta_s} \tag{1.76}$$

In (1.76), Z_s is the complex terminating impedance. Dividing B by A and substituting (1.76) for Γ_s gives:

$$B/A = |B/A|e^{j\psi} = -e^{-2(\rho_s + \alpha_L h)} e^{-2j(\beta_L h + \Phi_s)} \tag{1.77}$$

The magnitude and phase of B/A are:

$$|B/A| = e^{-2(\rho_s + \alpha_L h)} \tag{1.78a}$$

$$\psi = -2(\beta_L h + \Phi_s) \pm \pi \tag{1.78b}$$

Solving the above set of equations for ρ_s and Φ_s gives:

$$\rho_s = (1/2)\ell n|A/B| - \alpha_L h \tag{1.79}$$

$$\Phi_s = \pm\pi/2 - (\psi/2 + \beta_L h) \tag{1.80}$$

Equations (1.79) and (1.80) were used to evaluate the complex terminal function from the values of A, B, α_L and β_L that were obtained from the least-squares-fit program.

The complex terminal function was evaluated for dipole antennas placed

at heights of d/λ_0 = .01, .02, .05, .1 and .25 over the three media (fresh water, salt water, and moist earth) used for the measurements described in Part III. In all cases the θ_s value was obtained from the measured current distribution on a monopole, $1.5\lambda_0$ in length. Figure 1.20 depicts ρ_s and Φ_s as functions of d/λ_0 for each of the three media. As anticipated, ρ_s is an increasing function of d/λ_0 which indicates the increasing amount of energy that is radiated into the air. Figures 1.21 and 1.22 compare the theoretical wave numbers with the k_L values determined from the least-squares-fit program for the salt-water and moist-earth cases. Also included in these figures are the measured k_L values for the open-ended antenna. The measurements, taken from Part III, represent the effective α_L and β_L values since they include contributions due to end effects. For the salt-water case in Fig. 1.21, the α_L and β_L values determined with the program agree quite well with the theoretical predictions. The impact of the end effect on α_L is apparent, especially for $d/\lambda_0 \geq .05$, from a comparison of the attenuation obtained with the program and that measured on the open-ended antenna. For the moist-earth case in Fig. 1.22 in which condition (1.3b) is not satisfied, the k_L quantities evaluated with the least-squares program continue to exhibit a large variance with the theoretical predictions.

The tables below list the theoretical wave numbers evaluated from (1.7) together with the corresponding k_L and θ_s quantities determined with the least-squares program. The data are presented for the same range of d/λ_0 that is used throughout and for the same three media. An additional set of data is presented for the fresh-water case, namely, the measured k_L values determined from the data presented in Figs. 1.13 through 1.18. All experimental data are for measurements made at 300 MHz.

With the ρ_s and Φ_s values determined numerically from the measured data the new semi-empirical theory was compared to several cases of the fresh-water data measured previously and contained in Part III. The theory utilizes the measured ρ_s and Φ_s quantities in the zeroth-order expressions for the current, charge and admittance in (1.70), (1.73) and (1.72), respectively. In all cases only the theoretical values for k_L given by (1.7) were used. The results for the current and charge distributions and the input admittances are presented in Figs. 1.23 through 1.33.

For the current and charge distributions presented in the range $.02 \leq d/\lambda_0 \leq .13$ the agreement tends to be quite good. Note that there is no

FRESH WATER (ε_r = 82 and p_e = .067)

d/λ_0	.01	.02	.05	.1	.13	.25
Measured β_L/β_0	1.152	1.060	1.012	1.004	1.005	1.004
Measured α_L	1.043	.606	.234	.100	.071	.037
Theory β_L/β_0	1.143	1.052	1.009	1.002	1.002	1.000
Theory α_L	1.054	.6322	.2496	.1115	.0822	.038
Program β_L/β_0	1.144	1.056	1.015	1.010	1.005	1.010
Program α_L	1.031	.605	.2633	.1023	.0728	.047
Program ρ_s	-	.013	.017	.056	.061	.127
Program Φ_s	2°	3°	6°	8°	9°	11°

SALT WATER (ε_r = 81 and p_e = 2.885)

d/λ_0	.01	.02	.05	.10	.25
Theory β_L/β_0	1.109	1.047	1.015	1.006	1.002
Theory α_L	.512	.279	.108	.050	.017
Program β_L/β_0	1.111	1.058	1.023	1.016	1.015
Program α_L	.537	.291	.123	.054	.050
Program ρ_s	-	.017	.015	.046	.129
Program Φ_s	2°	4°	6°	8°	11°

MOIST EARTH (ε_r = 11.5 and p_e = .012)

d/λ_0	.02	.05	.10	.25
Theory β_L/β_0	1.143	1.044	1.014	1.002
Theory α_L	.901	.508	.270	.083
Program β_L/β_0	1.099	1.029	1.010	1.013
Program α_L	.719	.421	.234	.099
Program ρ_s	-	.022	.051	.105
Program Φ_s	3°	7°	8°	7°

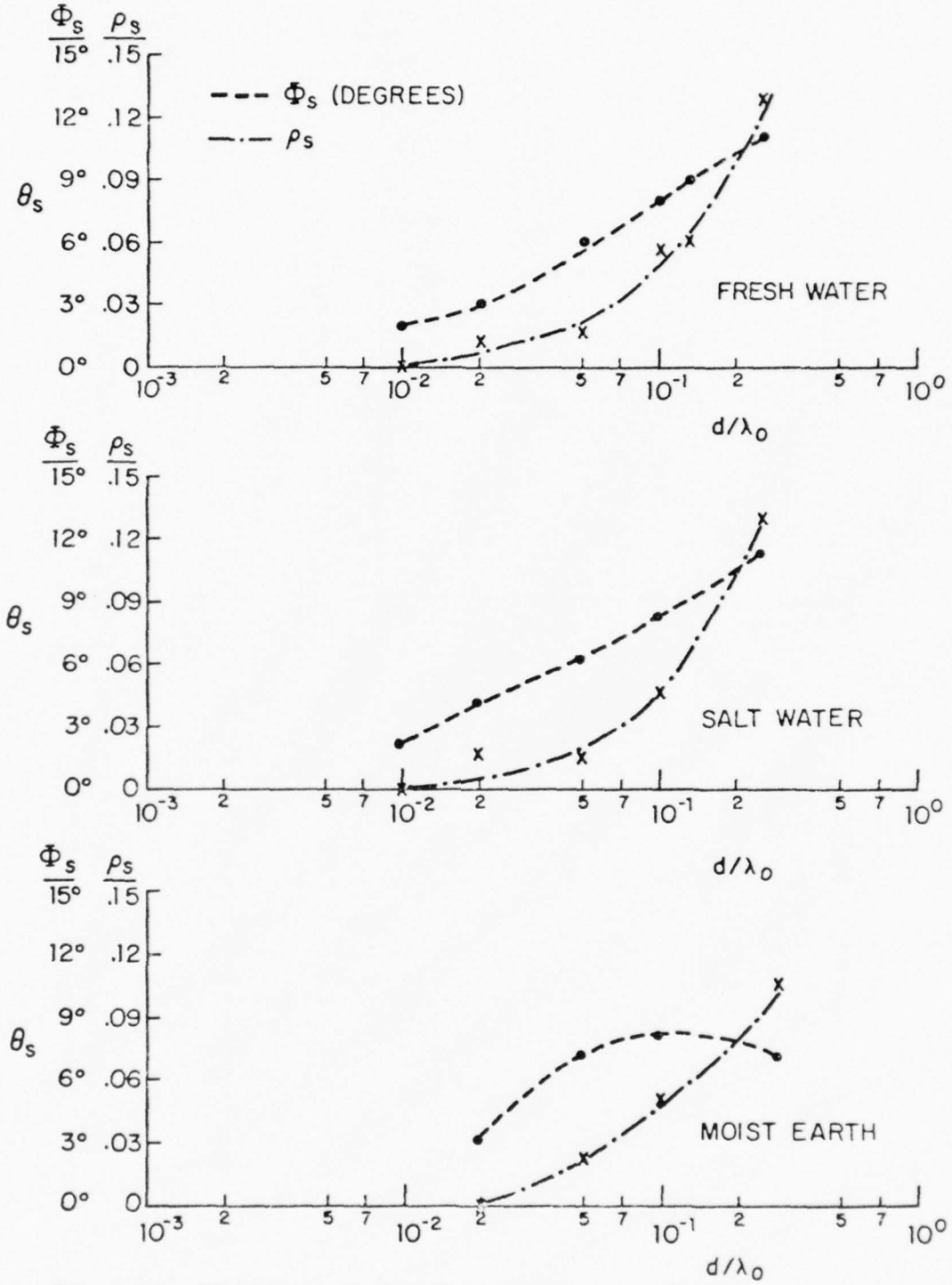


FIG. 1.20 PROGRAM-EVALUATED TERMINAL FUNCTIONS.

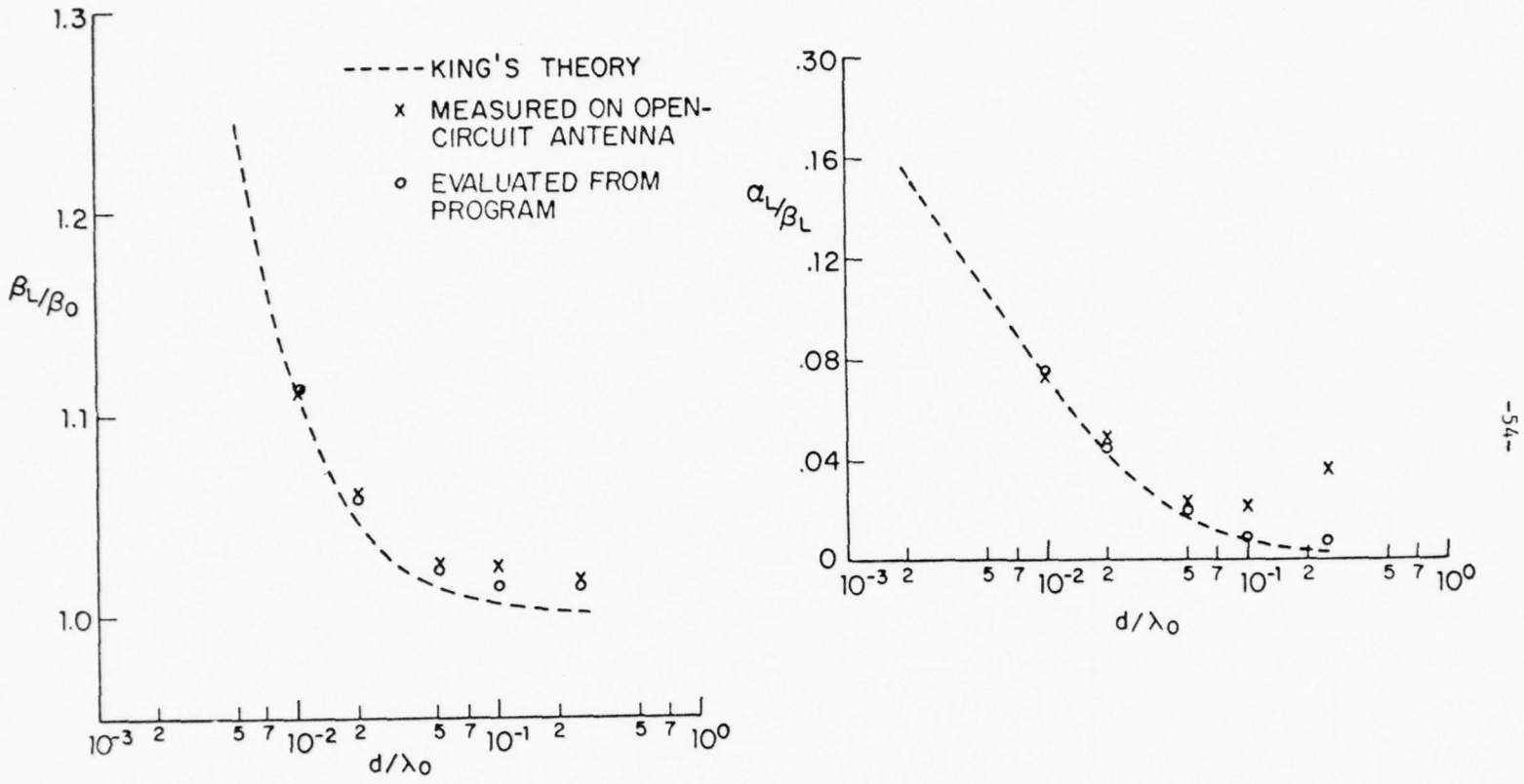


FIG. 1.21 WAVENUMBER ON HORIZONTAL WIRE OVER SALT WATER; $\varepsilon_r = 81$ AND $P_e = 2.885$

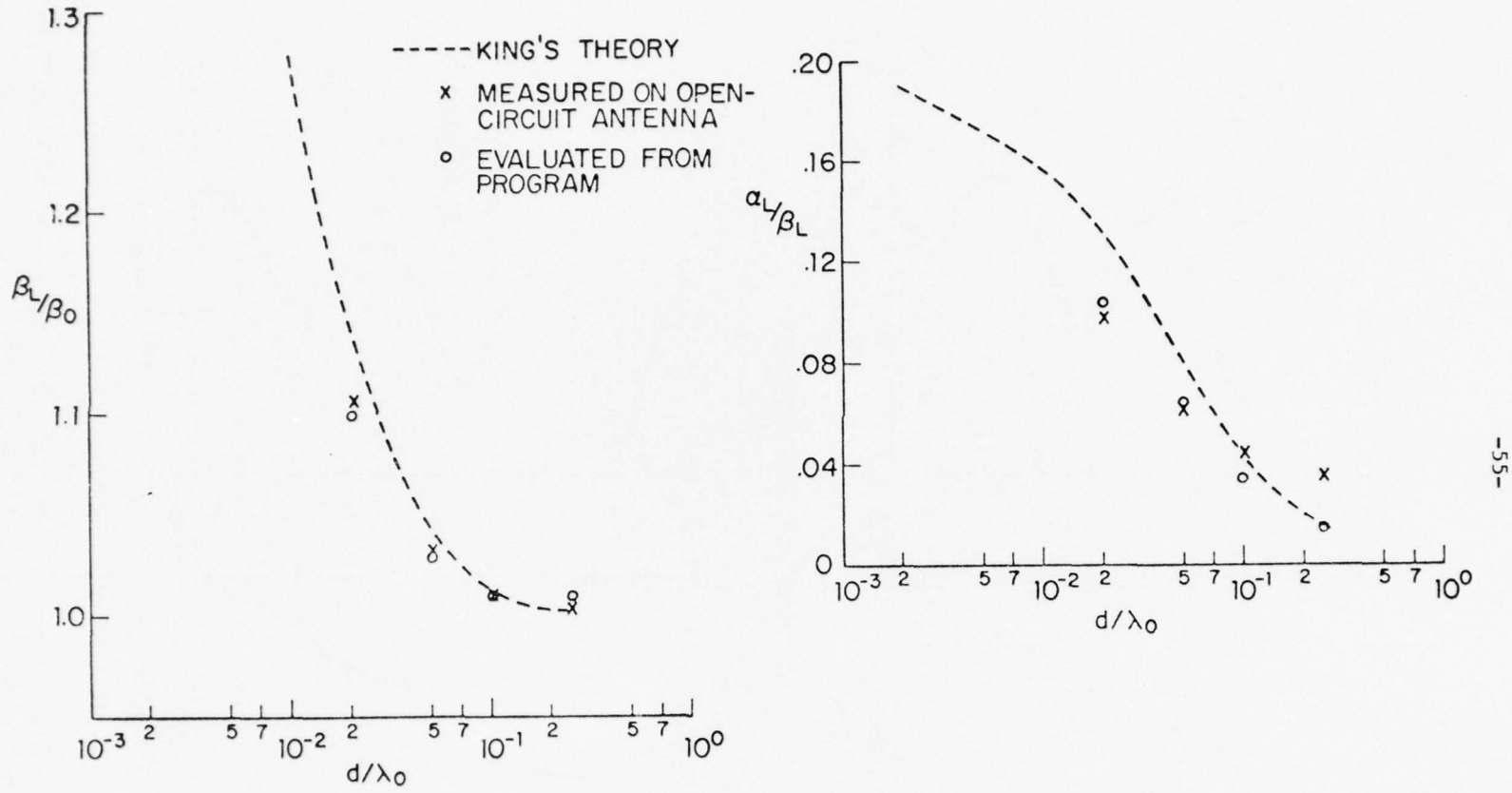
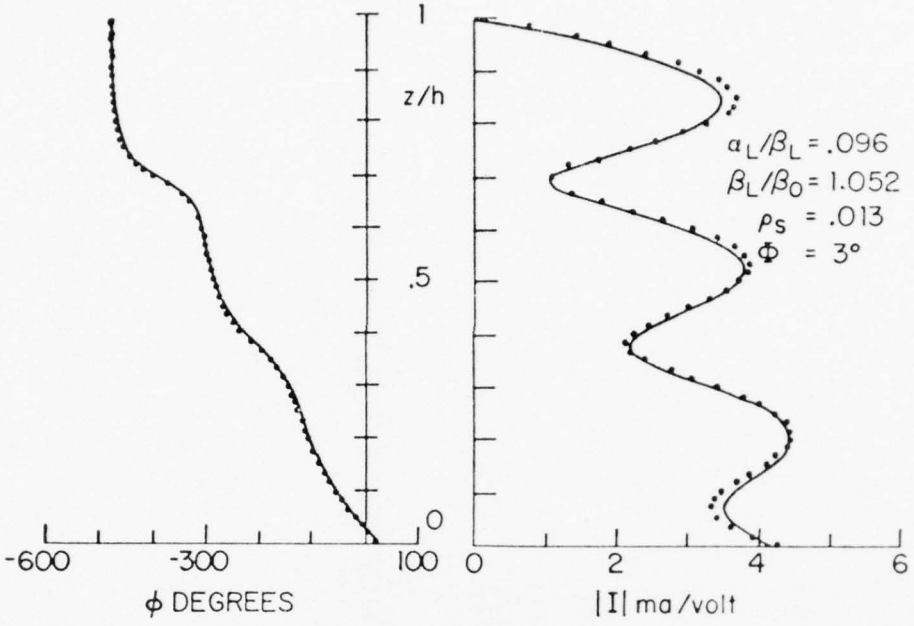
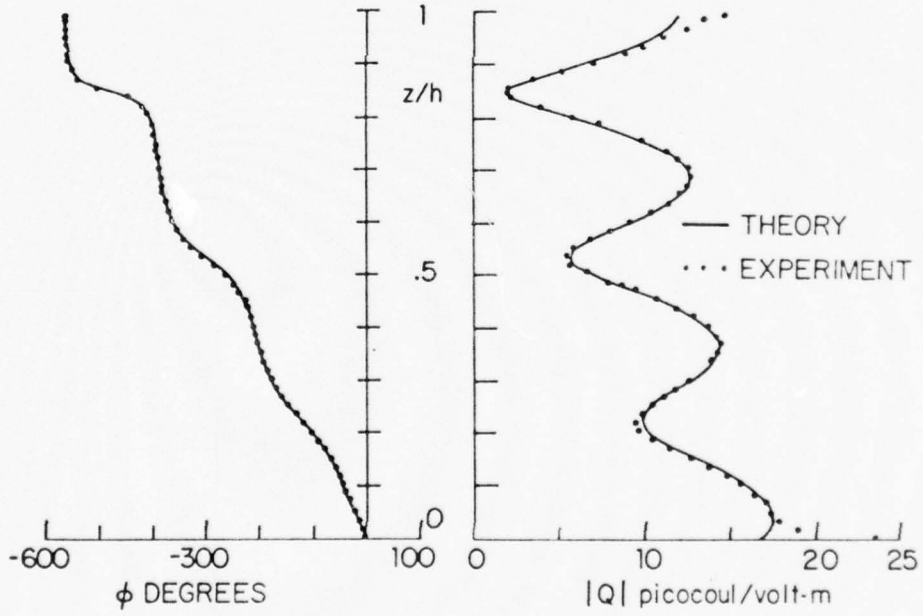


FIG. 1.22. WAVENUMBER ON HORIZONTAL WIRE OVER MOIST EARTH; $\varepsilon_r = 11.5$ AND $P_e = .012$.

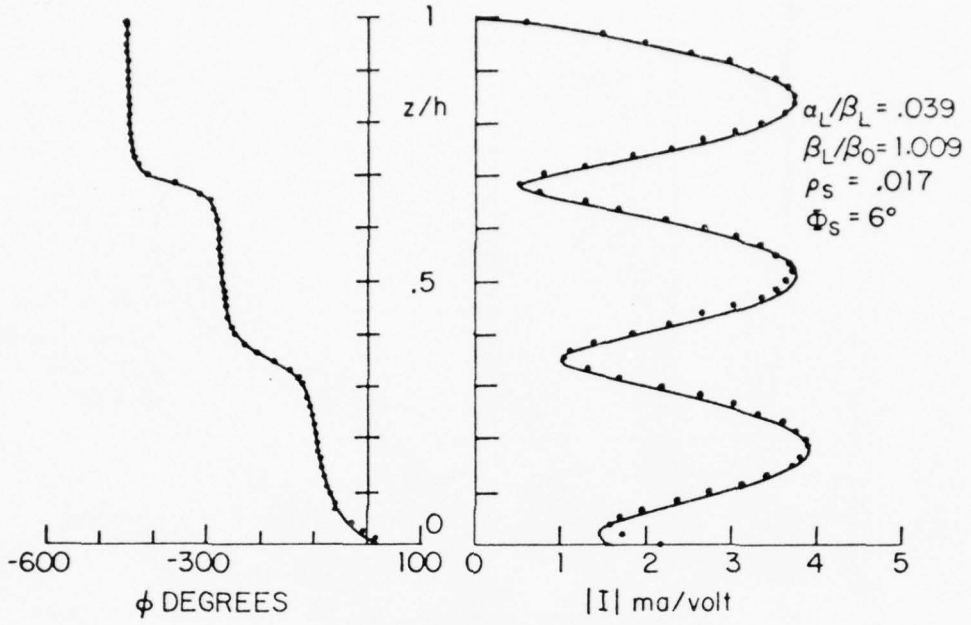


A) CURRENT DISTRIBUTION

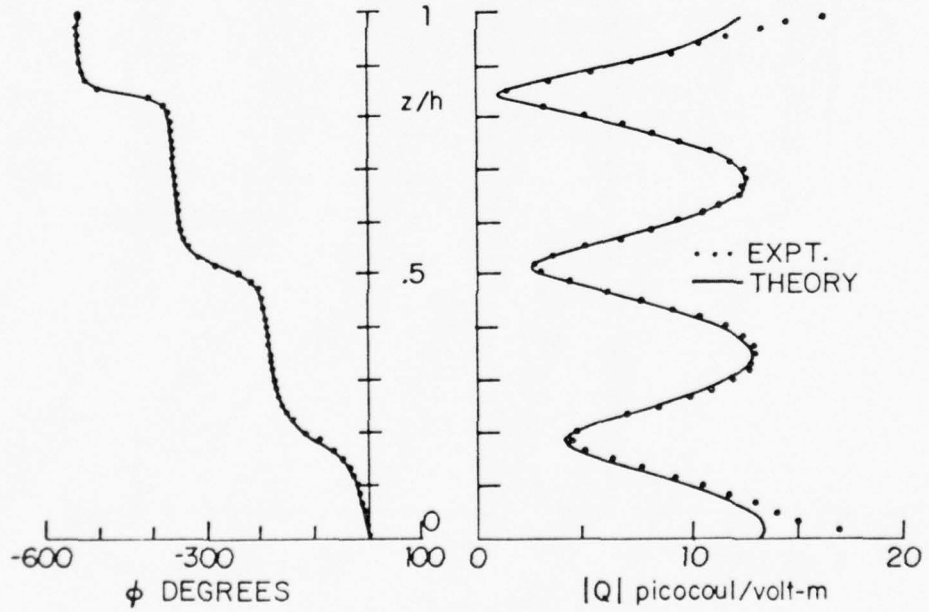


B) CHARGE DISTRIBUTION

FIG. 1.23. CURRENT AND CHARGE DISTRIBUTION ON MONOPOLE OVER FRESH WATER, $h/\lambda_0 = 1.5$ AND $d/\lambda_0 = .02$

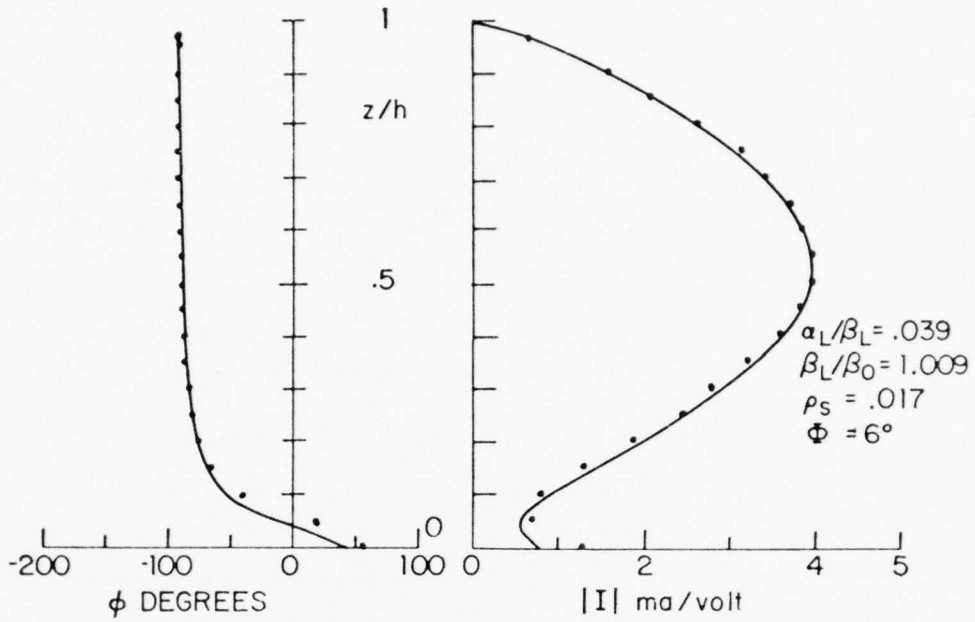


A) CURRENT DISTRIBUTION

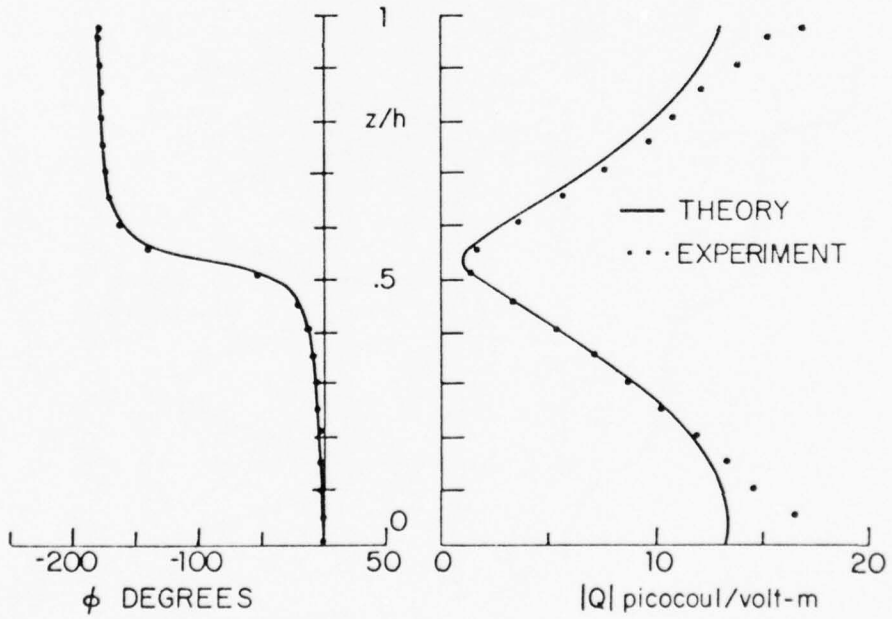


B) CHARGE DISTRIBUTION

FIG 1.24. CURRENT AND CHARGE DISTRIBUTION ON MONOPOLE OVER FRESH WATER, h/λ_0 = 1.5 AND d/λ_0 = .05

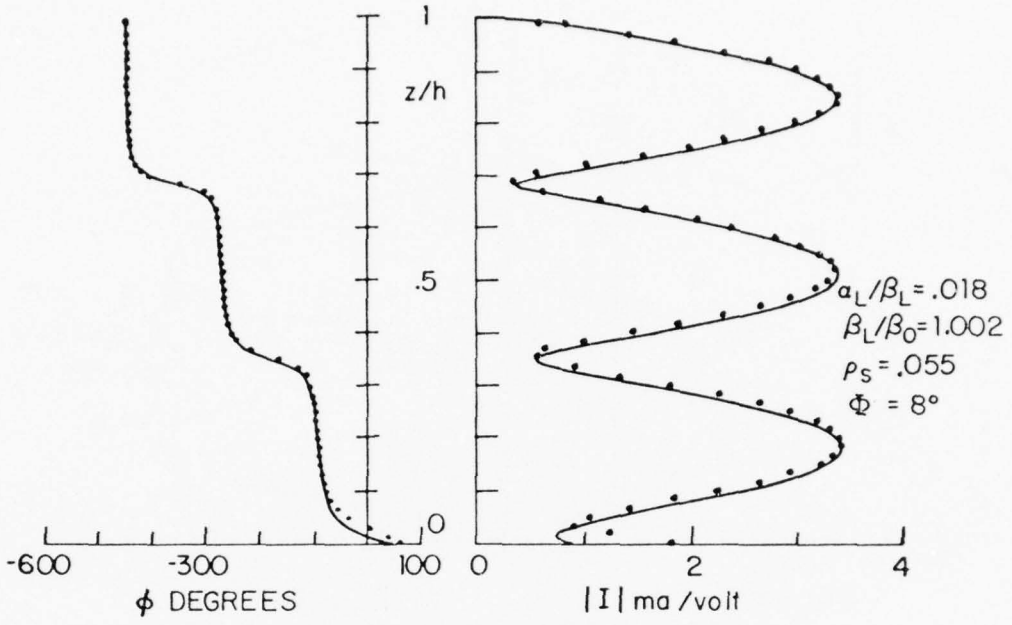


A) CURRENT DISTRIBUTION

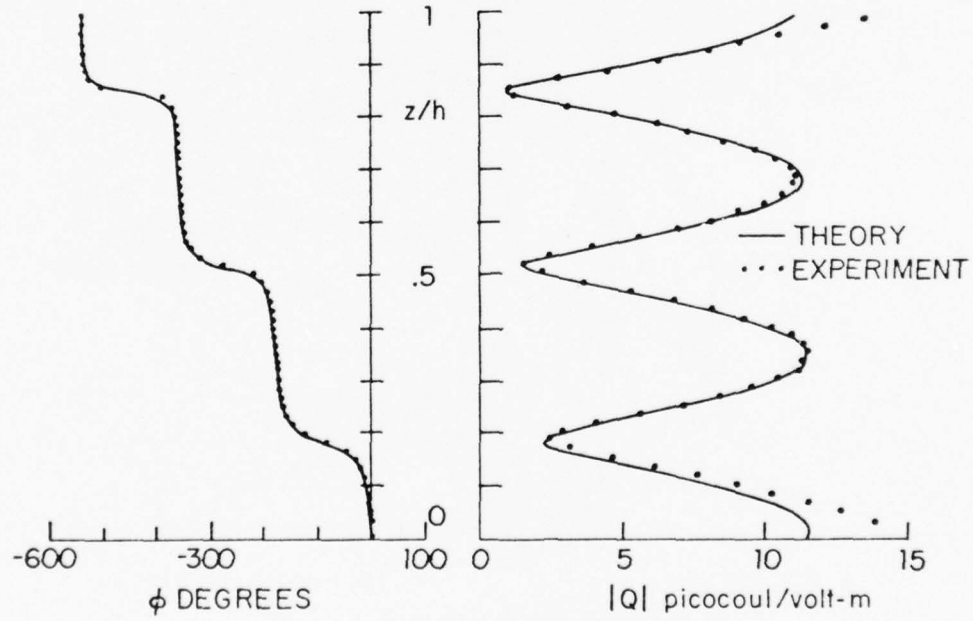


B) CHARGE DISTRIBUTION

FIG. 1.25 CURRENT AND CHARGE DISTRIBUTION ON MONOPOLE OVER FRESH WATER, $h/\lambda_0 = .5$ AND $d/\lambda_0 = .05$.

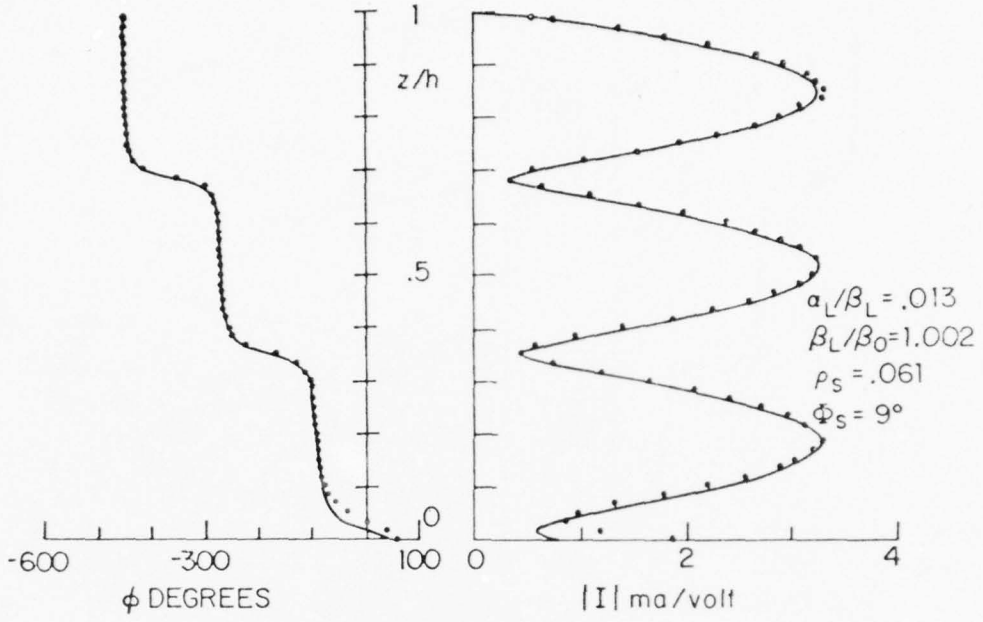


A) CURRENT DISTRIBUTION

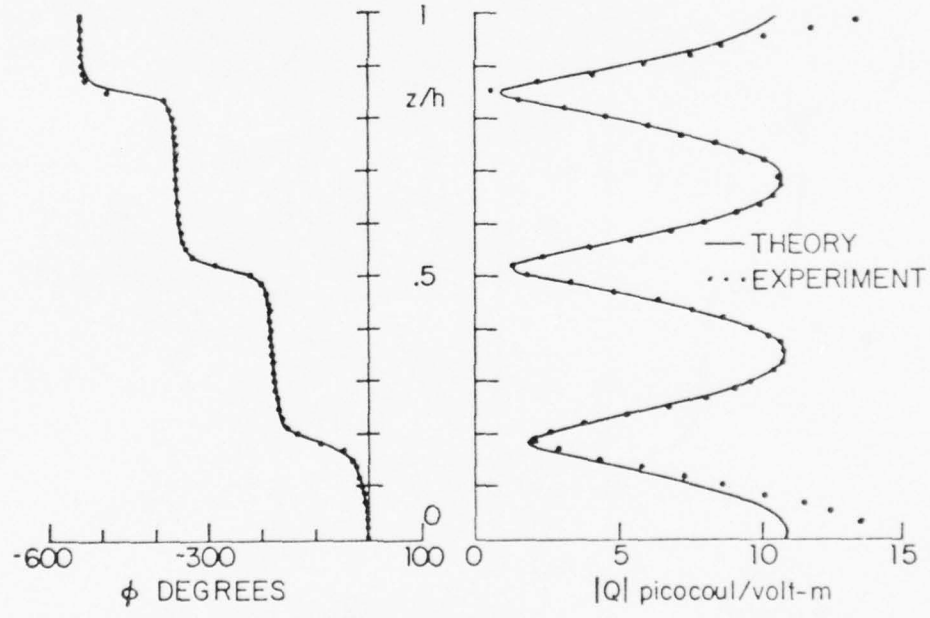


B) CHARGE DISTRIBUTION

FIG. 1.26. CURRENT AND CHARGE DISTRIBUTION ON MONOPOLE OVER FRESH WATER, $h/\lambda_0 = 1.5$ AND $d/\lambda_0 = .1$.

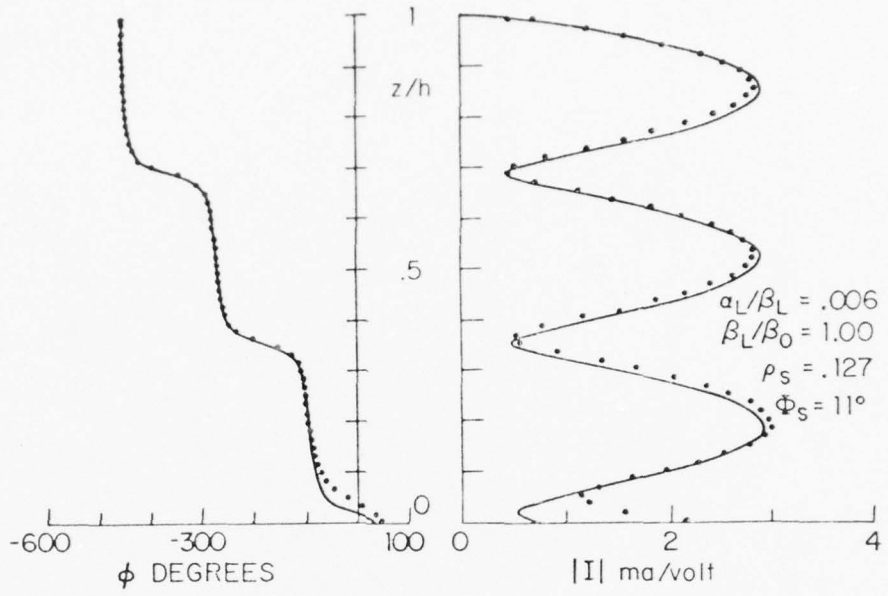


A) CURRENT DISTRIBUTION

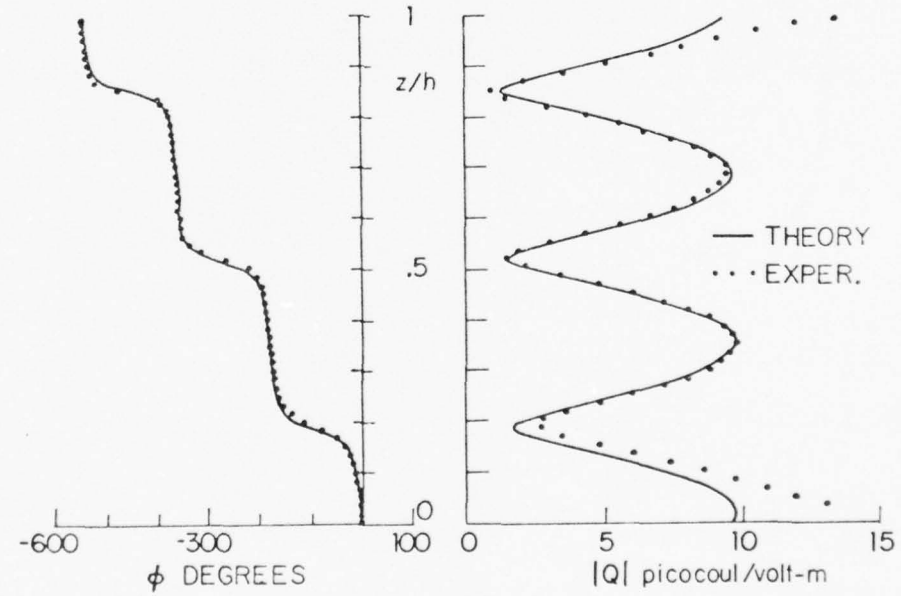


B) CHARGE DISTRIBUTION

FIG. 1.27. CURRENT AND CHARGE DISTRIBUTION ON MONOPOLE OVER FRESH WATER, $h/\lambda_0 = 1.5$ AND $d/\lambda_0 = .13$.

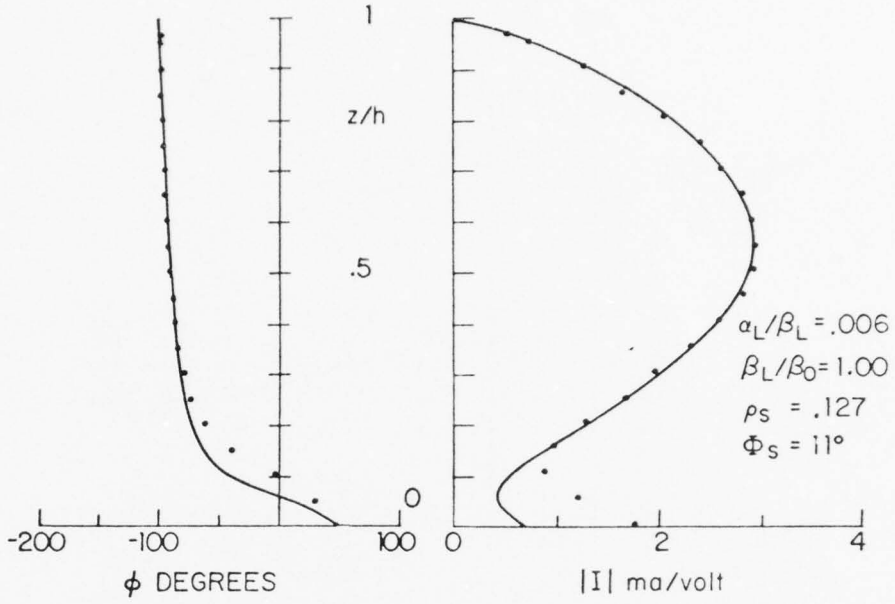


A) CURRENT DISTRIBUTION

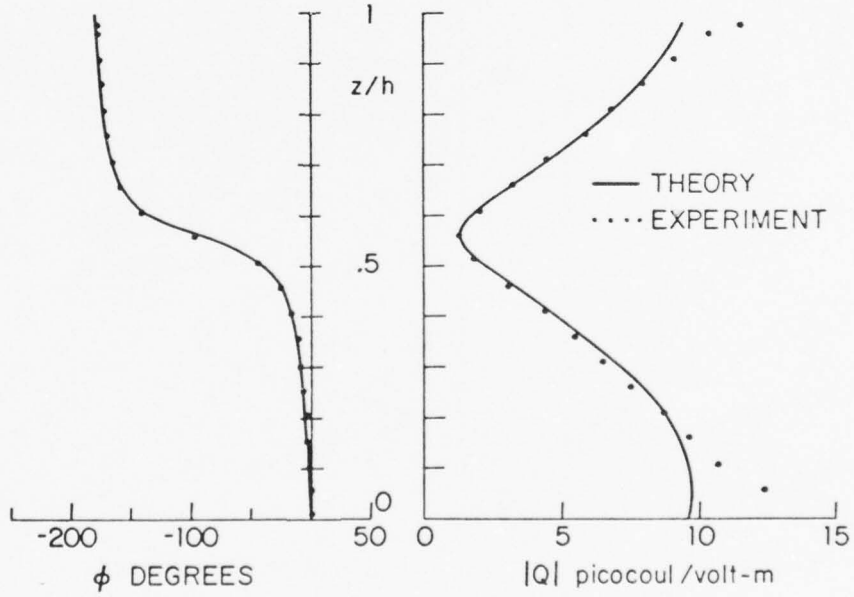


B) CHARGE DISTRIBUTION

FIG. 1.28. CURRENT AND CHARGE DISTRIBUTION ON MONOPOLE OVER FRESH WATER, $h/\lambda_0 = 1.5$ AND $d/\lambda_0 = .25$.



A) CURRENT DISTRIBUTION



B) CHARGE DISTRIBUTION

FIG. 1.29. CURRENT AND CHARGE DISTRIBUTION ON MONOPOLE OVER FRESH WATER, $h/\lambda_0 = .5$ AND $d/\lambda_0 = .25$.

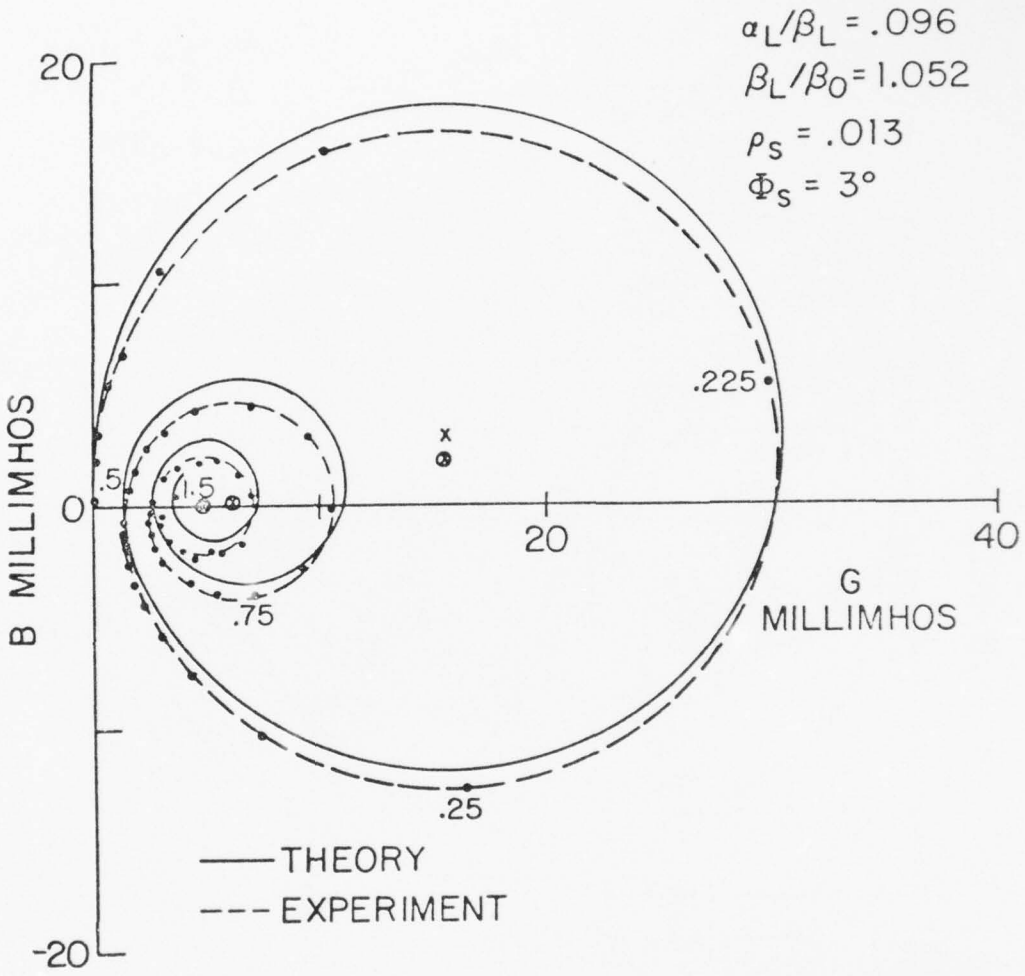


FIG. 1.30. INPUT ADMITTANCE CIRCLE DIAGRAM OF MONOPOLE OVER FRESH WATER; $d/\lambda_0 = .02$ AND $a/\lambda_0 = .0015$.

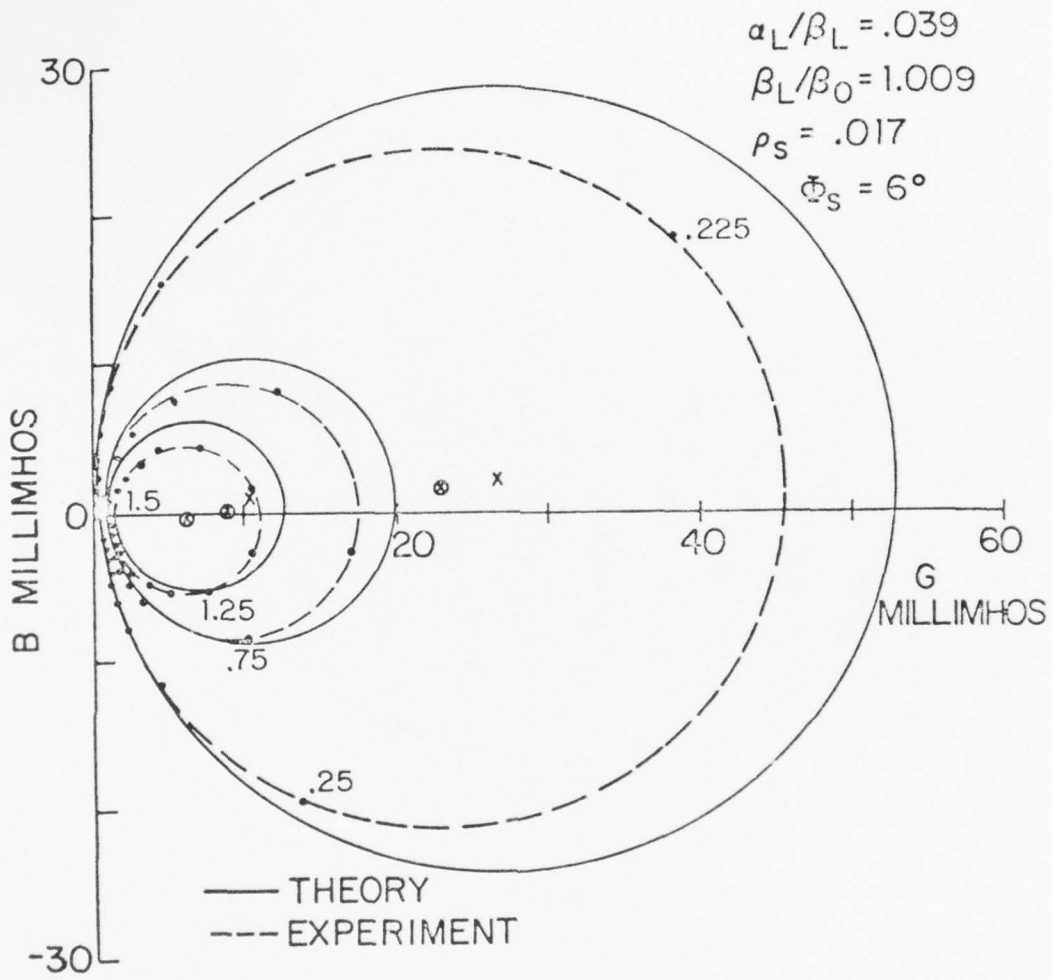


FIG. 1.31. INPUT ADMITTANCE CIRCLE DIAGRAM OF MONOPOLE OVER FRESH WATER; $d/\lambda_0 = .05$ AND $a/\lambda_0 = .0015$.

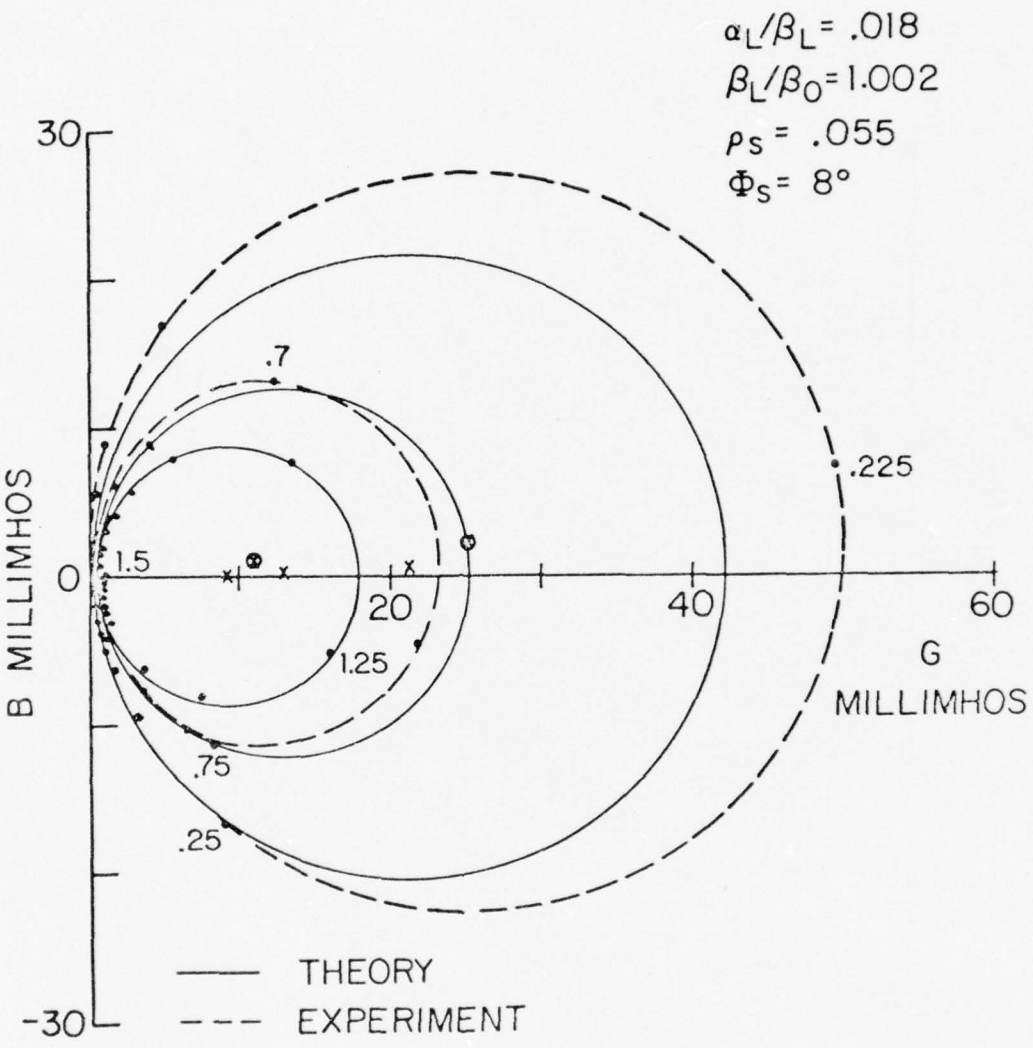


FIG. 1.32. INPUT ADMITTANCE CIRCLE DIAGRAM OF MONOPOLE OVER FRESH WATER; $d/\lambda_0 = .1$ AND $a/\lambda_0 = .0015$.

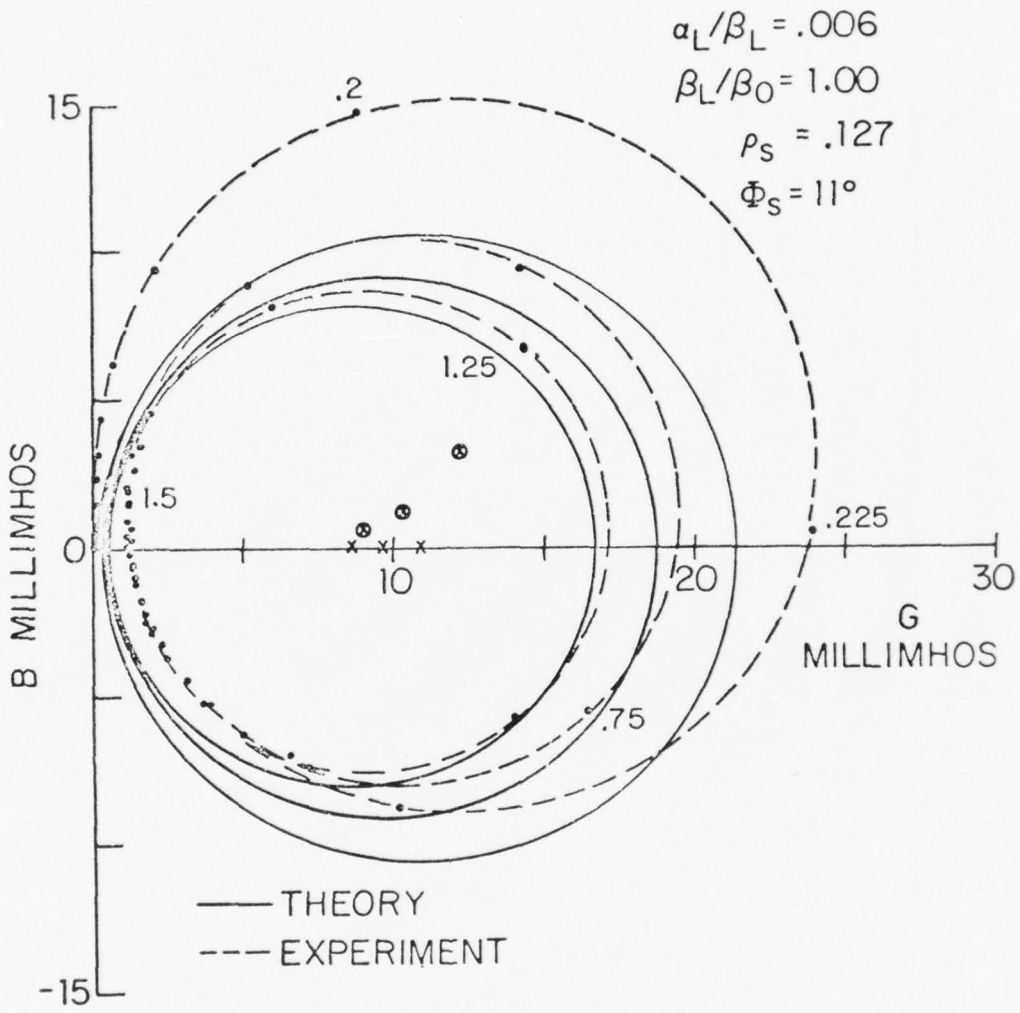


FIG. 1.33. INPUT ADMITTANCE CIRCLE DIAGRAM OF MONOPOLE OVER FRESH WATER; $d/\lambda_0 = .25$ AND $a/\lambda_0 = .0015$.

shift between the measured data and the theoretical curves. The inclusion of Φ_s into the theory is responsible for this. In each case, at the driving point there is some variation which tends to increase as d/λ_0 becomes larger. This is to be expected since the semi-empirical theory does not include any corrections for the junction effect at the driving point of the antenna. Like the end effect, the junction effect becomes more dominant as d/λ_0 becomes larger.

An interesting case is the one presented in Fig. 1.25. Even though h/d = 10 for this set of curves, the agreement is still good with only a small variation occurring at the driving point. For the distributions in Fig. 1.27 with $h/d \gtrsim 11.5$, the results again tend to confirm the validity of the semi-empirical approach. These figures also serve to reconfirm Wu's postulate by showing that for $h/d \gtrsim 10$ the zeroth-order theory can be used to obtain acceptable results. Figures 1.28 and 1.29 represent two cases, each with $d/\lambda_0 = .25$, and h/d = 8 and 2, respectively. In both cases the agreement between the measured data and theoretical results for distributions of current and charge is good with slightly greater variations observed at the driving point. Based on these two sets of curves it would appear that the semi-empirical theory will hold for all d/λ_0 values up to .25. However, the admittance curves will subsequently show that a significant departure from the transmission-line form begins to appear at this height.

Figures 1.30 through 1.33 compare the measured input admittance with that obtained with the semi-empirical theory for the cases with $d/\lambda_0 = .02$, .05, .1, and .25. One is able to compare the accuracy of the present theory to that of the initially employed semi-empirical theory developed in Part III by noting that Figs. 1.30 through 1.33 contain the same measured data as do Figs. 3.26 through 3.29, respectively. In the range $.02 \leq d/\lambda_0 \leq .10$ the agreement between the measured input admittance and the results of the semi-empirical theory is good. For $d/\lambda_0 = .05$ and $d/\lambda_0 = .1$, there is a large discrepancy in the first resonance. This, however, is most likely due to the junction effect which cannot be handled adequately by this theory. Note that a comparison of Fig. 1.31 with Fig. 3.27 and of Fig. 1.32 with Fig. 3.28 indicates that the present theory gives much better admittance agreement with measurement than the previous theory described in Part III. A more accurate experimental determination of ρ_s and Φ_s would probably improve the agreement

in the first resonance. Some of the discrepancy must still, however, be attributed to the junction effect. It is obvious from Fig. 3.29 that at this height the semi-empirical theory based on an effective k_L cannot adequately handle the input admittance. In contrast, Fig. 1.33 shows a much closer agreement between the present theory and the measurements. Nevertheless, the measurements indicate that the zeroth-order form for the admittance is not sufficient at this height. It appears that at $d/\lambda_0 = .25$ a higher-order theory is necessary for the input admittance owing to the fact that a radiation mechanism more characteristic of an antenna in free space may begin to dominate. The field-pattern measurements taken at $d/\lambda_0 = .25$ tend to confirm this fact further. In Figs. 2.13 and 2.18 of [25] the dip which begins to appear in the main beam of the surface wave indicates that the radiation is beginning to become more characteristic of a free-space antenna which would have a null along the axis.

With tables of the θ_s values provided, it is possible to make further comparisons between theory and experiment in both the fresh-water and salt-water cases. In the sample cases shown all the comparisons are for fresh water. The agreement is seen to be quite good. Since the salt-water case satisfies condition (1.3b) even better than the fresh-water situation, it can be expected that this semi-empirical theory based on measured ρ_s and Φ_s will also give good results for salt water over the same range of d/λ_0. For the moist-earth measurements it is necessary to develop a correction term to (1.7) in order to obtain theoretical wave numbers that agree more closely with the measurements. It is clear that a new expression for (1.7) is needed in the range where condition (1.3b) is not strictly satisfied. From all the appearances of the measured data, it would seem most likely that once the correct analytic expression for the wave numbers is known, the new semi-empirical theory could be utilized for these cases in the range $.02 \leq d/\lambda_0 \leq .25$.

The work presented in this final section has helped to refine and further clarify this investigation concerned with horizontal wires in the presence of a dissipative half-space. The section has dealt specifically with finite antennas and the development of a theoretical expression for them which can account for both the trends in the measured data and provide an adequate explanation for the physical phenomena involved. The main points emphasized and the conclusions drawn are as follows:

1) Condition (1.3c) has been shown not to be a necessary requirement for the validity of King's theory. Measurements tend to confirm Wu's postulate that for very long antennas over dense media (1.7) gives the correct wave number for spacings as high as $d/\lambda_0 = .25$. For finite antennas it was discovered that for values of $h/d = 10$ it is still possible to use King's theory and have (1.7) give the correct wave number. In many cases, however, this theory may have to be modified for end effects.

2) The semi-empirical theory developed in this section provides much better agreement with measured data and is more physically meaningful than the theory developed in Part III (Volume II). With the ability to determine end effects experimentally, there was no longer any necessity for using a theory based on effective wave numbers. The results in this section show that the semi-empirical theory gives good agreement for current and charge distributions for values up to $d/\lambda_0 = .1$. The admittances up to this height are also adequate and are shown to give much better agreement than the theory in Part III. Discrepancies in the first resonance may be due either to experimental error in the determination of θ_s or to junction effects or a combination of both.

3) For the case of $d/\lambda_0 = .25$ the semi-empirical theory gives adequate agreement for the current and charge distributions with some noticeable variations occurring at the driving point. The comparison for the input admittance clearly shows that the simple zeroth-order theory cannot handle the admittance and that a higher-order theory is necessary. The admittance curves indicate that the transmission-line behavior is no longer dominant at this height and that perhaps a behavior more characteristic of an antenna in free space is beginning to dominate.

4) The work to this point on horizontal-wire antennas over a dissipative half-space has brought about theoretical developments which can treat the problem over certain ranges of the parameters, but has also shown the need for more analytic investigations. For future work, it would be most beneficial to develop an analytic expression for θ_s to eliminate the empirical nature of the present theory. An extension of the theoretical expression for k_L to ranges for which the condition (1.3b) may not be completely satisfied is also worth investigating. Lastly, a more complete theory which can cover the entire range of d/λ_0 and approach the asymptotic limit of the free-space solution for $d/\lambda_0 \to \infty$ is also needed.

PART II
EXPERIMENTAL EQUIPMENT AND SYSTEM CALIBRATION

2.1. Experimental Modeling

Many problems in electromagnetic theory can be studied accurately by using an appropriate experimental model. In any analysis it is assumed t this "appropriate" model will not deviate greatly from physical reality. For many cases in antenna theory, the actual antenna dimensions may precl the use of a full-scale experimental model. Due to the linearity of the Maxwell equations, however, it is possible many times to scale antenna di mensions to sizes that can be readily handled experimentally [31], [32]. For antennas in free space this involves the proper scaling of the physic dimensions and operating frequencies.

When simple linear media other than the limiting cases of air or a p fect conductor are involved in the scaling process, it is necessary to sc properly the constitutive properties of the media in addition to all phys cal dimensions. When appropriately done, an experimental scale model wil accurately simulate a physically real situation with dimensions convenien scaled for experimental investigation.

For both the Beverage antenna and the horizontal-wire antenna above dissipative half-space, an experimental scale model was developed to inve tigate the validity of the mathematical models discussed in Sections 1.2 1.7. Sinclair [32] has shown that for practical, geometrical scale model the following relationships must hold:

$$\ell' = \ell/p \quad , \quad f' = pf \quad , \quad \lambda' = \lambda/p \tag{2.}$$

$$\sigma' = p\sigma \quad , \quad \mu' = \mu \quad , \quad \varepsilon' = \varepsilon \tag{2.}$$

where the unprimed quantities refer to the full-scale values and the prin quantities to the scaled values. The quantity p is the ratio of the full scale length to the model length. In almost all cases it is the general practice to simulate air in a full-scale system by air in the model syste With this one exception, (2.1b) applies to all other media. For the prob presently being considered, three different media are involved if one in- cludes the conducting wire along with the air and the dissipative half-sp

If the wire is assumed to be perfectly conducting, scaling the conductivity makes no sense and, therefore, the electrical properties of the wire are unaffected in the scale model.

Since most of the current interest in the Beverage antenna deals with operating frequencies in the HF band (5 MHz - 30 MHz; 10 m - 20 m wavelengths), it was necessary to scale down the antenna length, thereby requiring a corresponding increase in the operating frequency. A frequency of 300 MHz was chosen for the investigation. This provides an experimental model scaled down dimensionally by a factor of 10. In order to make a valid comparison between the actual full-scale situation and the scaled model, it was also necessary to scale up the conductivity of the dissipative half-space by a factor of 10. Due to the fact that the dielectric constant ε_2 is unaffected by the scaling procedure, it is common practice to use the same material in the experimental model and to vary its conductivity by mixing it with graphite [33], salt, or another type of ionic compound. Since the conductivity of most materials can only be varied over a limited range, either because of solubility limits or changes in ε_r caused by corresponding changes in σ, many times it is impossible to obtain an exact scale model for specified σ and ε_r, especially for extreme ranges of p.

With this in mind, the present approach has been to study experimentally the Beverage antenna and the horizontal wire over a wide range of media (salt water, fresh water, and moist earth). This investigation has specifically been concerned with measuring the current and charge distributions on and the input admittance of these antennas when placed at varying heights above the three different media. From this study an experimental check on King's theory (Section 1.2) and the related theory for the Beverage antenna (Section 1.7) can be made. It should then be possible to use the scale-model measurements to predict the antenna properties of the full-scale situations corresponding exactly to the experiment. It is hoped further that the favorable verification of the above theories should allow analytical predictions to be made for any full-scale situations unable to be modeled exactly.

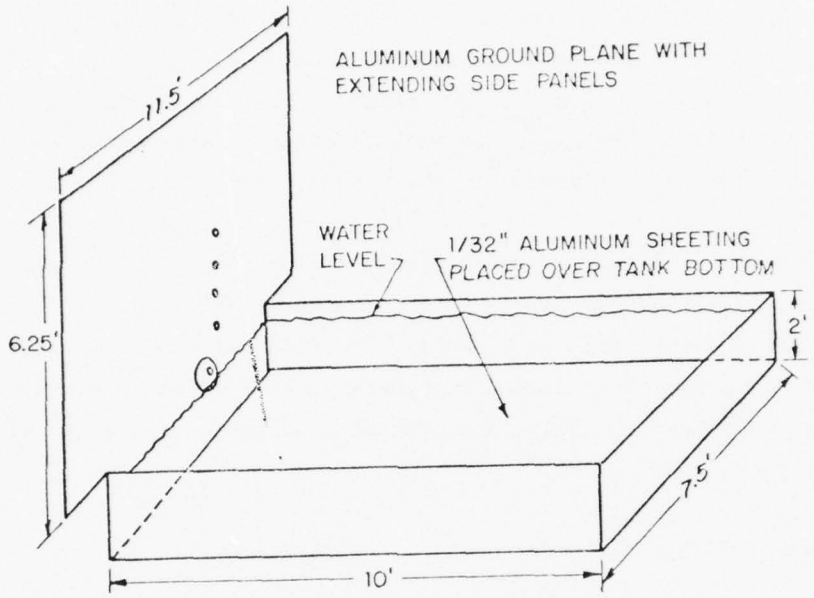
The matching technique used for the modified Beverage antenna in Section 1.5 allows it to be driven over water and a variety of media that would not have been possible with the conventional arrangement. The Beverage an-

tenna has been used exclusively, however, for measurements over the earth, and this situation is still of major interest. Modeling the Beverage antenna for the case over the earth is limited because of the difficulties encountered in varying the conductivity. Attempts have been made [33] to vary the earth's conductivity by mixing it with graphite or salt water but problems arose in obtaining uniformity in the conductivity. Modeling the Beverage antenna over water is quite different and, by adding salt, any conductivity from .04 - 10 mhos/m can be obtained with very little variation in ε_r. Therefore, scale models involving water can be easily handled when the specified σ falls within the above range. The difficulties associated with modeling the earth sometimes necessitate working with models for which σ cannot be properly scaled. Many times useful information can still be obtained under these conditions.

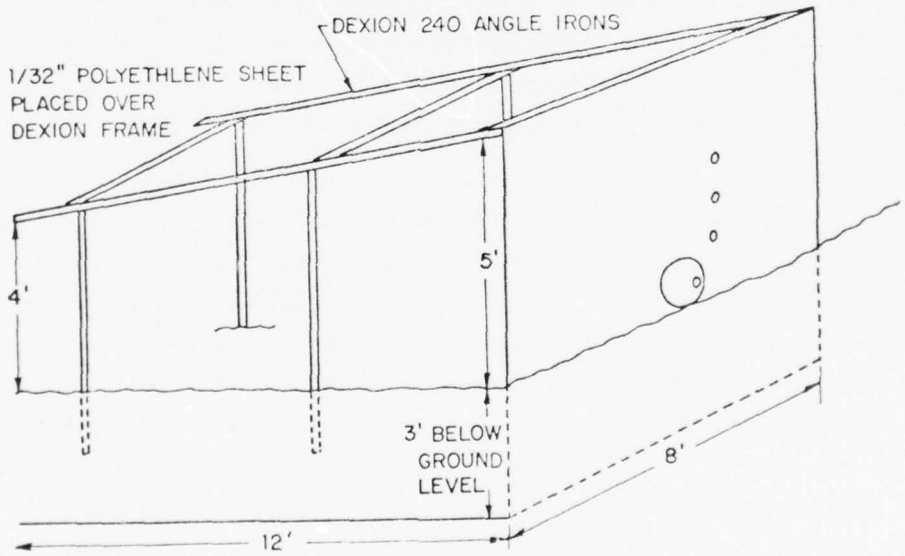
2.2. Half-Space Model and Choice of Operating Frequency

One of the first problems encountered in this experimental analysis was how to simulate properly the dissipative half-space. Due to size requirements it was necessary to use an area of convenient dimensions which would be large in comparison to a wavelength and could be assumed to behave as if infinite in extent without introducing serious errors. The accuracy of this assumption is critical to the validity of the experimental model.

Since the media over which the antennas were to be investigated had initially been determined, i.e., earth and water, it was necessary to construct experimental setups which could properly model a dipole antenna placed horizontally over these two different types of media. For water, a previously constructed tank (Fig. 2.1a) was filled and used to simulate an infinite half-space of water. The tank measured 10' × 7.5' × 2' and was constructed of 1/2" plywood. Along one side of the tank was fixed a large vertical ground plane, 11.5' × 8.25', made of 1/4" aluminum with extending side panels of fine mesh aluminum screening (Figs. 2.1a and 2.2a). The ground plane provides an imaging plane so that both the monopole, which is driven by extending the inner conductor of a coaxial line through a hole in the ground plane, and the medium in the tank may be perfectly imaged to simulate a center-driven dipole above a large body of dissipative material. For an accurate experimental model to be achieved, it is necessary that the ground plane be sufficiently large in terms of wavelengths that it can be considered infinite



a.) FACILITY FOR WATER HALF-SPACE MEASUREMENTS.



b.) FACILITY FOR EARTH HALF-SPACE MEASUREMENTS.

FIG. 2.1. EXPERIMENTAL HALF-SPACE MODELS FOR MEASURING ANTENNA PROPERTIES.

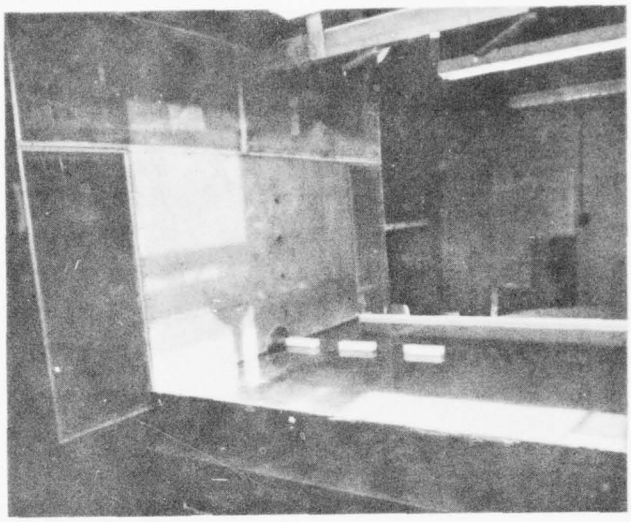


FIG. 2.2a EXPERIMENTAL SETUP FOR WATER MEASUREMENTS

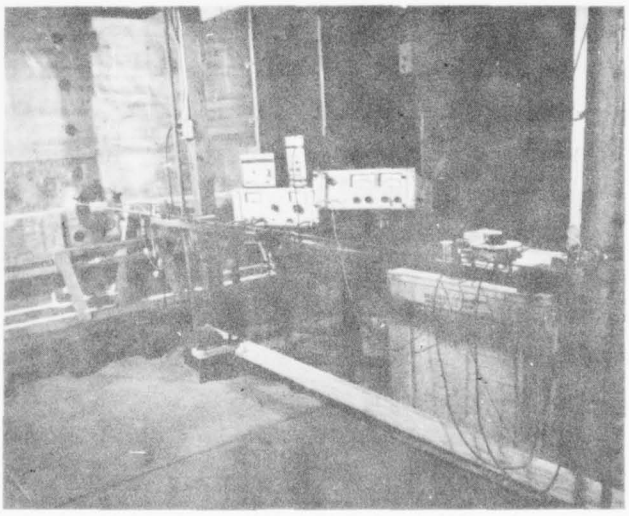


FIG. 2.2b BACK VIEW OF GROUND PLANE AND MEASURING EQUIPMENT

in extent.

For the measurements over the earth, a similar experimental setup was constructed. A vertical image plane, 8' by 8', of 1/4" aluminum was erected on a level section of ground. A trench was dug in order to allow the image plane to protrude approximately 3 feet below ground level (Fig. 2.1b). A metal frame was constructed behind the 5 feet of ground plane extending above the surface of the earth. Over this was spread a large sheet of polyethylene, 1/32" thick, to provide an enclosed working area where the equipment could be kept (Figs. 2.1b and 2.3b). Due to the size of the large field surrounding the ground plane, the earth could be considered infinite in extent for all practical purposes, eliminating the types of problems that can arise when using a finite-sized tank for the water measurements. The problems associated with the size of the ground plane remain to be considered for both cases.

Obviously, the operating frequency becomes a critical parameter for the two experimental setups described, in that areas of finite dimension must accurately replace infinitely large areas. Too low a frequency could produce wavelengths comparable in size to the tank or ground plane which would cause considerable diffraction effects and produce large errors in the measurements. It was also desirable to analyze antennas that could range up to several wavelengths in length. Due to these physical constraints, a lower bound on the operating frequency was imposed. To work at very high frequencies eliminates many problems (e.g., the ground plane and tank can be a large number of wavelengths in size), yet causes several others. Specifically, it is necessary to select an operating frequency which allows the radius of the antenna to be a small fraction of a wavelength in size. Since the construction of the antenna line (Section 2.3) necessitates a system of movable probes, the smallest mechanically feasible line was 1/8" or approximately 3 mm. in diameter. With the major purpose of the experimental investigation concerned with observing the effects of the half-space on the antenna properties as the height of the wire is varied over a large range of spacings ($.01\lambda_0$ - $.25\lambda_0$), the ratio of antenna radius to height, a/d, must be kept quite small. If this were not the case, at very small spacings above the medium ($.01\lambda_0$ and $.02\lambda_0$) the radius of the wire would be an appreciable part of the height, giving the distorted image of a thick antenna close to an imperfect conductor. The most important criterion in placing an

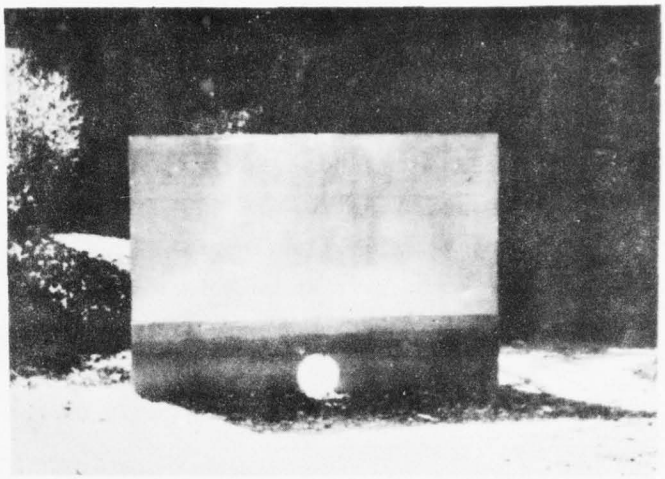


FIG. 2.3a GROUND PLANE FOR EARTH MEASUREMENTS

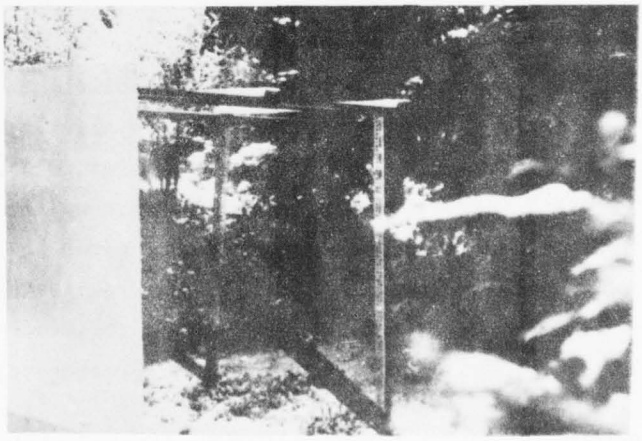


FIG. 2.3b REAR VIEW OF GROUND PLANE

upper bound on the frequency is concerned with the physical distances involved in the spacing from $.01\lambda_0$ to $.02\lambda_0$. Since the ability to work with increments of this size is desirable, it would be extremely difficult to insure uniformity of height along the length of the wire if the spacings were any less than 1 cm.

The discussion above provides various reasons for constraining the frequency range over which the available experimental setup could be used to model accurately a dipole antenna over an imperfect half-space. After all the above factors were taken into account, an operating frequency of 300 MHz was chosen. This frequency was selected with the hope that it would provide an optimal experimental model subject to the previously discussed constraints. The following reasons were considered:

1) At 300 MHz, $.01\lambda_0$ = 1 cm. This was determined to be just about the smallest distance above the water or earth that the wire could be placed and still insure that the spacing would be constant and that significant errors would not be introduced. At spacings very close to the interface, $d/\lambda_0 < .01$, height variations of $.001\lambda_0$ can result in significant changes in the wave number on the wire. Due to the thinness of the brass tubing, fluctuations of ±1 mm could easily exist on the long 150 cm antenna length used. To insure that this would not be a problem, spacings of at least 1 cm were determined to be the limit of accuracy possible.

2) At 300 MHz, $a/\lambda_0 = .0015$, which certainly obeys the thin-wire approximation and insures that a is considerably smaller than the closest spacing used.

3) At 300 MHz, the tank measures $3.1\lambda_0 \times 2.3\lambda_0$ while the ground plane is $3.4\lambda_0 \times 2.85\lambda_0$. In the water, the tank and ground plane appear considerably larger, almost by a factor of ten, due to the large relative dielectric constant. For the earth measurements, the ground plane measures $2.5\lambda_0 \times 2.5\lambda_0$ with the 3 ft. section underground appearing about 4 times larger. Although none of these dimensions seem large enough to assume realistically that they may be considered infinite in extent, a series of calibration checks were performed (Section 2.8) to show that these setups represent very accurate experimental models.

4) The chosen frequency of 300 MHz provides a convenient scaling factor of 10 to 1 in order to compare scale-model measurements with full-scale

systems being developed in the HF band.

2.3. Coaxial Measuring Line

The most important single piece of equipment used in this experimental analysis is the coaxial measuring line (Fig. 2.4). The antenna is formed by extending the inner conductor of the coaxial line out over the water or earth while mounting the outer conductor flush with the vertical ground plane (Fig. 2.2a). A series of holes, 1-1/2" in diameter, was cut in the ground plane through which the flanged outer conductor of the coaxial line could be mounted. Four individual holes were placed at heights of $.25\lambda_0$, $.5\lambda_0$, $.75\lambda_0$ and $1.0\lambda_0$ above the water level in the tank, where $\lambda_0 = 1$ m. For spacings ranging from just touching the water level to heights of $.125\lambda_0$ a large brass plate, 10-1/4" in diameter, was fitted into the ground plane. A hole, 1-1/2" in diameter, through which the coaxial line could be mounted and the center conductor extended, was placed eccentrically in the plate. The plate (Fig. 2.2a) could be rotated allowing the eccentric hole to vary in height above the water continuously. For the earth measurements, a similar arrangement with the brass plate was used (Fig. 2.3). Since the earth could not be extended above the 10-1/4" diameter hole in the ground plane used for the brass plate, the closest spacing obtainable was $d/\lambda_0 = .02$. The upper section of the ground plane contained a series of holes at heights of $d/\lambda_0 = .25, .5, .75$ and 1.0, identical to those made in the tank.

The actual construction of the coaxial measuring line is depicted in Fig. 2.4. The line was fabricated almost entirely of brass. The coaxial-feed section consisted of an outer conductor 5/8" in diameter with .032" wall thickness and an inner conductor 1/4" in diameter with .042" wall thickness. These sizes were chosen in order to obtain a 50 ohm characteristic impedance for the feed line. Two N-type connectors, through which an external power source could be coupled, were mounted on the coaxial line. These connectors were placed 25 cm and 62.5 cm, respectively, from the shorted end of the coaxial line. The distances, corresponding to $\lambda_0/4$ at 300 MHz and $5\lambda_0/4$ at 600 MHz, were chosen to insure sufficient power transfer to the antenna end of the line. A flange mounting was soldered to the antenna end to enable the line to be fastened securely to the ground plane. At this end, a 1/4" piece of rexolite was press-fitted between the inner and outer conductors to insure that the inner conductor remained centered.

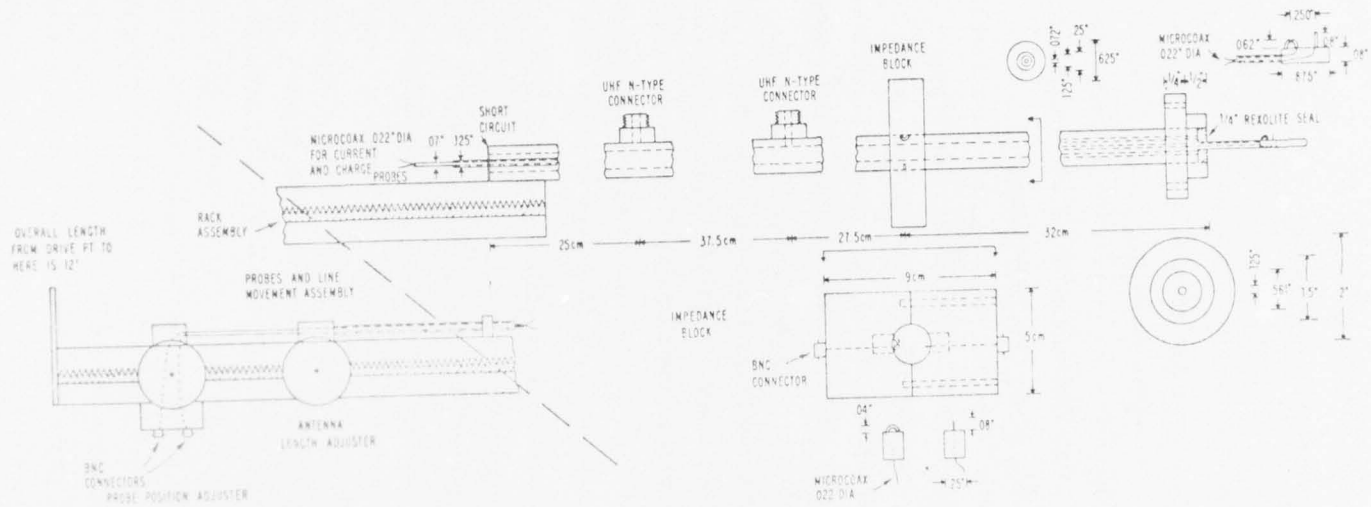


FIG 2.4 COAXIAL MEASURING LINE AND ANTENNA

Several other rexolite spacers were placed inside the feed line to accomplish the same purpose. At the antenna driving point the radius of the 1/4" section of inner conductor surrounded by the rexolite was decreased accordingly to insure a uniform 50 ohm characteristic impedance to the end of the line.

The antenna was constructed of 1/8" brass tubing with .02" wall thickness. This tubing was placed inside the inner conductor of the feed line and could be extended from or withdrawn into the feed line by a carriage mechanism attached to the short-circuited end of the feed line. With the present design the antenna could be extended out to a length of 2 meters. A scale was placed along the carriage, making it possible to calibrate accurately the antenna length while working behind the ground plane. A slot, .032" in width, was cut along the antenna. This slot provides a path for a small movable loop and monopole.

There are three important quantities that can be measured with the coaxial line. Two of them are the current and charge distributions that exist along the wire antenna. These measurements are accomplished by having a small shielded loop, .062" in radius, and a short monopole, .08" in height, move along the slot in the antenna (Figs. 2.4 and 2.5a). The loop responds to the tangential magnetic field which is directly proportional to the axial current, making the loop a sensitive current-detecting probe. The monopole makes an excellent charge probe since it is responsive to the radial electric field which is proportional to the charge distribution. The probes are constructed of microcoaxial cable, .022" in diameter, and are mounted on a strip of brass, .08" in width by .875" in length. The two microcoaxial cables, each over 12 feet long, were placed inside a stainless steel needle tubing, .070" in diameter with .01" wall thickness. One end of the stainless steel tube was soldered to the brass strip on which the probes were mounted. The stainless steel tubing containing the microcoaxial cable was passed inside the 1/8" antenna tube all the way back through the coaxial feed line and attached to a movable carriage assembly. The overall length of the stainless steel tubing is about 12 feet.

The carriage assembly enables the probes to be moved back and forth along the slot in the antenna by rotating the rack-mounted carriage knob from the rear of the ground plane. At the probe carriage knob the two mi-

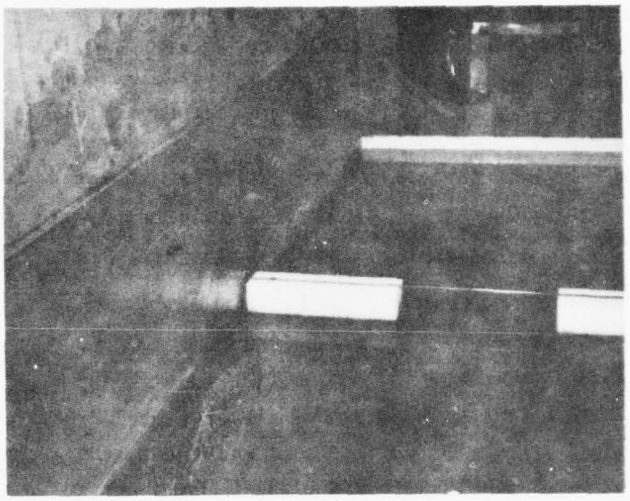


FIG. 2.5a ANTENNA DRIVING POINT AND CURRENT AND CHARGE PROBES

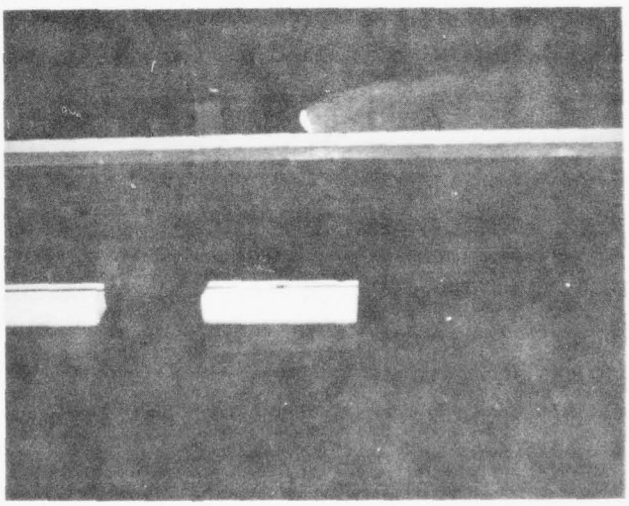


FIG. 2.5b RESISTOR AND QUARTER-WAVE SECTION

crocoaxial cables extend out from the stainless steel tubing into a small aluminum box where each is soldered to a BNC connector. Through the use of a vector voltmeter attached to the connector, continuous readings of current or charge distribution are possible.

Figure 2.2b shows the complete coaxial line and carriage assembly along with the accompanying measuring equipment. The entire apparatus extends for more than 12 feet back from the ground plane and is supported by a pulley system and locking clamps.

2.4. Impedance Measuring Probes

Along with the current and charge distributions, the third important antenna quantity to be measured with the coaxial line is the input impedance. This is accomplished by means of the impedance measuring block [34], [35] located on the coaxial feed line (Fig. 2.4). Inside the block are a small loop, .04" in radius, and a short monopole, .08" in length, which extend into the transmission line feeding the antenna and sense the current and voltage at that point on the line. BNC connectors located on the outside of the aluminum block allow the voltages from the probes to be monitored by a vector voltmeter. Figures 2.6a and 2.6b show the location of the impedance block in the feed line and a disassembled view of the block exposing the small sensing probes. Through an appropriate calibration procedure consisting of measuring the voltage and current probes' responses to both a match and a short circuit placed at the antenna driving point, it is possible to measure accurately the input impedance of the antenna.

The operation of the impedance measuring block is as follows. The antenna represents a lumped impedance at the end of the coaxial feed line. The monopole has a voltage output, V_B, proportional to the transmission-line voltage at that point while the loop's output voltage, V_A, is proportional to the current at this point. The Hewlett-Packard 8405A vector voltmeter is used to measure the voltage outputs and provide the relative phase information between V_A and V_B. Therefore, the input impedance of the transmission line at the plane of the probes is the ratio of the two measured voltages multiplied by an appropriate complex constant K.

$$Z_{AB} = |Z_{AB}| \, e^{j\phi_{AB}} = R_{AB} + jX_{AB} = |K| \frac{|V_B|}{|V_A|} e^{j[\phi_B - \phi_A + \phi_K]} \qquad (2.2)$$

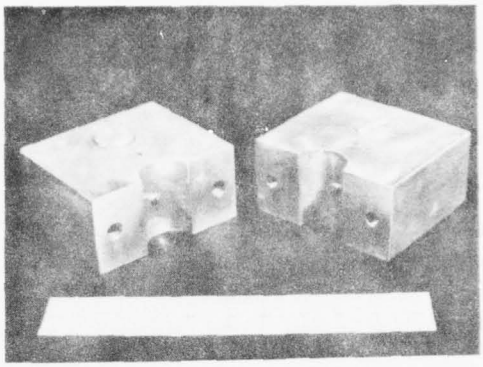


FIG. 2.6a IMPEDANCE MEASURING PROBES

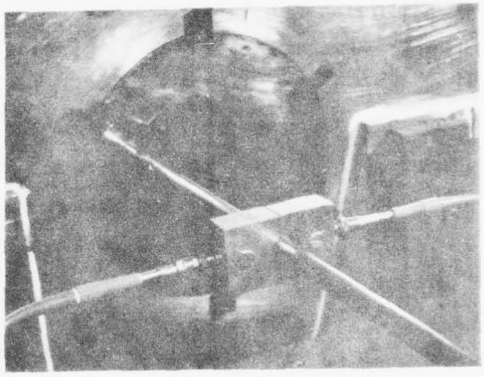


FIG. 2.6b IMPEDANCE BLOCK IN COAXIAL LINE

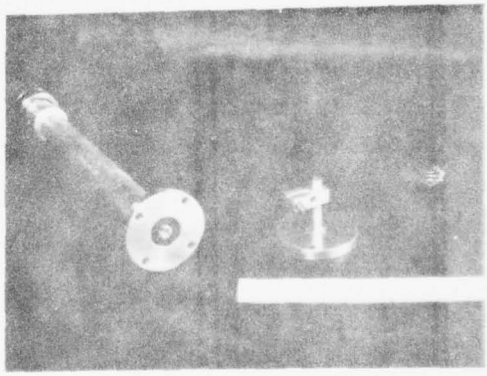


FIG. 2.6c 50Ω AND SHORT-CIRCUIT ADAPTERS

where

$$V_A = |V_A| e^{j\phi_A} , \quad V_B = |V_B| e^{j\phi_B} , \quad K = |K| e^{j\phi_K} \tag{2.3}$$

By knowing the characteristic impedance of the coaxial line and the distan from the plane of the probes to the driving point of the antenna, the inpu impedance of the antenna can be found by the impedance transformation equa tion, namely,

$$Z_{ant} = |Z_{ant}| e^{j\phi_{ant}} = Z_c \left[\frac{Z_{AB} - jZ_c \tan \beta_L \ell}{Z_c - jZ_{AB} \tan \beta_L \ell} \right] \tag{2.4}$$

For the coaxial line used, $Z_c = 50$ ohms and $\beta_L = \beta_0$ for a lossless section of transmission line. Thus, in order to measure the antenna input impedan it is necessary to determine the constant K and the electrical length $\beta_0 \ell$ the operating frequency of 300 MHz.

In order to measure K and $\beta_0 \ell$ accurately, the following calibration procedure was used:

1) Terminate the coaxial line with a precision 50 ohm load and adjust the input power level so that a signal of 5 mV is read on V_B, the voltage probe. Measure the voltage V_A at the current probe. This voltage now becomes a reference level used throughout to measure unknown impedances. Fr this measurement, $|K|$ is determined as follows:

$$|K| = \frac{50 \text{ ohms}}{5 \text{ mV}} V_A \tag{2.5}$$

2) Replace the 50 ohm load with a short-circuit adapter which terminates the coaxial line at the ground plane with a short circuit. Set V_A t the previously measured reference voltage and measure the voltage V_B. Uti izing the formula for the impedance transformation of a short-circuit section of lossless transmission line, this measurement gives:

$$\beta_0 \ell = \tan^{-1} \left[\frac{V_B(\text{short circuit})}{5 \text{ mV}} \right] \tag{2.6}$$

3) With the short circuit still in place, adjust the phase offset on the vector voltmeter such that the phase difference between V_A and V_B is

zero. Connect both probes of the voltmeter through a tee to V_A and measure the phase difference ϕ_{AB}. This is the constant phase offset due to the response of the probes. The vector voltmeter must be adjusted to this offset when making impedance measurements. On a short-circuited section of transmission line the impedance is reactive at all points with the current and voltage always 90° out of phase. Therefore, from this measurement ϕ_K is:

$$\phi_K = 90° - \phi_{REF} \tag{2.7}$$

With all the necessary quantities determined, the procedure to follow in measuring an unknown impedance is:

i) Set voltage V_A to the reference level determined in step 1. Measure voltage V_B and calculate the magnitude of the unknown impedance by:

$$Z_{AB} = [50V_B/5 \text{ mV}] \text{ ohms} \tag{2.8}$$

ii) Connect both probes through a tee to voltage V_A and adjust the phase difference between the probes to ϕ_{REF}. Measure the phase difference between V_A and V_B and calculate the angle of the unknown impedance by:

$$\phi_{AB} = (\phi_B - \phi_A) + 90° \tag{2.9}$$

iii) Use (2.4) to evaluate the unknown impedance at the driving point of the antenna.

In the calibration procedure, several special pieces of equipment (Fig. 2.6b) had to be fabricated to provide a match and short circuit at the antenna driving point. In the design of the coaxial feed line, it was necessary to place the impedance block far enough away from the end of the line to insure that higher-order modes due to the end effect were sufficiently attenuated. A distance greater than 10(b - a) is usually considered sufficient for this purpose. The impedance block should also be located so that with a short-circuit termination the probes do not lie close to a null. If otherwise, the accuracy of calibration would be seriously jeopardized. Since an operating frequency of 300 MHz had been predetermined, the block was placed at 32 cm from the driving point in the hope of avoiding any serious calibration problems. Using the procedure in step 2, the physical distance between the end of the line and the impedance block was determined to

be 32.47 cm at 300 MHz. The additional length is due to the end effect of the coaxial line and the piece of rexolite located at the junction.

2.5. Measurement of the Electrical Properties of Water

Numerous techniques have been utilized to measure the electrical properties of dissipative media [36]-[38]. All have been shown to give accurate results over various frequency ranges. In order to make an accurate experimental analysis of antennas over dissipative media, a suitable determination of the electrical properties of the media is necessary. Fresh water and salt water having previously been chosen as two of the media of interest, it was essential to be able to determine accurately their electrical properties. For a given frequency and temperature the electrical properties of either of the above solutions can be fully characterized by an effective permittivity ε and an effective conductivity σ. It can be assumed that the permeability of these two solutions is equal to that of free space, i.e., $\mu_0 = 4\pi \times 10^{-7}$ Henry/m. The real and imaginary parts of the propagation constants of these media are related to ε and σ by the following relationships:

$$k = \beta - j\alpha = \omega[\mu_0\varepsilon(1 - jp)]^{1/2} = \omega(\mu_0\varepsilon)^{1/2}[f(p) - jg(p)] \tag{2.10a}$$

$$f(p) = \{(1/2)[(1+p^2)^{1/2} + 1]\}^{1/2} \quad , \quad g(p) = \{(1/2)[(1+p^2)^{1/2} - 1]\}^{1/2} \tag{2.10b}$$

where

$$p = \sigma/\omega\varepsilon \tag{2.10c}$$

and

$$\varepsilon_r = \varepsilon/\varepsilon_0 = \frac{1}{\omega^2\mu_0\varepsilon_0}(\beta^2 - \alpha^2) \tag{2.11a}$$

$$\sigma = \frac{2}{\omega\mu_0}\alpha\beta \tag{2.11b}$$

An experimental apparatus previously designed by Smith [35] was used to measure the values of α and β for the fresh-water and salt-water solutions. The measuring apparatus, shown in Fig. 2.7a, consists of a water-filled section of transmission line. A signal is introduced at one end of the line

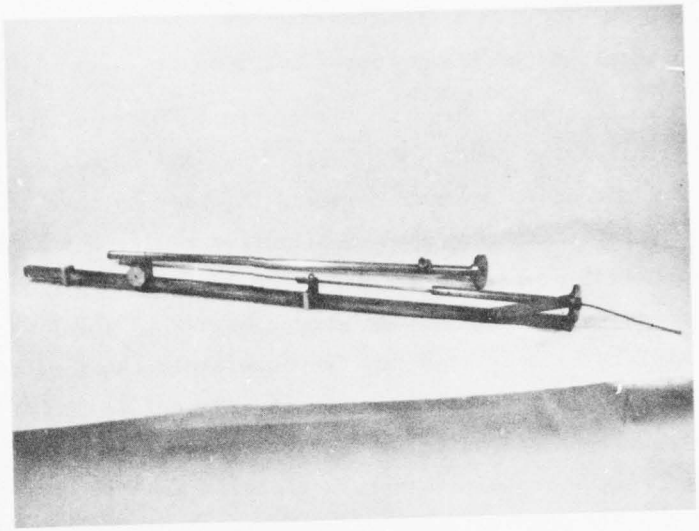


FIG. 2.7a TRANSMISSION LINE FOR MEASURING THE ELECTRICAL PROPERTIES OF WATER

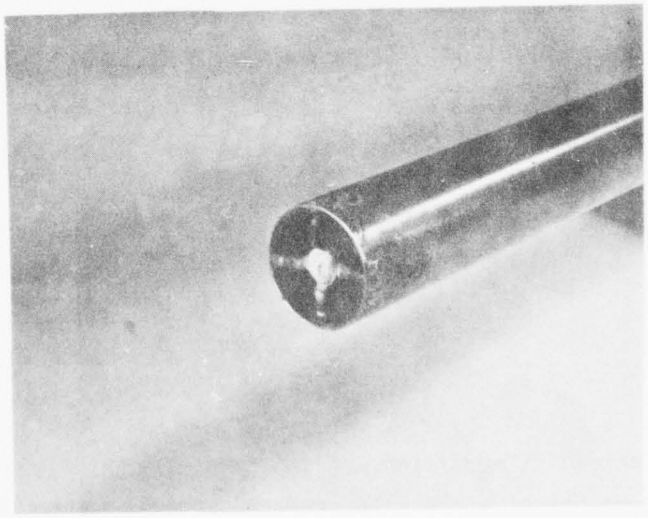


FIG. 2.7b MATCHING RESISTORS TERMINATING THE COAXIAL LINE

and the opposite end is terminated in a match. The inner conductor has a slot cut in it and a current probe is allowed to move along the slot by means of a carriage assembly similar to the antenna line. The probe is connected to a vector voltmeter which measures the relative amplitude and phase of the signal on the transmission line. With this apparatus the attenuation and phase shift per unit length can be measured and the components of the propagation constant determined as follows:

$$\alpha \text{ (Nepers/m)} = 11.51 \times \alpha' \quad \text{(measured attenuation dB/cm)} \tag{2.12a}$$

$$\beta \text{ (radians/m)} = 1.745 \times \beta' \quad \text{(measured phase shift °/cm)} \tag{2.12b}$$

The matching was accomplished by resistively loading the end of the coaxial line (Fig. 2.7b). With the line placed in a distilled-water solution the characteristic impedance is determined to be 8.05 ohms. A parallel combination of two 27 Ω and two 36 Ω resistors equivalent to 7.8 Ω, was soldered to the end of the line and shown to provide a good match [35]. When the conductivity of the solution is increased, the line will no longer be matched. To correct for this, the load was located well beyond ($> 5\ \lambda_w$) the position of maximum probe travel. Hence, with increased conductivity the incident and reflected waves in this extension were sufficiently attenuated so that a good match would still exist along the section of probe travel.

The above analysis assumes that only a TEM wave exists on the coaxial line. The construction of the line consists of a 1/4" inner conductor and 7/8" outer conductor with .03" wall thickness. For a coaxial line of these dimensions, immersed in a salt-water solution with $\sigma = 6$ mhos/m and $\varepsilon_r = 80$, the condition $f << 600$ MHz must be satisfied to insure only the presence of the TEM mode. Subject to this restriction, all measurements were made at 100 MHz to avoid higher-order modes. Smith [35] has shown that this apparatus can be used to give acceptable results at frequencies as high as 100 MHz. Measurements [39] have shown that the electrical properties of water change insignificantly over a range of 100 MHz to 300 MHz. Therefore, measurements made at 100 MHz should introduce very little error into the experimental analysis being carried out at 300 MHz.

The electrical properties of three different solutions were measured using the above technique. The amplitude and phase distributions for each of the solutions are illustrated in Fig. 2.8. The traveling-wave nature of

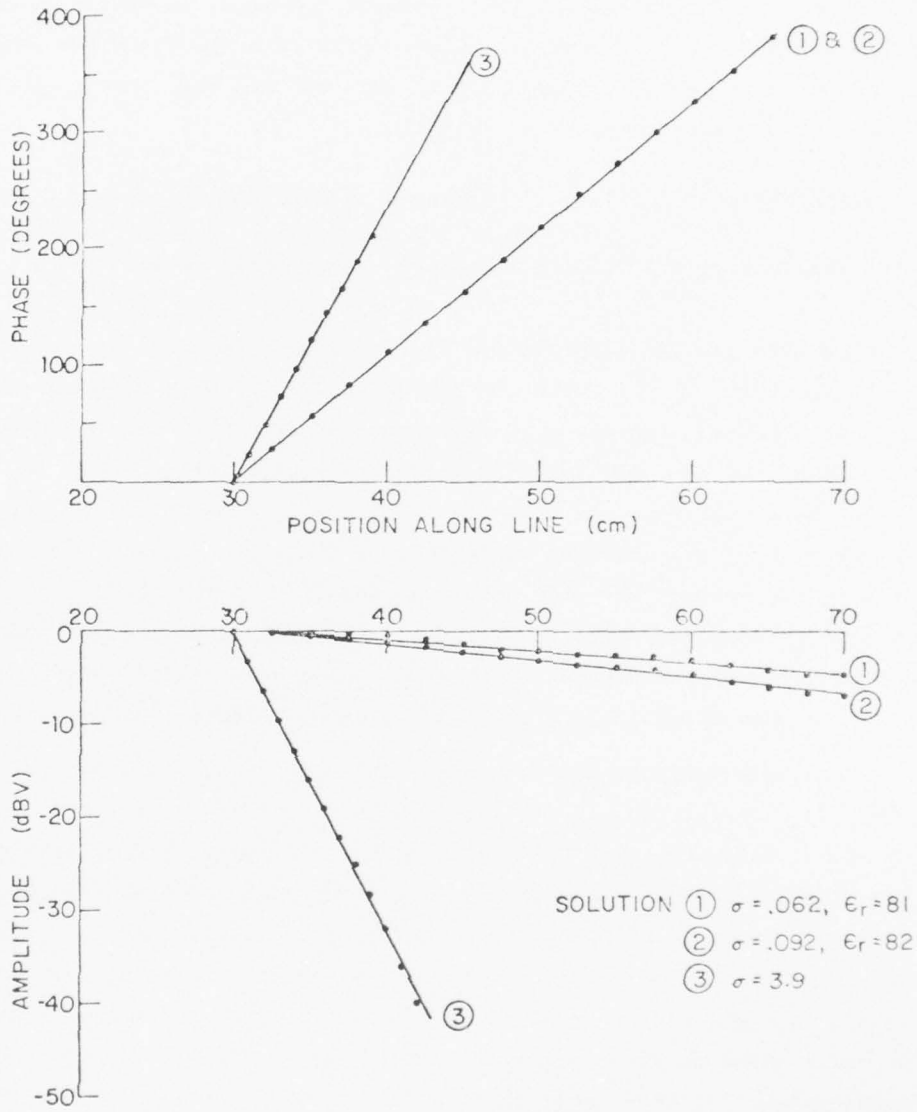


FIG. 2.8. MEASURED AMPLITUDE AND PHASE IN WATER FILLED COAXIAL LINE AT 100 MHZ.

the signal is evident. The measured σ and ε_r of each solution are also given in Fig. 2.8. Note that due to the inherent inability to measure ε_r accurately for highly conducting solutions [35], [38], erroneous results occur for ε_r in solution 3. This difficulty is overcome by assuming that ε_r remains significantly unchanged from the values measured in solutions 1 and 2.

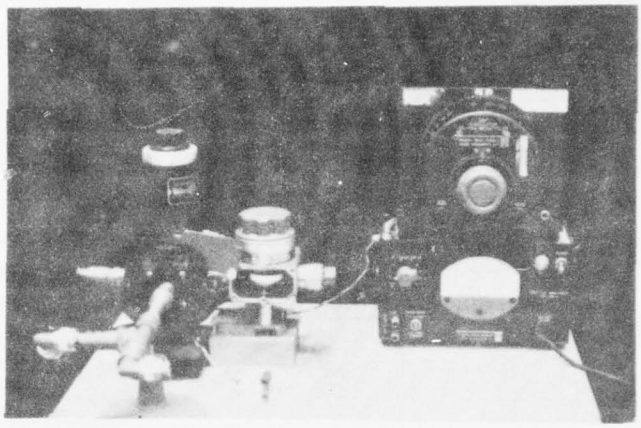
2.6. Measurement of the Electrical Properties of Earth

With earth being the third medium over which antenna measurements were to be made, it was necessary to be able to determine its electrical properties. It is obvious that the previous technique in Section 2.5 for measuring the properties of saline solutions cannot be used for earth. Standard techniques have been developed [26], [39], [40] to measure accurately the electrical properties of solid materials as well as of granular-type materials such as powders or earth. For present purposes, a Hartshorn-type dielectric sample holder [41] corresponding to ASMT standards was used to measure ε_r and σ of various earth samples. The sample holder, which is essentially an air-filled capacitor with variable plate spacing, was used in conjunction with a General Radio 1602-B admittance meter (Fig. 2.9a) to measure the admittance of the earth samples.

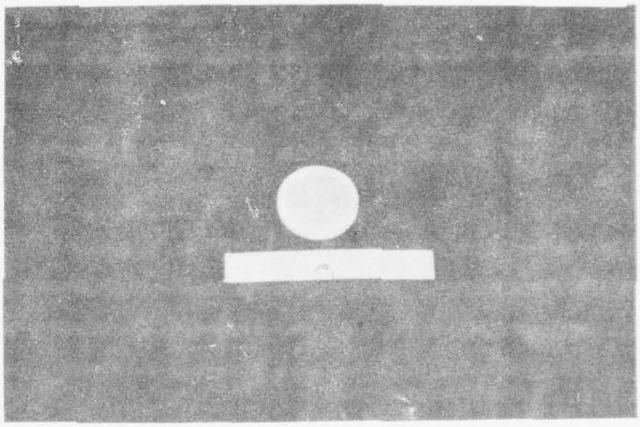
The samples were prepared by placing a small amount of the earth to be measured inside a ring of Teflon (Fig. 2.9b). The ring measured .254" thick with an inner diameter of 1.249" and an outer diameter of 1.638". Over the top and bottom of the ring was placed aluminum foil, sandwiching the earth sample and providing good electrical contact to the plates of the sample holder.

The block diagram for the sand measurements is shown in Fig. 2.10. The sample is placed in the holder and its admittance determined by means of the General Radio admittance meter [42]. The meter is a 5-port device with two ports used for signal input and signal detection. The signal at the operating frequency desired is fed into one port while a heterodyne detector is placed on the output port. The other three ports are terminated, respectively, with a conductance standard (50 Ω load), an admittance standard, and the unknown consisting of the sample in the dielectric holder. A coupling loop is found in each of these three ports and the combined output of the three loops is fed in parallel to the detector. By adjusting the coupling

a)



b)



c)

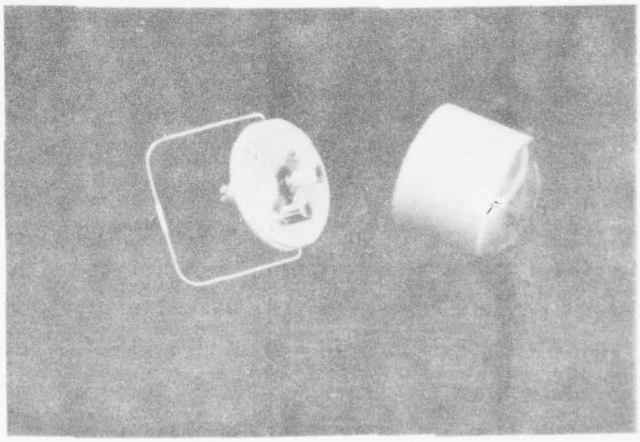


FIG. 2.9 a) EXPERIMENTAL SETUP FOR MEASURING THE ELECTRICAL PROPERTIES OF EARTH b) TEFLON RING WITH EARTH SAMPLE c) GENERAL RADIO COMPONENT MOUNT

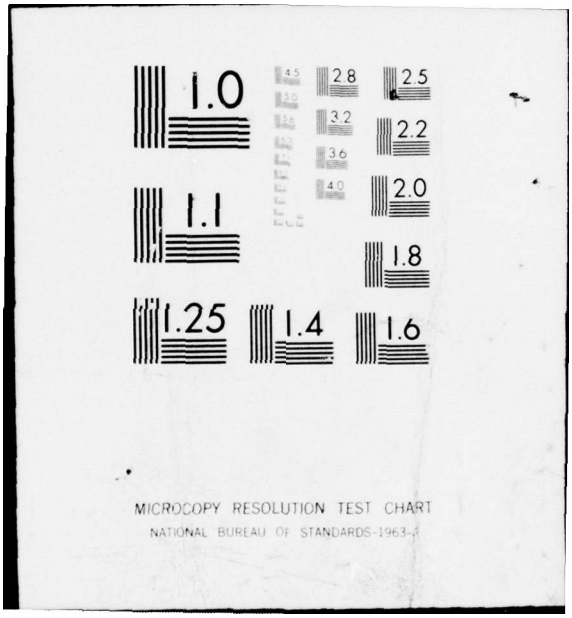
AD-A040 377 HARVARD UNIV CAMBRIDGE MASS GORDON MCKAY LAB F/G 9/5
THE BEVERAGE WAVE ANTENNA: CURRENTS, CHARGES AND ADMITTANCES. V--ETC(U)
FEB 77 R M SORBELLO F19628-76-C-0057
UNCLASSIFIED SCIENTIFIC-1 RADC-TR-77-82-VOL-1 NL

2 OF 2
AD
A040 377



END

DATE
FILMED
6-77


1.0
1.1
1.25
1.4
1.6
1.8
2.0
2.2
2.5
2.8
3.2
3.6
4.0
4.5
5.0
5.6
MICROCOPY RESOLUTION TEST CHART
NATIONAL BUREAU OF STANDARDS-1963-A

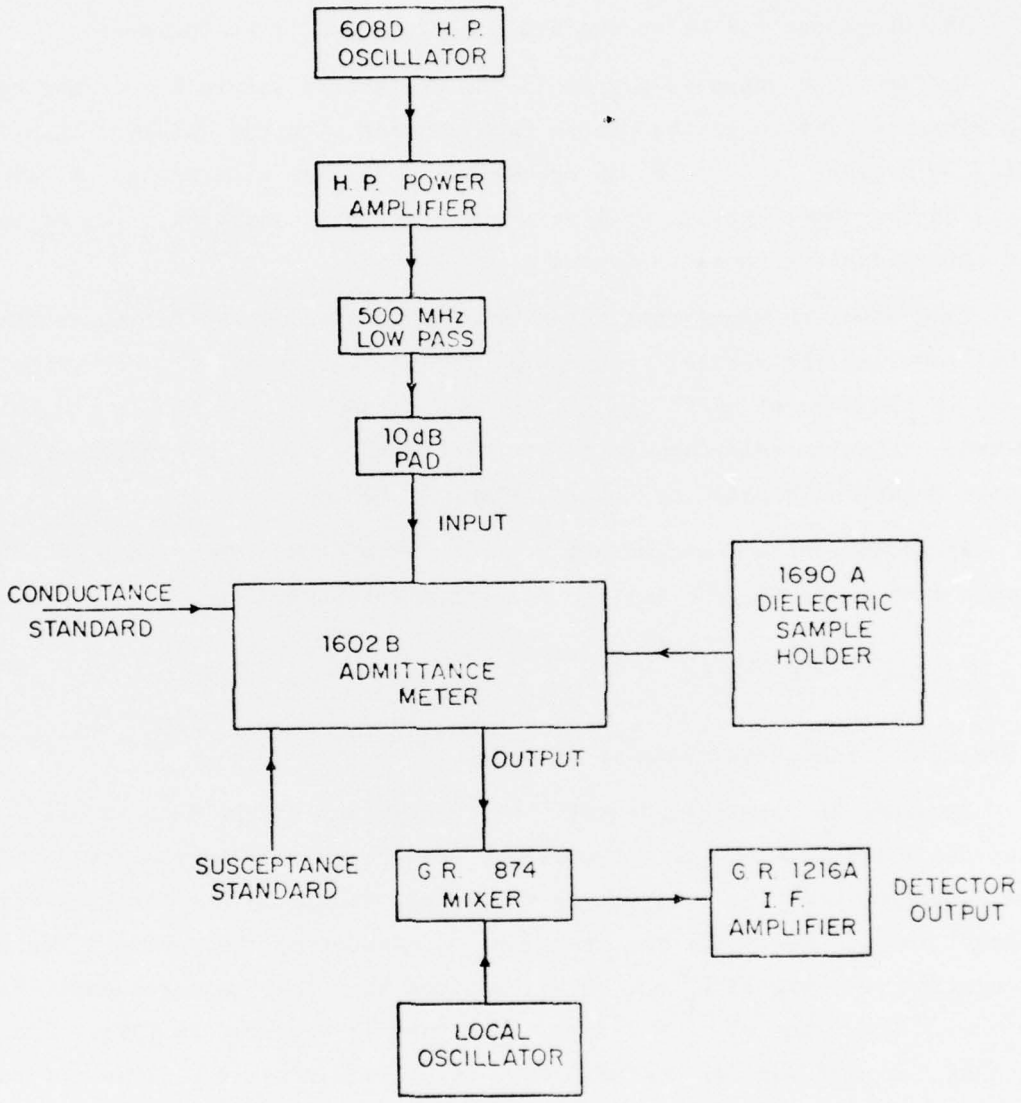


FIG. 2.10. BLOCK DIAGRAM FOR MEASUREMENT OF ELECTRICAL PROPERTIES OF EARTH.

of each loop it is possible to reduce the detector reading to zero and obtain the admittance of the unknown sample through the calibrated scales associated with each of the three loops.

The procedure for measuring σ and ε_r for sand is as follows:

1) Place the prepared sample in the dielectric sample holder and adjust the plate spacing until the plates make contact with the sample. This is noted by a clutch release which prevents any further tightening. A vernier scale on the sample holder will give the exact plate spacing, t_1. Adjust the three coupling loops to obtain a null.

2) Remove the sample and adjust the plate spacing and G loop to obtain a null, noting the vernier reading for the plate spacing, t_2. By using formulas in the General Radio manual, the capacitance of the sample can be obtained. Relating this capacitance to the capacitance C_0 of the air-filled sample holder with plate spacing t_1 gives ε_r for the earth.

3) To determine σ one merely needs to obtain the conductance of the sample from the meter and use the following relationship,

$$G = \sigma C_0/\varepsilon_0 \tag{2.13}$$

where C_0 has been determined in step 2.

In order to obtain accurately the capacitance of the sand sample in step 2, it is necessary to subtract out the capacitance of the Teflon ring. The capacitance of the ring can be determined easily by the procedures in steps 1 and 2. When this was done and the dielectric constant for Teflon determined, a value of $\varepsilon_r = 1.98$ was arrived at. This compares quite favorably with the value of $\varepsilon_r = 2$ to 2.2 obtained from handbooks [39]. Since most of the sand samples measured were relatively low-loss, it was often difficult to measure small changes in conductance accurately on the admittance-meter scale. To obtain more accurate conductance readings a technique developed by Smith [43] was utilized in which a small vernier capacitor associated with the sample holder was used to obtain the equivalent change in capacitance associated with the conductance of the sample.

The admittance-meter technique has been shown to be accurate for frequencies between 20 and $900/\varepsilon_r^{1/2}$ MHz. Since ε_r was unknown, it was decided to have all measurements made at 100 MHz. Again it was assumed that the

electrical properties of the sand would not drastically change from 100 MHz to 300 MHz.

2.7. Measurement of Load Resistors

For the Beverage antenna, it is necessary to resistively load the horizontal wire in addition to placing a quarter-wave section of line behind the resistor as shown in Fig. 2.5b. The loading was accomplished by inserting a 1/2 Watt ohmite carbon resistor into the line. The resistor leads were cut short and brass collars were soldered on the leads so that at one end the resistor could be press-fitted into the line while the other end was soldered directly to the quarter-wave section. The 1/2 Watt size was chosen because the diameter of the cross section measures .140" which is comparable to the .125" cross-sectional diameter of the antenna. Due to a small bulging effect caused by the slot cut along the tubing, the diameter of the cross section is actually somewhat larger than .125", providing a fairly smooth transition from tubing to resistor.

With measurements being made at 300 MHz, it was necessary that the resistors used be accurate up to this frequency and produce as little stray inductance as possible. To determine this, a systematic set of measurements was made on the resistors used. Initially the face-values of the resistors were compared to the d.c. resistances measured on a Simpson meter and a 8000A Fluke DVM. Next, the impedance of each resistor was measured at 300 MHz on a slotted line. This was accomplished with the use of a General Radio 874 ML component mount, shown in Fig. 2.9b. The complex impedance of the resistor was determined by terminating a slotted line with the component mount containing the resistor under test. By measuring the VSWR and null shift [26] on the slotted line, the impedance of the resistor could be determined. The ohmite carbon resistors proved to have excellent characteristics at 300 MHz. Almost negligible inductance was measured and the resistances determined were within 10% of the measured d.c. values.

2.8. System Calibration

It has been previously noted that for this experimental analysis certain assumptions have been made concerning the models used. Specifically, no justification has been given to determine when a finite-sized object such as a ground plane or tank can be approximated as being infinitely large or,

for that matter, how much error is involved in making this assumption. It is also important to investigate how accurate the measuring techniques and equipment used in the analysis are. To solidify the foundation of this work it was necessary to calibrate accurately the critical components of the experiment and provide precise checks on the major assumptions involved.

Impedance Calibration

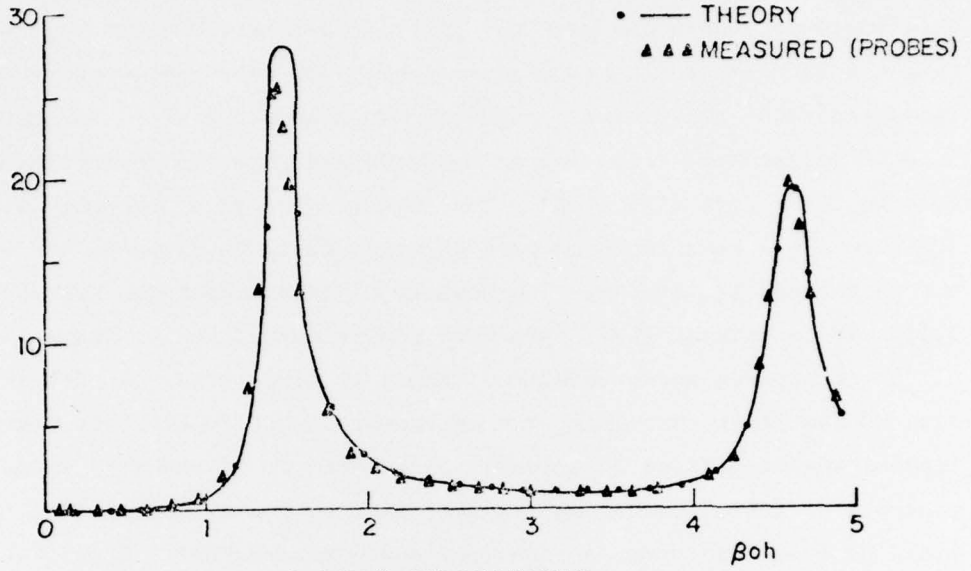
Precision impedance measurements require that the ground plane be as large as possible. Due to physical limitations in size, the ground plane used measured approximately $3\lambda_0 \times 3\lambda_0$. The effects of finite-sized ground planes on impedance measurements have been investigated by several authors [44], [45]. The work done by Hahn and Fikioris leads to the conclusion that the impedance of full-wave monopoles measured on a circular ground plane will be in error by less than 2% if the radius of the plane is at least 6λ, and in error by less than 4% for a radius of 4λ. Meier and Summers have shown that by making the image plane rectangular, the error can be decreased even further. With the present ground plane having an equivalent radius of only $1.5\lambda_0$, the anticipated error might be expected to exceed 10%. Along with the utilization of a rectangular ground plane, Andrews [46] has shown that by placing the antenna off center the image plane can be made effectively larger, thus further reducing the impedance error. This technique of placing the antenna off center was employed for all the impedance measurements made throughout this analysis.

The above arguments would tend to suggest that, for the experimental arrangement used, large errors could arise in the impedance measurements. Fortunately, these arguments hold only for measurements on free-space antennas. In the presence of the dissipative half-space, interaction between the antenna and the medium causes the fields to be concentrated in a region closely surrounding the wire. In fact, one of the major assumptions in King's theory is to presume that the radiation into the air is insignificant compared to the radiation into the dissipative medium. If this assumption is shown to be valid, then it is possible to use a much smaller ground plane and still obtain quite accurate measurements. Finally, it is worthwhile to note that the previous investigations [44], [45] represent a worst-case analysis and essentially only place an upper bound on the possible errors involved.

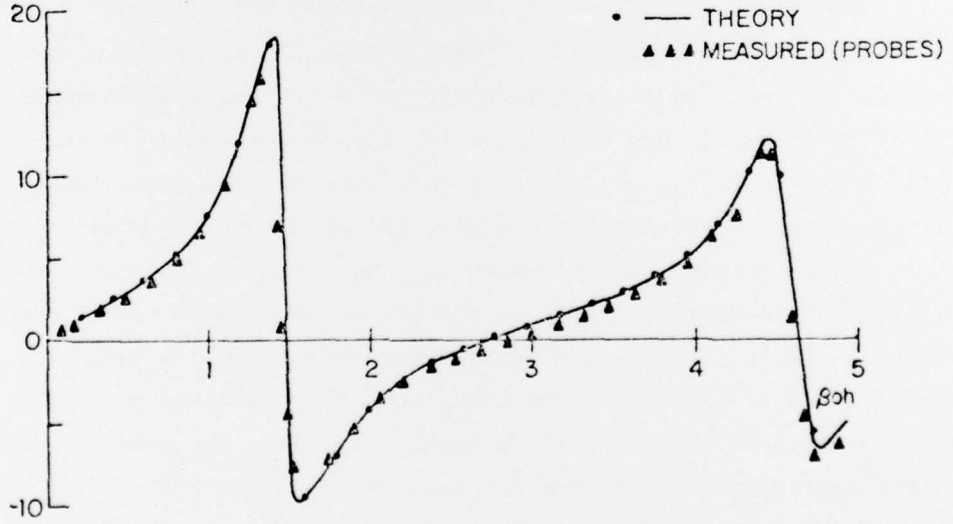
Using the present measuring facilities, it was decided to determine approximately how much error would be involved in the impedance measurements. This would provide a check on the finite-sized ground plane and could also give a good measure of the accuracy obtainable from the impedance block and its associated calibration procedure. To accomplish this, the input impedance of an isolated monopole was measured and compared to tabulated results for the TEM theory [47], [48]. For electrically thin antennas ($a/\lambda_0 \leq .01$), TEM theory has been shown to give accurate approximations to the actual apparent antenna admittance. The results of this comparison are shown in Fig. 2.11. It is evident that, even with the relatively small image plane, the agreement between measurement and theory is quite good. In the critical area of the first resonance, the agreement is within 10%, but for all other lengths the comparison is actually much better. If the wire were in the presence of a dissipative half-space, it can be anticipated that the error would be even less than for the free-space measurement. Thus, accurate results can be obtained through the use of the impedance block and, by using this technique along the ground plane, available impedance measurements can be accurate to within 5%.

Calibration of Current and Charge Measurements

Critical to the accuracy of any current or charge distribution measurement is the need for precise measuring probes. The probes should be made sufficiently small such that, ideally, they would sense yet not disturb the field being measured. In practice this becomes impossible; yet, for most cases, if the probes are quite small, the effect of the presence of the probe can be neglected. An extensive investigation into the use of electrically small loops and dipoles as electromagnetic field probes was made by Whiteside [49]. From this investigation, Whiteside concluded that center-loaded circular loops with diameters less than .01λ and monopoles of comparable height make excellent field-sensing probes. The monopole responds only to the tangential E field and for lengths less than .01λ the averaging effect of the probe is small. The loop is sensitive to the B field normal to the surface area of the loop but may also be responsive to the axial E field. Whiteside showed that it is advantageous to make the shielded loop even smaller than .01λ in order to decrease the averaging effect of the loop and to reduce its sensitivity to the axial E field, which may become a source of error in current measurements near the end of the antenna.



a) INPUT CONDUCTANCE



b) INPUT SUSCEPTANCE

FIG. 2.11 COMPARISON OF MONOPOLE APPARENT ADMITTANCE MEASURED BY IMPEDANCE PROBES WITH PREDICTED THEORY. $a/\lambda_0 = .0015$ AND $b/a = 2.3$.

The probes used for this experimental analysis consisted of a current-sensitive, shielded loop with $a/\lambda_0 = .0015$ and a charge-sensitive monopole with $h/\lambda_0 = .002$. Both were constructed of microcoaxial cable of .022" diameter and are small enough to fall well within the range predicted for accurate field measurements.

In order to provide a check on the accuracy of the probe response, the loop and monopole were calibrated against a known field by comparing the measured probe responses on a transmission line to the actual sinusoidal current and charge distributions that are known to exist on the line. This comparison is given in Fig. 2.12. The agreement is very good over a dynamic range of at least 30 dB. Therefore, one can expect the measured current and charge distributions to be quite accurate and to have very little error introduced due to the probes.

Effects Due to the Finite-Sized Tank

Throughout the previous discussions on the experimental tank model the assumption was made that a 7.5' × 10' × 2' body of water could accurately represent a dissipative half-space. This assumption is vital to the overall accuracy of the experiment. Specifically, it presumes that reflections from the bottom and side walls of the tank are negligible and that any diffraction effects due to the finite size of the tank can be neglected. A series of experimental checks were made to determine the validity of this assumption.

In the original modifications on the tank it was decided to place a 1/32" aluminum sheet along the bottom of the tank in order to evaluate the exact nature of the reflections. This determination is critical since, if reflections should be shown to present a problem, it would become necessary to model this situation mathematically as two coupled antennas between which is sandwiched a lossy medium - a problem different from the one originally intended to be studied. It was decided that if reflections from the bottom of the tank were found to be significant, a sufficient amount of salt would be added to the water to attenuate the unwanted reflections. This would necessarily place a limit on the conductivity range that could be used in the tank.

To determine what effect, if any, reflections from the bottom surface of the tank would have, two sets of impedance measurements were made at

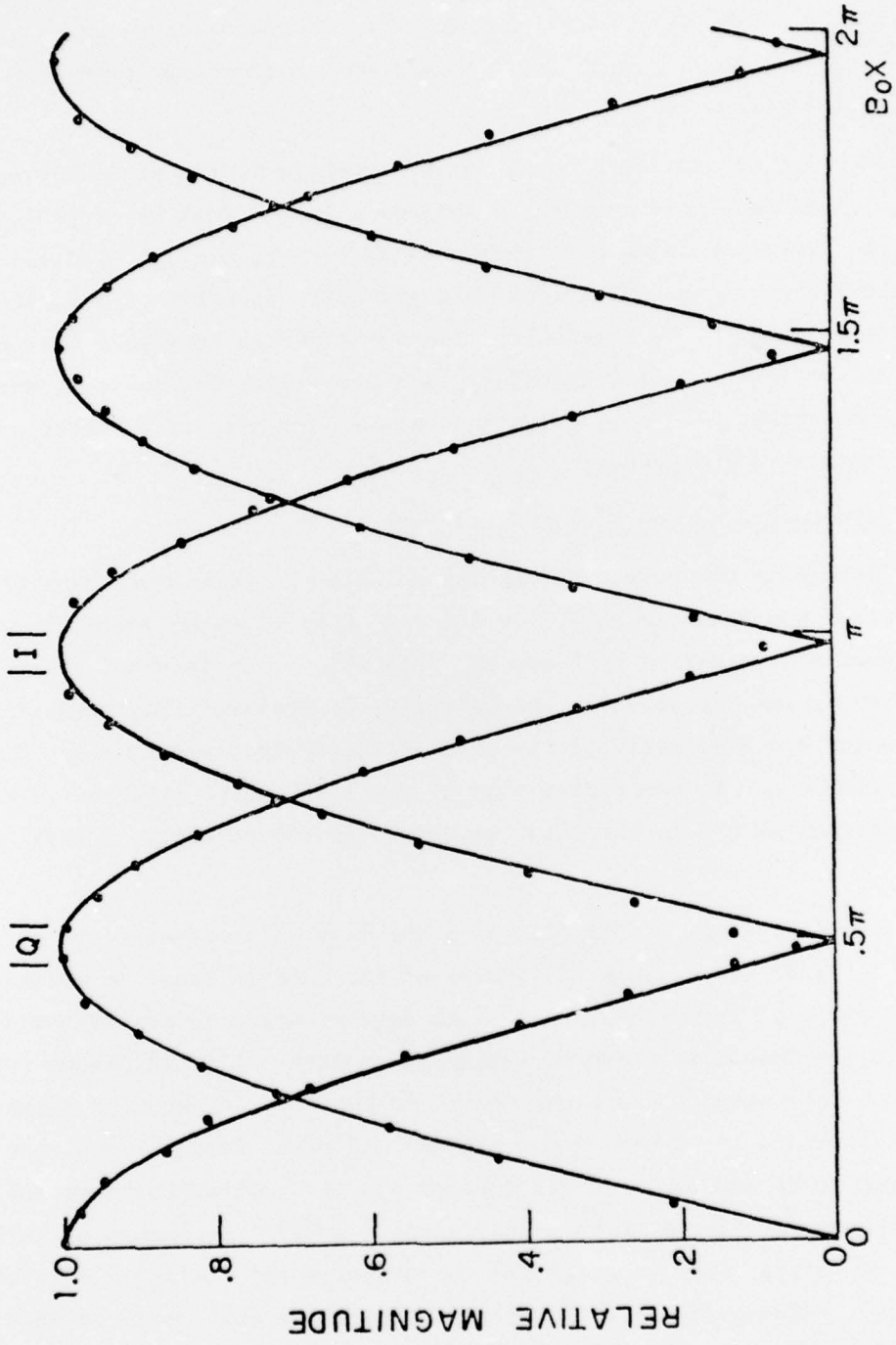


FIG. 2.12. CALIBRATION CURVES FOR CURRENT AND CHARGE PROBES

$d/\lambda_0 = .02$. In one case, the water depth was 54 cm, while in the other the depth was increased to 57 cm. The antenna input impedance is quite sensitive to the presence of any reflecting bodies and tends to be a much more accurate indicator than either the current or charge distribution. For the initial fresh-water measurements ordinary tap water with measured constitutive parameters $\varepsilon_r = 81$ and $\sigma = .04$ mhos/m was used. At 300 MHz the skin depth for this solution is 1.2 m, considerably larger than the 57 cm water depth. Figure 2.13 compares the input admittance of a monopole over fresh water with $d/\lambda_0 = .02$ for water depths of 54 cm and 57 cm.

The three-centimeter difference in water depth, which is equivalent to approximately a $.3\lambda_w$ change in the water, shows that the input admittance is dependent on water depth and, therefore, significant reflections are present from the tank bottom. To eliminate this, salt was added to the water. It was previously determined that, by making the conductivity $\sigma = .09$ mhos/m, the skin depth becomes approximately 52 cm, insuring that the reflections are eliminated. Since the conductivity in local fresh-water lakes such as Upper Mystic Lake was measured to be $\sigma = .063$ mhos/m, the additional salt does not alter the solution significantly from a real fresh-water situation. With $\sigma = .09$ mhos/m, a similar set of admittance measurements was made for the two different water depths. The results are given in Fig. 2.14. The two admittance curves agree quite well with a maximum variation of about 7% occurring at the first resonance. Since exact comparisons in the resonance region are difficult to obtain even for identical sets of measurements, it is reasonable to assume that the conductivity has all but cancelled the reflections from the tank bottom. Thus, for water solutions with $\sigma \geq .09$ mhos/m the tank appears to be infinitely deep.

It was previously noted that when an antenna is in close proximity to a dissipative half-space, the electromagnetic field remains in a region closely surrounding the wire with most of the radiation going into the dissipative medium. Anticipating this type of behavior, it is reasonable to assume that only a small area, consisting of the section of interface directly under the wire, is strongly coupled to the antenna. If this is the case, then only a finite section of medium is actually needed to approximate accurately an infinite half-space.

It also became necessary to determine if the tank was wide enough to preclude any erroneous contributions due to "edge effects." Since the dis-

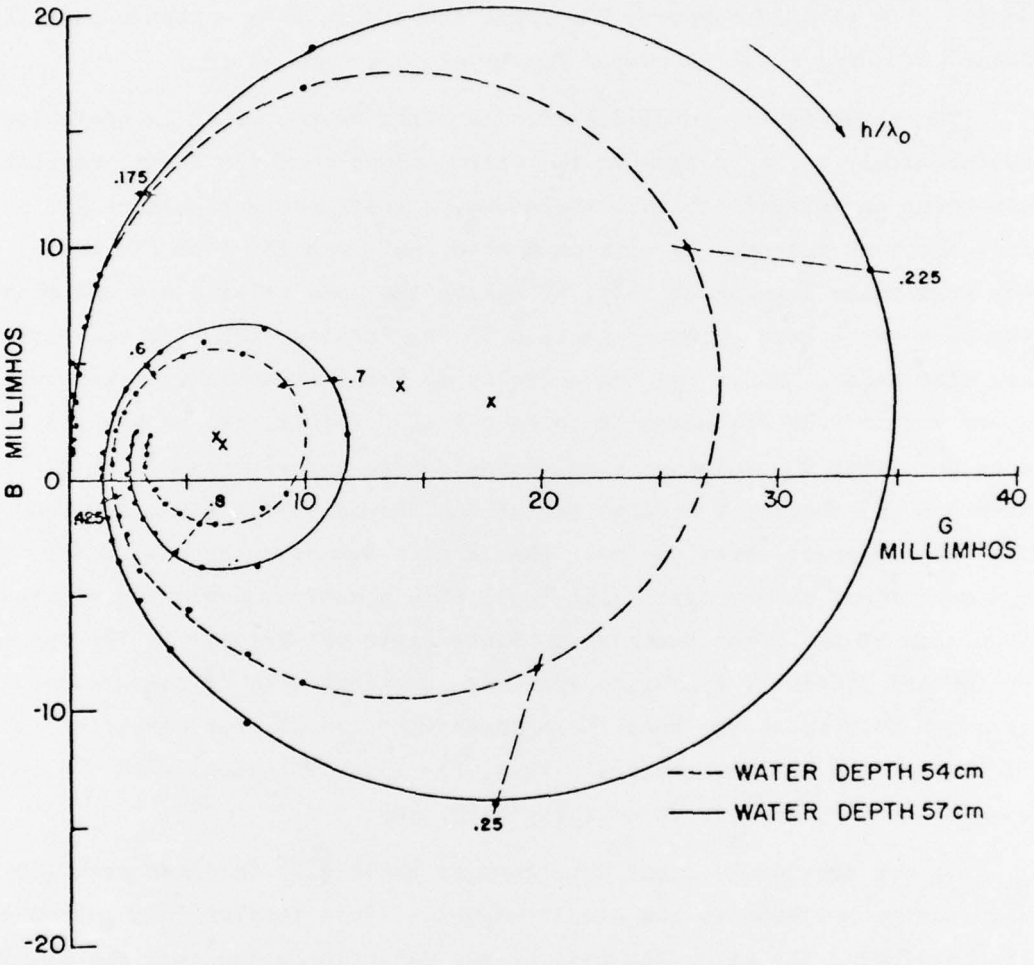


FIG. 2.13. EFFECT ON MEASURED INPUT ADMITTANCE DUE TO VARYING WATER DEPTH $\sigma = .04$ MHOS/M AND $d/\lambda_o = .02$.

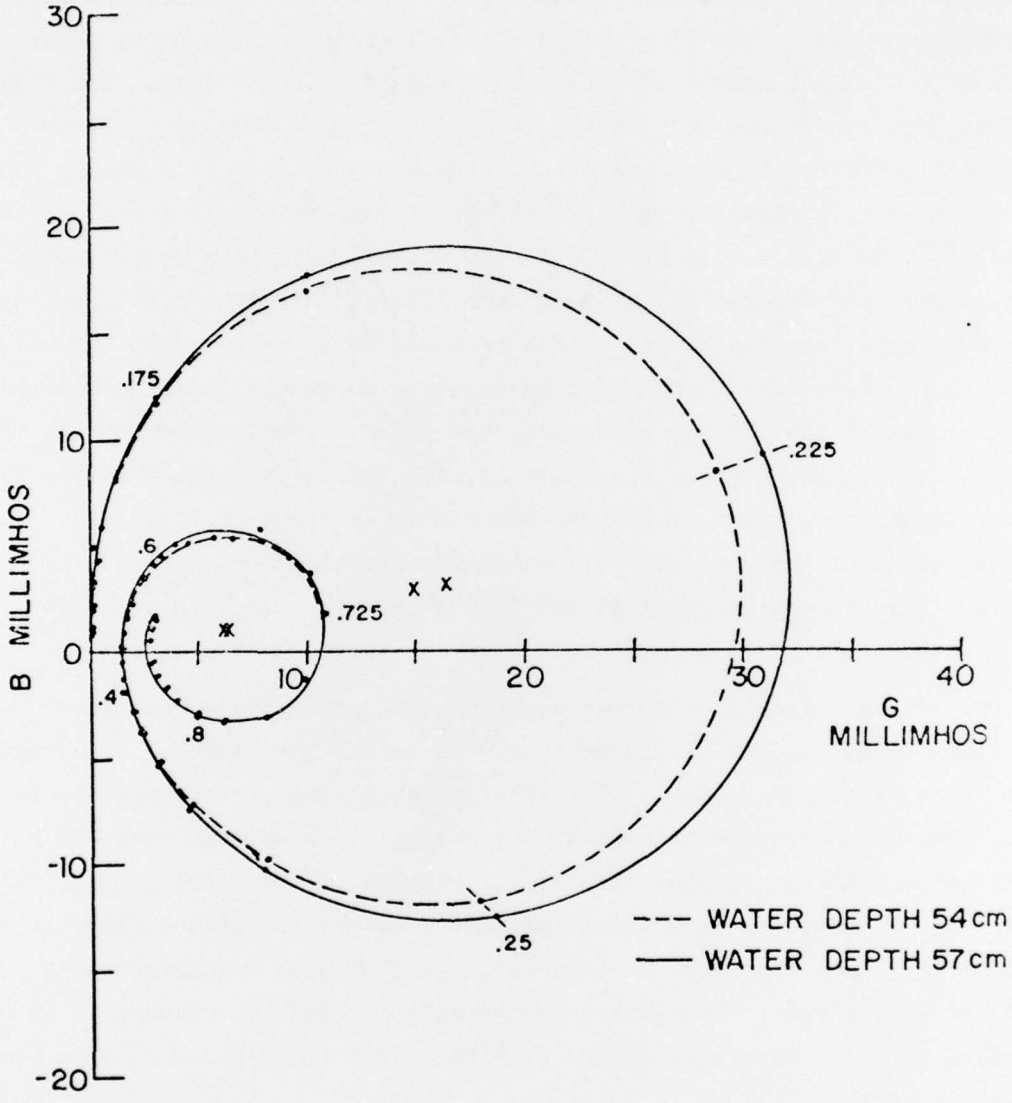


FIG. 2.14. EFFECT ON MEASURED INPUT ADMITTANCE DUE TO VARYING WATER DEPTH. σ = .09 MHOS/M AND d/λ_0 = .02.

tance from the wire to the side wall of the tank is at least two times greater than the water depth, reflections from the walls should be unnoticed. In order to determine this, along with the effect caused by the discontinuity in the air-water interface at the walls, two sets of impedance measurements were compared - one with the normal tank arrangement and the other with a 6' × 8' aluminum sheet placed along one side of the tank. The idea was that any significant reflections from the walls or edge of the tank would be altered by the presence of the aluminum sheet and this change could be observed by its effect on the driving-point impedance. If the fields at the edge of the tank are small, the aluminum sheet will have no influence on the driving-point impedance. Although the aluminum sheet is not large enough to produce a perfect image, its effect is essentially to increase the width of the tank. Since the field would be expected to become less concentrated as the height of the wire is increased, the impedance measurements were made with $d/\lambda_0 = .25$, the highest spacing studied. This represents a worst-case analysis. The comparison of the two impedances is shown in Fig. 2.15. The results show that the presence of the aluminum panel has no effect on the input admittance, confirming that very little error is introduced by the finite-sized tank.

The original ground plane was equipped with side panels constructed of fine aluminum mesh. The panels were used to extend the width of the ground plane by an extra three feet. As a final check on the performance of the ground plane, impedance measurements for $d/\lambda_0 = .25$ were made with and without the side panels. A comparison of the results is presented in Fig. 2.16 and appears to indicate that any error introduced by the ground plane is insignificant. Since the ground plane used for the earth measurements is identical to the one in the tank when the side panels are removed, it is anticipated that any error associated with the earth image plane will be small.

In conclusion, the series of experimental checks performed appear to provide reasonable evidence to presume the validity of the experimental models used in this analysis. The error introduced by the finite-sized tank is quite small and, with the accuracy exhibited by the measuring probes, favorable results can be anticipated.

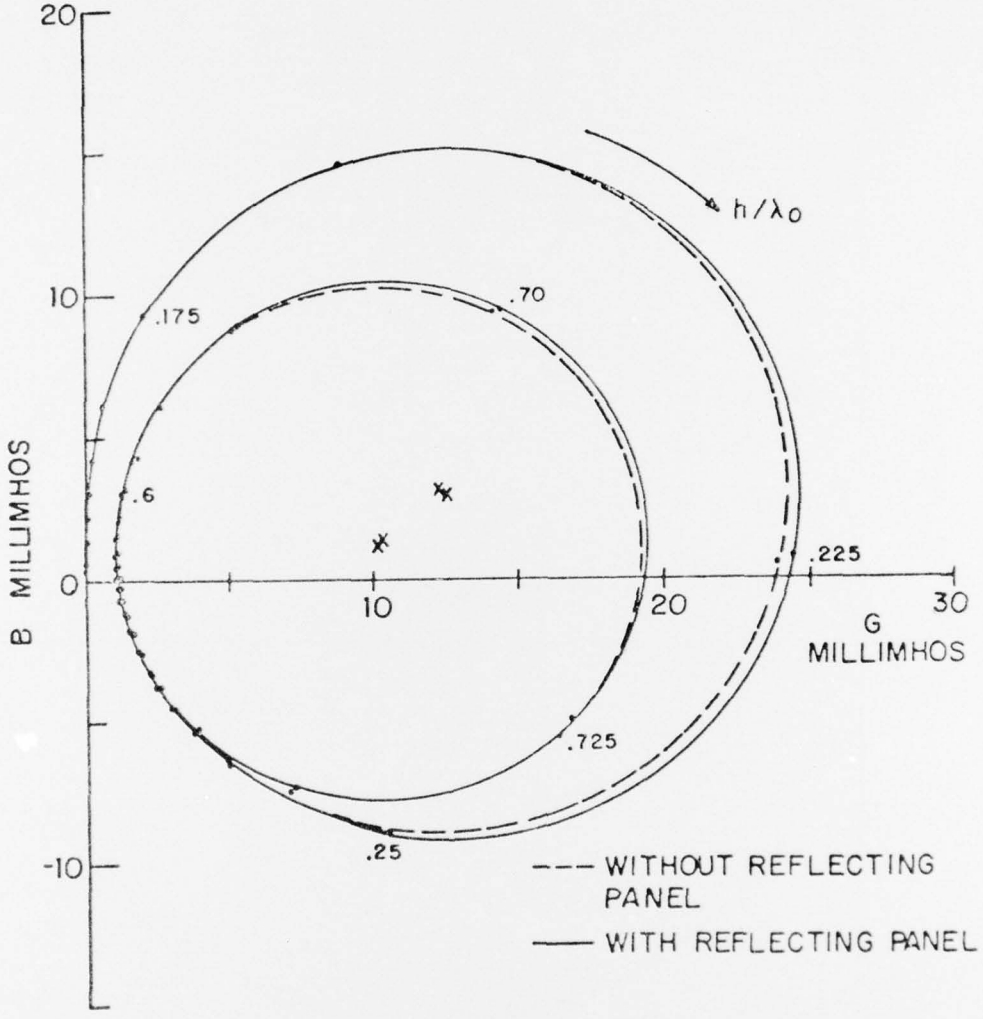


FIG. 2.15. EFFECT ON MEASURED INPUT ADMITTANCE DUE TO FINITE TANK SIZE. $d/\lambda_o = .25$.

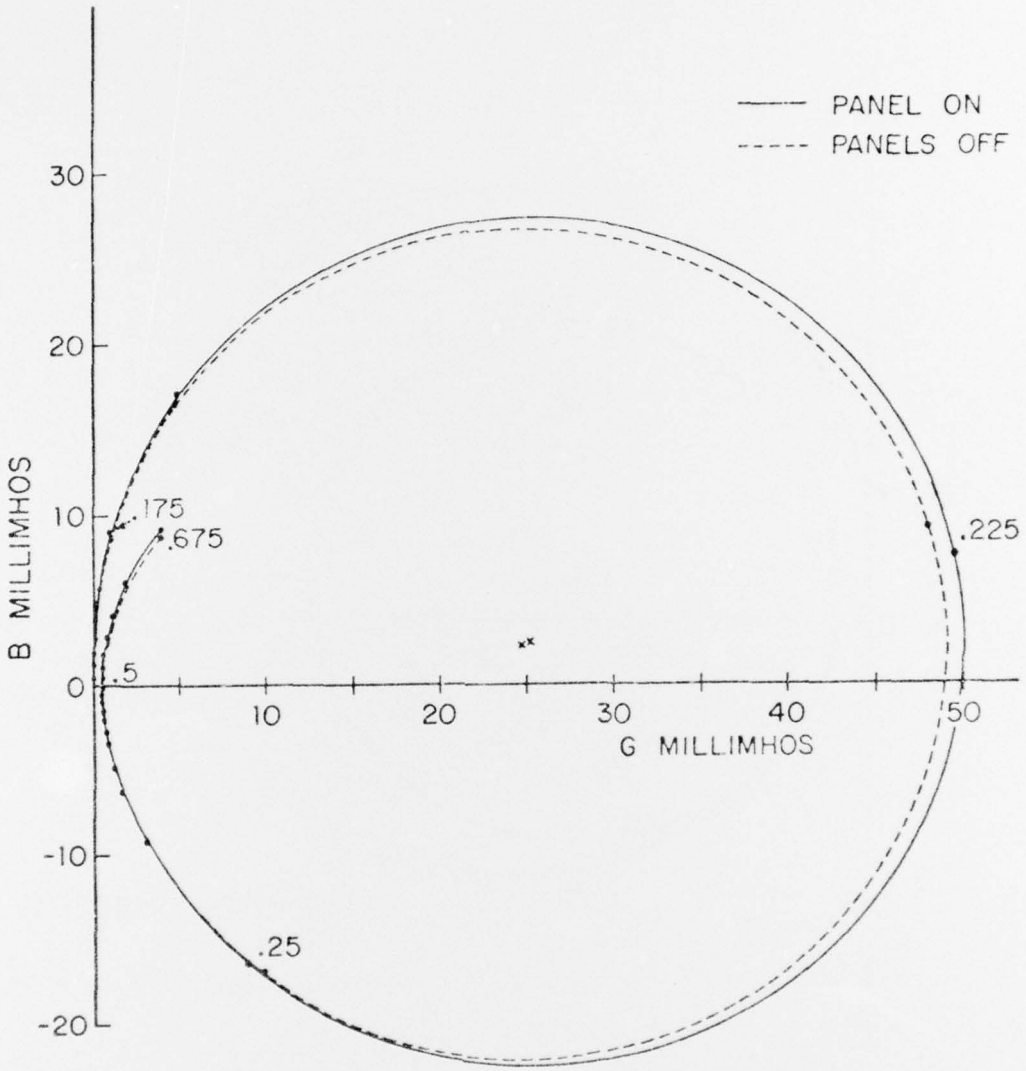


FIG. 2.16. EFFECT OF GROUND PLANE SIZE ON ADMITTANCE MEASUREMENTS ; $d/\lambda_0 = .1$

REFERENCES

[1] Arnold Sommerfeld, Partial Differential Equations in Physics. New York: Academic Press, 1949.

[2] Alfredo Baños, Jr., Dipole Radiation in the Presence of a Conducting Half-Space. New York: Pergamon Press, 1966.

[3] Marvin Siegel, "The electromagnetic fields of dipoles, antennas, and arrays in a dissipative half-space," Ph.D. Thesis, Harvard University, Cambridge, Mass., 1970.

[4] R. W. P. King and B. Sandler, "Subsurface communication between dipoles in general media," paper presented at Annual URSI/USNC Conference, Boulder, Colorado, 1975; IEEE Trans. Antennas Propagat., accepted for publication.

[5] J. R. Carson, "Wave propagation in overhead wires with ground return," Bell Syst. Tech. Jour., pp. 539-544, 1926.

[6] H. Kikuchi, "Wave propagation along a wire above ground at high frequencies," Electro Tech. Jour. Japan, pp. 73-78, 1956.

[7] A. S. Knyazev, "Engineering computation of the resistance of line conductors taking into account the earth's influence," Radiotechnika, pp. 21-32, 1960.

[8] C. H. Walters, Traveling Wave Antennas. New York: McGraw-Hill, 1965, pp. 315-317.

[9] J. D. Kraus, Antennas. New York: McGraw-Hill, 1950.

[10] M. T. Ma, Theory and Application of Antenna Arrays. New York: Wiley-Interscience, 1974.

[11] T. K. Sarkar and B. J. Strait, "Analysis of radiation by wire antennas over imperfect ground," AFCRL Scientific Report No. 6, 1975.

[12] E. K. Miller and F. J. Deadrick, "Computer evaluation of large low-frequency antennas," paper presented at IEEE AP-S Symposium, Williamsburg, Virginia, 1972.

[13] W. C. Kuo and K. K. Mei, "Computation of the scattered electric field by a buried wire," paper presented at IEEE AP-S Symposium, Urbana, Illinois, 1975.

[14] J. R. Wait, "Theory of wave propagation along a thin wire parallel to an interface," Radio Science, vol. 8, pp. 675-679, 1972.

[15] R. W. P. King, T. T. Wu, and L. C. Shen, "The horizontal-wire antenna over a conducting or dielectric half-space: current and admittance," Radio Science, vol. 9, pp. 701-709, 1974.

[16] T. T. Wu, R. W. P. King, and D. V. Giri, "The insulated dipole antenna in a relatively dense medium," Radio Science, vol. 8, pp. 699-709, 1973.

[17] T. T. Wu, L. C. Shen, and R. W. P. King, "The dipole antenna with eccentric coating in a relatively dense medium," IEEE Trans. Antennas Propagat., vol. AP-23, pp. 57-62, 1975.

[18] M. Abramowitz and I. A. Stegun, Handbook of Mathematical Functions. New York: Dover Press, 1965.

[19] H. H. Beverage, C. W. Rice, and E. W. Kellogg, "The wave antenna," Trans. A.I.E.E., 1923.

[20] J. M. Headrick and M. I. Skolnik, "Over-the-horizon radar in the HF band," Proc. IEEE, vol. 62, 1974.

[21] Private communications, Charles Drane and John McIlvenna.

[22] R. M. Sorbello, "Properties of the horizontal-wire antenna over an imperfect conductor," paper presented at Annual URSI/USNC Conference, Boulder, Colorado, 1975.

[23] E. E. Altshuler, "The traveling-wave linear antenna," Ph.D. Thesis, Harvard University, Cambridge, Mass., 1961.

[24] R. W. P. King, Theory of Linear Antennas. Cambridge, Mass.: Harvard University Press, 1955.

[25] R. M. Sorbello, "The Beverage wave antenna: radiation field patterns," Rome Air Development Center Contract F19628-75-C-0057, Scientific Report No. 2, Cambridge, Mass. (in preparation).

[26] R. W. P. King, Transmission-Line Theory. New York: Dover Press, 1965.

[27] E. Hallén, "Exact treatment of antenna current wave reflection at the end of a tube-shaped cylindrical antenna," IRE Trans. Antennas Propagat., vol. AP-4, pp. 479-491, July 1956.

[28] L. C. Shen, T. T. Wu, and R. W. P. King, "A simple formula of current in dipole antennas," IEEE Trans. Antennas Propagat., vol. AP-16, pp. 542-547, Sept. 1968.

[29] R. W. P. King, L. C. Shen, and T. T. Wu, "The horizontal-wire antenna over a conducting or dielectric half-space," Radio Science, vol. 9, pp. 701-709, 1974.

[30] L. C. Shen, R. M. Sorbello, R. W. P. King, K.-M. Lee, and T. T. Wu, "The horizontal-wire antenna over a dissipative half-space: Generalized theory and measurements," (to be published).

[31] R. W. P. King, Fundamental Electromagnetic Theory. New York: Dover Press, 1963.

[32] George Sinclair, "Theory of models of electromagnetic systems," Proc. of the IRE, vol. 37, pp. 1364-1370, Nov. 1949.

[33] Kussen, Maley, Chang, and Wait, "Experimental investigation of the impedance of a horizontal linear antenna above a dissipative homogeneous earth," paper presented at the 1973 International IEEE/AP-S Symposium.

[34] L. D. Scott, "Apparatus for studying the properties of antennas in an effectively infinite dissipative medium," NASA Scientific Report No. 6, Harvard University, Cambridge, Mass., Dec. 1969.

[35] G. S. Smith, "A theoretical and experimental study of the insulated loop antenna in a dissipative medium," JSEP Technical Report No. 637, Harvard University, Cambridge, Mass., April 1973.

[36] K. Iizuka, "An experimental study of the insulated dipole antenna immersed in an conducting medium," IEEE Trans. Antennas Propagat., vol. AP-11, pp. 518-532, Sept. 1963.

[37] L. D. Scott, "Antennas in homogeneous isotropic media," Ph.D. Thesis, Harvard University, Cambridge, Mass., 1970.

[38] L. D. Scott and G. S. Smith, "Measurement techniques for antennas in dissipative media," IEEE Trans. Antennas Propagat., vol. AP-21, pp. 499-507, July 1973.

[39] A. R. von Hippel, Dielectric Materials and Applications. Cambridge, Mass., M.I.T. Press, 1954.

[40] J. B. Birks and J. Hart, Progress in Dielectrics, Vol. 3. New York: Wiley & Sons, 1961, Section 4, pp. 132-136.

[41] General Radio Co., "Instruction Manual, Type 1690A Dielectric Sample Holder," Concord, Mass., 1968.

[42] General Radio Co., "Operating Instructions for Type 1620B Admittance Meter," Concord, Mass., 1954.

[43] G. S. Smith, "A comparison of electrically short bare and insulated probes for measuring the local r.f. electric field in biological systems," IEEE Trans. Biomedical Engrg., vol. BME-22, Nov. 1975.

[44] R. F. Hahn and J. G. Fikioris, "Impedance and radiation patterns of antennas above flat discs," IEEE Trans. Antennas Propagat., vol. AP-21, pp. 97-100, Jan. 1973.

[45] A. S. Meier and W. P. Summers, "Measured impedance of vertical antennas over a finite ground plane," Proc. of the IRE, vol. 37, p. 609, 1949.

[46] H. W. Andrews, "Image plane and coaxial line measuring equipment at 600 Mc.," JSEP Tech. Rept. No. 177, Harvard University, Cambridge, Mass., 1953.

[47] C.-Y. Ting, "A theoretical study of a cylindrical antenna with a hemispherical cap," AFCRL Scientific Report No. 2, Harvard University, Cambridge, Mass., 1963.

[48] R. W. P. King, Tables of Antenna Characteristics. New York: Plenum Publishing Co., 1971.

[49] H. Whiteside, "Electromagnetic field probes," JSEP Technical Report No. 381, Harvard University, Cambridge, Mass., Oct. 1962.

MISSION
of
Rome Air Development Center

RADC plans and conducts research, exploratory and advanced development programs in command, control, and communications (C^3) activities, and in the C^3 areas of information sciences and intelligence. The principal technical mission areas are communications, electromagnetic guidance and control, surveillance of ground and aerospace objects, intelligence data collection and handling, information system technology, ionospheric propagation, solid state sciences, microwave physics and electronic reliability, maintainability and compatibility.

Printed by
United States Air Force
Hanscom AFB, Mass. 01731